Alkali-activated materials with organics: A critical review

Shengqian Ruan [a,b], Rongfeng Gao [a], Wenlin Tu [b], Dongming Yan [a,*], Mingzhong Zhang [b,*]

[a] *College of Civil Engineering and Architecture, Zhejiang University, Hangzhou 310058, China*

[b] *Department of Civil, Environmental and Geomatic Engineering, University College London, London WC1E 6BT, UK*

Corresponding authors. E-mail addresses: dmyan@zju.edu.cn (D. Yan), mingzhong.zhang@ucl.ac.uk (M. Zhang)

Abstract: This paper represents a critical review on alkali-activated materials (AAM) containing organics with high homogeneity at nano-scale (<1 μm). Organics including organosilicons, surfactants, water-soluble polymers and epoxy resins can contribute to performance enhancement and tailorability of AAM based on their molecular characteristics. Hence, AAM with organics can generally possess improved characteristics between organic and inorganic components and may even exhibit emerging functional properties. According to the hybridisation modes between AAM and organics such as chemical bonding, physical adsorption, electrostatic attraction or phase crosslinking, these AAM with organics are categorised into four distinct types: organic-grafted, organic-adsorbed, phase-crosslinked and phase-separated AAM. In this paper, the hybridisation modes and reaction mechanisms of AAM with organics are summarised, for the first time, followed by a comprehensive discussion on the phase assemblage, microstructure, mechanical properties, durability and potential applications. Afterwards, the fundamental insights are gained and the remaining challenges for future research are identified and discussed.

Keywords: Alkali-activated materials; Organics; Reaction mechanisms; Microstructure; Mechanical properties; Durability

1. Introduction

Alkali-activated materials (AAM) are a class of inorganic aluminosilicate materials formed by the reaction of solid precursors including fly ash, slag and metakaolin with alkaline activator such as sodium or potassium silicate and hydroxide [1-2]. AAM have been regarded as a promising alternative to ordinary Portland cement (OPC) [3-6]. The global production of OPC reached 4.1 billion tonnes in 2020, accounting for approximately 6–8% of global anthropogenic emissions [7-8]. AAM have a significantly lower carbon footprint, with production energy consumption and carbon emissions being only 40% and 20% of OPC, respectively [3,9-10]. The predominant reaction products within AAM

are sodium aluminosilicate hydrate (N-A-S-H) or/and calcium aluminosilicate hydrate (C-A-S-H) gels, depending on the chemical composition of the precursors [11-12]. Specific designations are employed to represent these AAM systems: AAMK for alkali-activated metakaolin, AAF for alkali-activated fly ash, and AAS for alkali-activated slag. Moreover, mixtures of alkali-activated fly ash-slag or metakaolin-slag are denoted as AAFS and AAMKS, respectively. AAM, when prepared with appropriate material mix design and curing conditions, exhibit exceptional properties in terms of early-age strength, ductility, bonding characteristics and fire-resistance, making them highly suitable for a variety of applications, including building restoration, structure protection and 3D printing [6,13-16]. However, certain performance deficiencies and controversies of AAM, such as pronounced capillary water absorption [17-19], high drying shrinkage [20-22] and susceptibility to efflorescence [23-24], would impede their broad utilization in engineering applications. AAM exhibit high hydrophilicity (with a water contact angle of less than 30°) and rich pore structure (total porosity of 30–45% for AAMK), resulting in their high water absorption and corrosive transport performance [17-18,25]. A comparative study revealed that the water permeability of AAF concrete (1.52×10^{-10} m/s) is approximately 10 times greater than that of OPC concrete (1.73×10^{-11} m/s) [26]. Additionally, the drying shrinkage of AAM is about 2–4 times higher than that of OPC, which promotes the formation of cracks and leads to negative effect on durability and long-term performance of civil infrastructure made with AAM [27-28]. To tackle these limitations, the incorporation of various additives is a commonly employed strategy to enhance the performance of AAM [14,29-30]. Among them, the synthesis of organic-containing AAM with improved properties or even new functional performance through organic-inorganic hybridisation strategies has recently gained a lot of attention.

In recent years, organic-containing AAM characterised by high homogeneity at nano-scale (<1 μm) have garnered significant attention in engineering materials, particularly construction materials. According to the IUPAC standard, these AAM with organics are generally composed of an intimate and uniform mixture of the inorganic and organic components, which usually interpenetrate at nano-scale of less than 1 μm [31]. Thus, they exhibit features that are intermediate between the organic and inorganic components and may even have new functional properties, e.g., hydrophobicity, water and corrosion resistance [32]. AAM with organics can be synthesised by blending organics with fresh AAM via direct-incorporation, pre-dissolution or pre-emulsification [33-34]. The organics encompass a range of categories, including micromolecular organosilicons (e.g., silane coupling

agents and ionic organosilicons), surfactants (e.g., micromolecular surfactants, superplasticisers and alcohol organic compounds), silicone oil, water-soluble polymers or their emulsions, and epoxy resin. These organics may be grafted on the initial and final gel matrix through chemical bonding, attached to precursor particles and matrix through physical adsorption or crosslinked with the inorganic gel network [35-37]. In final AAM systems, the inorganic gel usually plays the role of providing the main foundation that is the source of strength. The effect of organics on the synthesis reaction and performance of AAM depends on their chemical structure and active functional groups, as well as the characteristics of raw materials and the inherent structure within the AAM system.

Organic-containing AAM with nano-scale homogeneity was initially reported in 2005 in a research on the synthesis and thermal behaviour of the epoxy-AAMK composite [38], and numerous investigations on these AAM have been subsequently reported, particularly after 2013 [39-43]. To date, literature reviews on topics related to the processing routes of organic liquids into AAM [33], the rheology of AAM incorporating chemical additives [44-45], hydrophobically modified AAM [46-47] and the adsorption of organic pollutants on AAM [48-50] have been reported. However, a comprehensive review on AAM with organics in terms of hybridisation modes and reaction mechanisms between organic and inorganic components is still lacking.

This paper presents a state-of-the-art review on AAM with organics, focusing on the reaction mechanisms, phase assemblage, chemical composition, microstructure, mechanical properties and durability in terms of wettability, water absorption, corrosion resistance, volume deformation and thermal stability. The potential applications of these AAM are also discussed. **Fig. 1** shows the outline of this review, where the main focus is placed on inorganic systems of AAM derived from fly ash, slag and/or metakaolin as precursors. Organics with stable chemical structures including but not limited to rubbers, cottons, superabsorbent polymers, organic fibres, vegetable oils and mineral oils are excluded. They can be used as aggregates or toughening materials but are generally considered incompatible with cementitious materials at micro-scale [30,51-58].
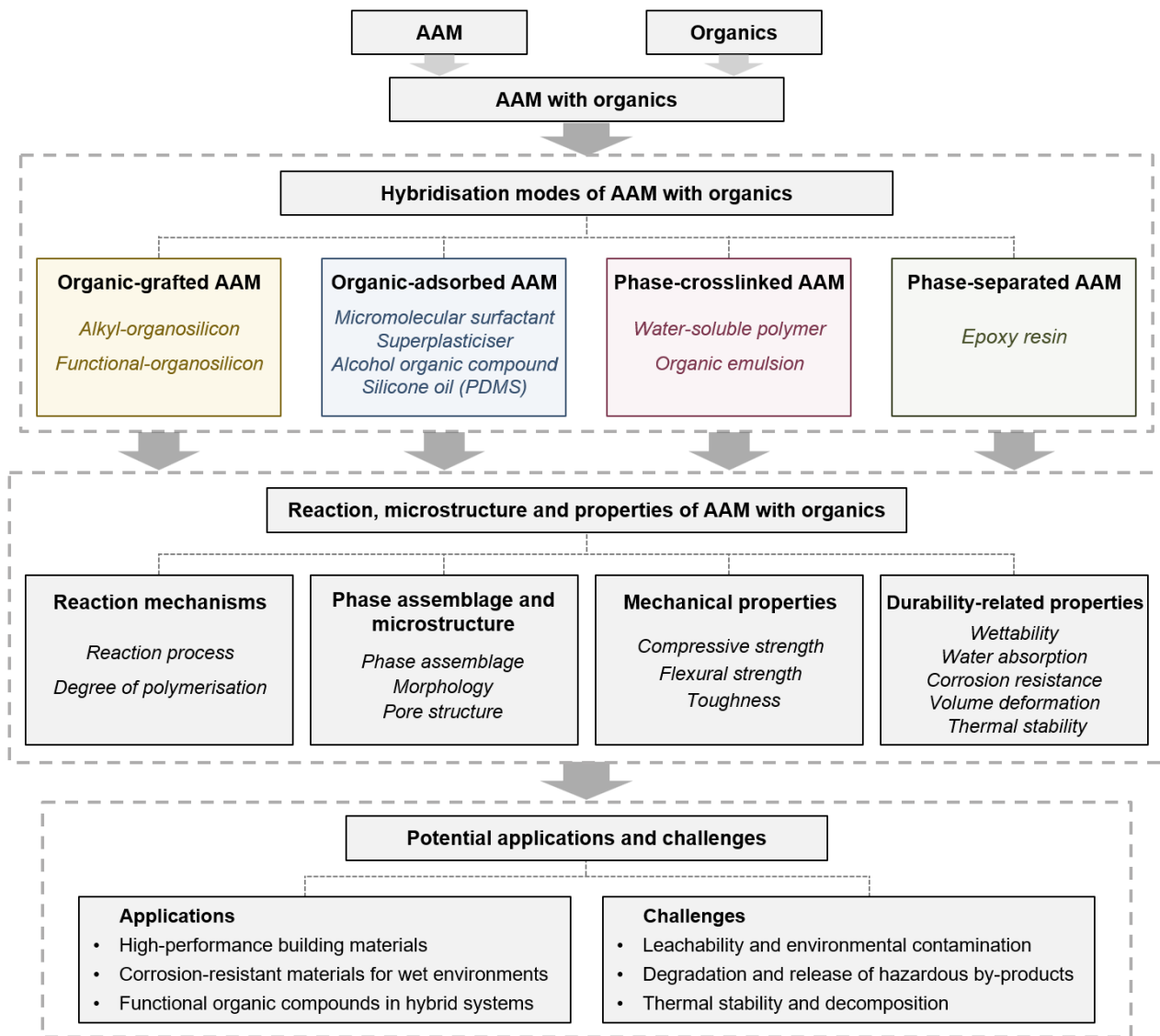
Fig. 1. Outline of this review.

2. Hybridisation modes of AAM with organics

Due to the different molecular structures, sizes and functional group types of organics, their binding forms and sites with inorganic materials are significantly different. Based on the hybridisation modes of organic and inorganic components, AAM with organics can be categorised into the following four distinct types (**Fig. 2**).
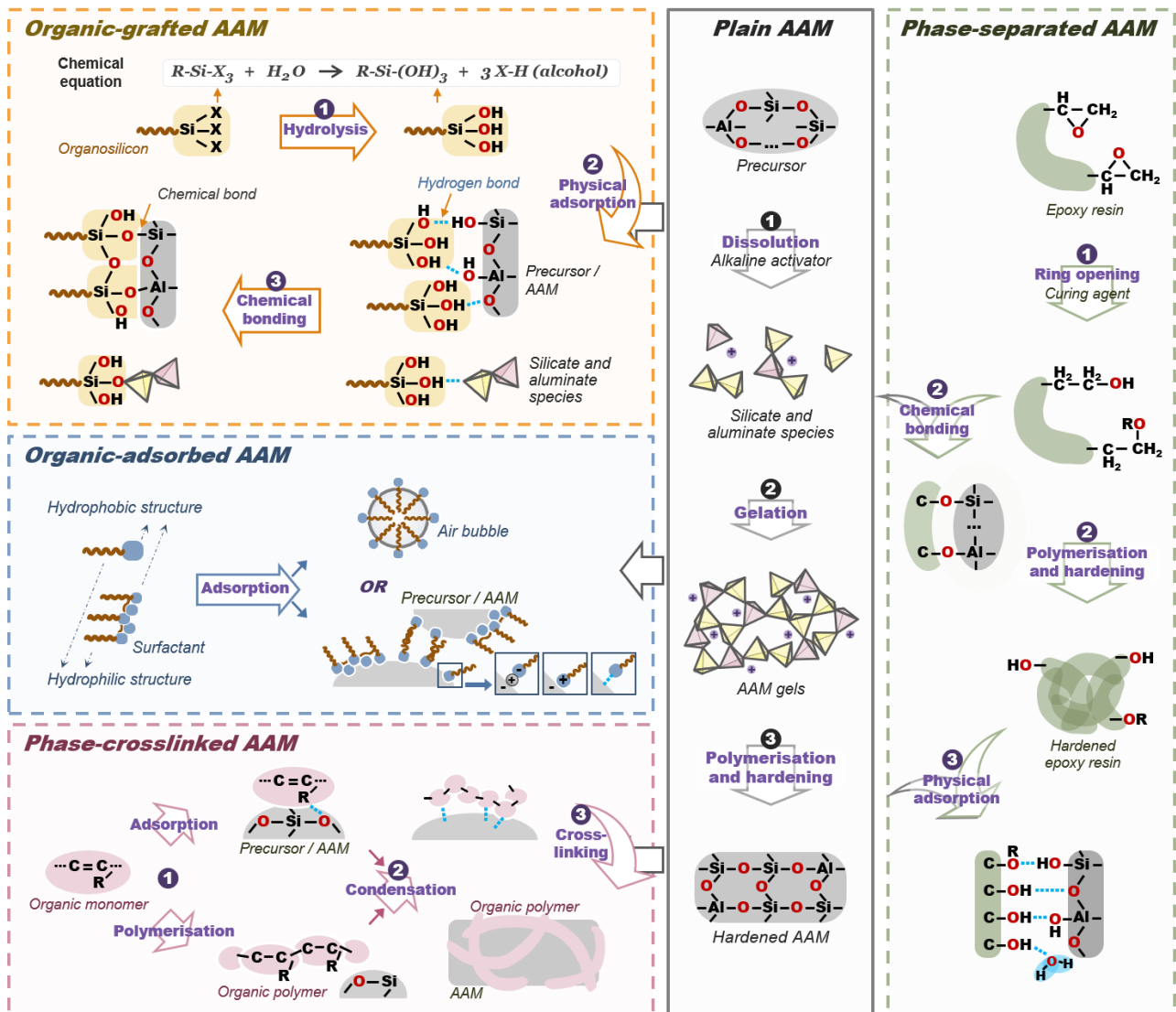
Fig. 2. Schematic illustration of hybridisation modes and synthesis reaction mechanisms of four types of AAM with organics.

2.1. Organic-grafted AAM

In organic-grafted AAM, organics and AAM are mainly combined through chemical bonds, and supplemented by van der Waals forces, hydrogen bonds and electrostatic attraction, as illustrated in **Fig. 2**. The main organics are micromolecular organosilicon compounds (hereinafter referred to as organosilicons) such as silane coupling agents and ionic organosilicons, which can undergo chemical bonding with inorganic species and phases in alkaline solutions (**Tables 1** and **2**) [59-61]. The general chemical structure of organosilicons is R-Si-X$_3$, where R represents an organic structure, typically a carbon or -C-O- chain that may incorporate various functional groups such as vinyl, amino, epoxy, ester and urea [62-63]. X denotes a hydrolysable functional group, containing methoxy, ethoxy, chlorine, etc. These groups can undergo hydrolysis in alkaline solution, yielding silanol active

structures (Si-OH). Then, covalent bonds of Si-O-Si or Si-O-Al can be formed through condensation reactions, facilitating the coupling reactions with inorganic materials [64-65]. Ionic organosilicons such as sodium methyl siliconate (SMS) and potassium methyl siliconate (PMS) can also be hydrolysed in alkaline solution and engage in polymerisation, leading to the direct chemical graft onto aluminosilicate hydrate gels [59,66-67]. These organosilicons typically have molecular weights below 300 g/mol and exhibit favourable solubility and dispersion characteristics in alkaline solution or fresh AAM slurries (**Table 1**). They can establish consistent and robust chemical bonds with AAM at micro-scale, thereby inducing alterations in chemical composition and microstructure of gel particles and clusters [66,68]. Organic-grafted AAM are emerging materials with broad development prospects, and more than 90% of related research was reported after 2019 (**Table 1**).

2.2. Organic-adsorbed AAM

In contrast to organosilicons, most organics that can be used as additives for cementitious materials lack active structures analogous to Si-OH, rendering them incapable of chemical bonding with gels in AAM. In organic-adsorbed AAM, the organics predominantly combine with the solid precursors, initial gel particles or final gel network of AAM through physical adsorption caused by van der Waals forces and hydrogen bonds [44,69]. Additionally, specific instances may involve the presence of ionic and covalent bonds to a lesser extent [69-70].

The organics frequently employed in the synthesis of organic-adsorbed AAM are surfactants and silicone oil (**Tables 3** and **4**). Surfactants are amphiphilic compounds composed of hydrophilic structures (polar groups such as carboxylic acid, sulfonic acid, sulfuric acid, amino, hydroxyl, amide group, and ether bond) and hydrophobic structures (non-polar hydrocarbon chain). Their primary function is to mitigate the interfacial tension within target suspensions or emulsions [71-72]. For AAM, three types of surfactant additives are commonly adopted: micromolecular surfactants, superplasticisers and alcohol organic compounds (hereinafter referred to as alcohols). Micromolecular surfactants in cementitious materials primarily offer two essential functions as dispersants for various raw materials (e.g., solid precursors, carbon nanotubes, graphene, and fibres) [44,73-78] and as stabilisers for foam or oil in fresh systems [48,79-80]. As seen in **Table 4**, foamed AAM are the most common specimen type of micromolecular surfactant-adsorbed AAM, and the additive dosage generally does not exceed 2.5% [81-83]. The additive dosage in this review represents the mass ratio of organics to the inorganic binder (i.e., AAM paste). Superplasticisers are a special

type of polymer surfactant [84]. Superplasticiser molecules have multiple hydrophilic and hydrophobic structures, facilitating their adsorption onto precursors and enhancing the workability of fresh AAM [69,85]. Alcohols, including ethylene glycol (EG) and propylene glycol (PG) monomer/polymer and other glycols, represent a distinct category of non-ionic surfactants. The molecular structure of alcohols consists solely of hydroxyl groups and hydrocarbon chains, which are often used as shrinkage reducing agents for cementitious materials [86-87]. Polydimethylsiloxane (PDMS), a type of silicone oil, has recently been approved effective as a typical organic polymer for hydrophobic and anti-corrosion modification of AAM [18,88-94]. In addition to the controversy over the stability of superplasticisers in strong alkaline solutions, micromolecular surfactants, alcohols and PDMS exhibit robust physical and chemical stability in fresh AAM, implying that they generally do not form chemical bonds with AAM [95-96].

2.3. Phase-crosslinked AAM

In phase-crosslinked AAM, organics and AAM predominantly form interconnections via the crosslinking of two self-condensation systems, with significant contributions from van der Waals forces and hydrogen bonds. The organics involved in this type of AAM are water-soluble polymers or their emulsions. Water-soluble polymer monomers possess a molecular structure of carbon-carbon double bonds (C=C), providing them the capability to condense and create organic polymer networks or films, which can crosslink with inorganic gel networks (**Table 5** and **Fig. 2**) [97-98]. The majority of these polymers are esters, capable of preserving their inherent structures and material characteristics within AAM systems [99]. With uniform dispersion in water, water-soluble polymers can be mixed with surfactants, catalysts and other ingredients in aqueous solutions to prepare organic emulsions or latex, which are used to regulate the mechanical properties, bonding characteristics and durability of building materials [97,100-101]. The commonly used polymers for enhancing cement-based materials include polyacrylate, ethylene vinyl acetate (EVA), styrene butadiene rubber, styrene-acrylic copolymer and polyvinyl alcohol with main functional groups such as ester, alkyl, amino and benzene rings [101-105]. Although water-soluble polymers have been widely used in cement-based materials, the hybridisation mechanisms and impact of them on performance of AAM have been rarely studied (**Table 6**).

2.4. Phase-separated AAM

Phase-separated AAM stand for a composite system where organics and AAM each harden into

separated phases connected by hydrogen bonds. Epoxy resin is a polymer compound that exhibits a phase transition when exposed to heat or reacting with a curing agent, resulting in the formation of a hardened 3D network with high density [106]. In epoxy resin-containing AAM, AAM generally dominate as a continuous phase, and hardened epoxy resin primarily exists in the form of solid particles with dimensions ranging from 1 to 20 μm [41,107-108]. There exists strong adhesion between organic epoxy resin and AAM because of the presence of a nano-scale hybrid interfacial transition zone (ITZ) between them [41,107], which can enhance the mechanical properties and durability of AAM composite, making the system worthy of discussion in this review (**Table 7**) [41,109-111].

3.   Reaction, microstructure and properties of organic-grafted AAM

3.1. Reaction mechanisms

The incorporation of organosilicons significantly affects synthesis reaction mechanisms of organic-grafted AAM by direct participating in the gelation and polymerisation processes. As seen in **Fig. 2**, when organosilicons are introduced into either water or alkaline solution, they undergo swift hydrolysis, which leads to the rupture of silicon-oxygen bonds between the silicon atom and hydrolysable functional groups (X), resulting in the formation of silanol structures within the organosilicon molecules. A state of hydrolysis dynamic equilibrium is typically attained within 20–30 min upon mixing [68,112-113]. The organosilicon dosage in AAM is generally less than 7% and mainly below 2% (**Table 2**). When organosilicons or their hydrolysates are added into fresh AAM slurry, the molecules typically manifest the following distinct physical and chemical behaviour [60,114]. Firstly, organosilicon molecules can rapidly adsorb onto precursor, oligomers or gel particles through hydrogen bonds. Such physical adsorption in the early-age stage of reaction facilitates favourable spatial positions for subsequent chemical bonding. As reaction progresses, the adsorbed organosilicons participate in the synthesis of gels in AAM through continuous chemical bonding reactions. Some adjacent organosilicon molecules grafted onto the gel can form organic networks or films through further self-condensation [60,115].

Fig. 3 displays the evolution of heat flow of AAMK and AAFS containing molecular or ionic organosilicons. All reaction heat curves exhibit distinct peaks characterised by exceptionally high heat flow values within the initial 30 min of the experiment. These peaks are indicative of the swift dissolution of aluminosilicate precursors, leading to the release of monomers and oligomers into the

alkaline solution [116]. As the reaction proceeds, both AAMK and AAFS experience an induction period with low reaction heat lasting around 6–12 h with heat flow less than 0.5 J/g, followed by a distinct exothermic peak at 12–48 h, which corresponds to the rapid formation of initial N-A-S-H and/or C-A-S-H gels [36,59,117]. In contrast to AAMK, AAFS exhibits a specific exothermic peak at about 3 h after the reaction initiation, lasting for approximately 5 h (**Fig. 3**g), which can be ascribed to the initial reaction between the dissolved silicate and calcium sources [118]. The incorporation of 0.8–3.2% organosilicons of 3-aminopropyltriethoxysilane (KH550), 3-methacryloxypropyltrimethoxysilane (KH570), triethoxyoctylsilane (S823) and SMS notably accelerates the early-age heat release rate of organic-grafted AAM (**Fig. 3**). Their initial 30-min cumulative heat release is almost doubled compared to the plain AAM, primarily owing to the rapid hydrolysis of organosilicons accompanied by the heat release in alkaline environments [60]. The nature of organosilicons can alter this effect on the early-age reaction of AAM. As seen in **Fig. 3**a and c, adding 0.8% KH550, 1% S823, 1% dodecyltrimethoxysilane, (S1213) and 1% KH570 leads to a change in the maximum rate of heat release of AAMK by 138%, 103%, -10% and 62%, respectively. Except for S1213 that has a long hydroxyl chain, other organosilicons can be rapidly hydrolysed in the first 10 min of the reaction, and the hydrolysis by-products adsorb onto solid particles, with concurrent formation of hydrogen bonds that also release thermal energy [115,119]. The reaction progress including precursor dissolution and initial gel formation is further facilitated, attributed to heat accumulation and heightened alkalinity [60]. Moreover, it can be found that all these organosilicons can delay the time reaching the maximum rate of heat release by 0.4–3 min, suggesting that the hydrolysis and adsorption rates of organosilicons may be slightly lower than the hydrolysis rate of AAM precursor.

The early-age reaction mechanisms of AAM can be reflected by the evolution of fresh properties to some extent. The incorporation of 1–2% KH550 rises the fluidity and consistency of AAMK by 7–13% and 32–66% respectively [120], whereas 5% KH550, [(2,3-epoxypropoxy)propyl]trimethoxysilane (KH560) or KH570 reduces the fluidity of AAS by 18–20% [121]. The change in fresh properties of AAM results from the competitive balance between the dispersion and agglomeration effects following silanol adsorption [120,122]. An appropriate dosage of organosilicons (≤2%) can increase the zeta potential of the precursor in alkaline solution, thereby reducing particle agglomeration [121,123]. Hydrophobic groups on organosilicons can also diminish

the surface energy of precursor particles, consequently enhancing their dispersion characteristics. However, organosilicons with over-dosage (>2%) may induce the formation of spherical micelles in the system, thereby resulting in particle agglomeration and a subsequent reduction in the mobility of fresh AAM [122,124].
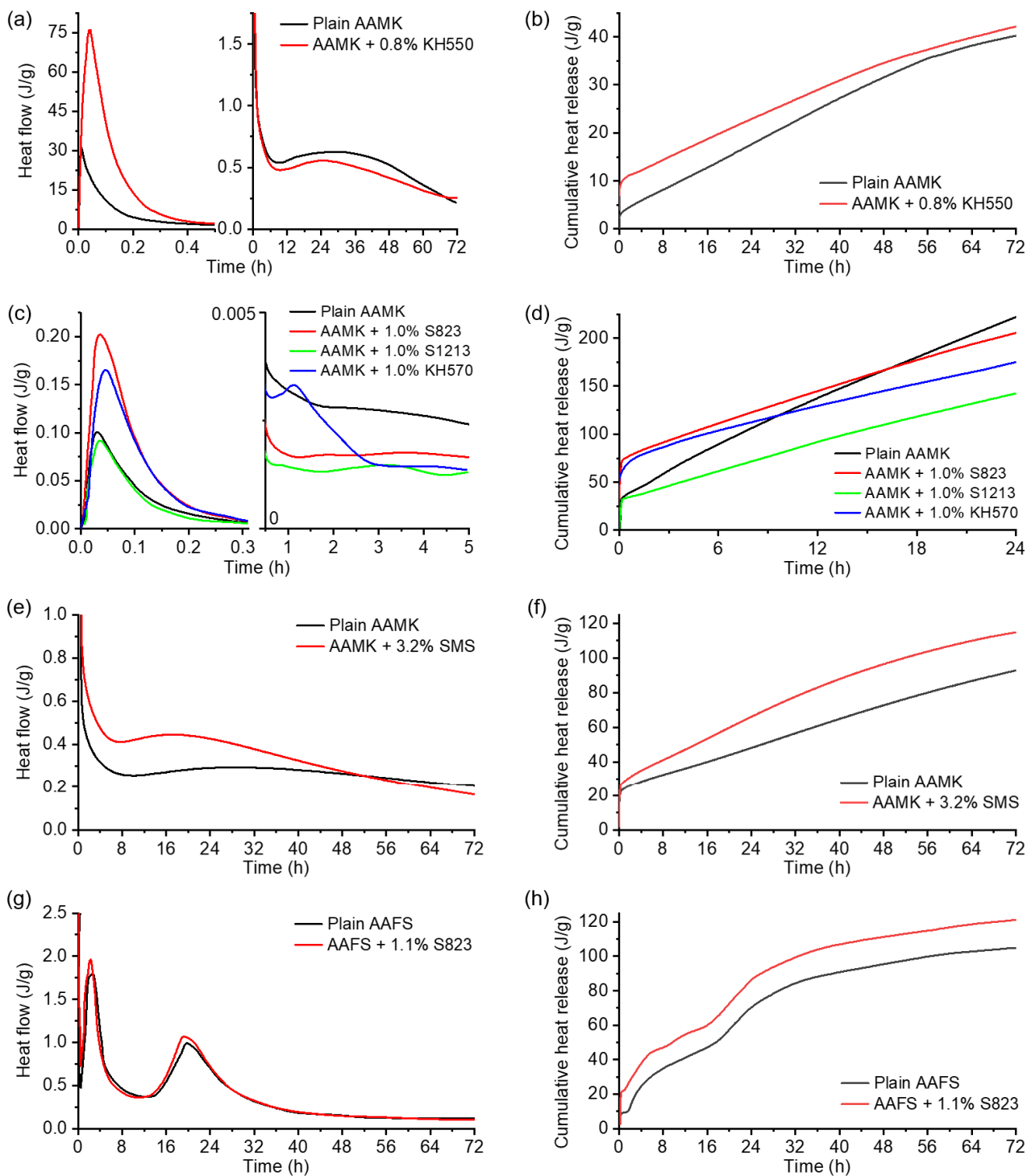

Fig. 3. Evolution of (a, c, e, g) heat flow and (b, d, f, h) cumulative heat release of (a, b) AAMK with 0.8% KH550, (c, d) AAMK with 1.0% S823/S1213/KH570, (e, f) AAMK with 3.2% SMS, and (g, h) AAFS with 1.1% S823 [41,59-60,68].

As for the overall reaction, the degree of polymerisation in AAM drops with the addition of organosilicons with long hydrophobic hydrocarbon chains or alkyl groups (alkyl-organosilicons), e.g., S823, methyltrimethoxysilane (MTMS), SMS and PMS [59-60,66]. The incorporation of S823 contain a hydrocarbon chain of C8 results in a notable reduction in the intensity of the humps representing amorphous phases in AAM detected by the X-ray diffraction (XRD) technique [60]. The presence of organic hydrocarbon chains in the gels hinders the condensation of oligomers due to the steric hindrance effect [36]. The addition of SMS and PMS, featuring methyl groups, also reduces the degree of polymerisation of the final gels. The initial gels bonding with the organic structure [R-Si(OH)$_3$] exhibits less binding sites compared to the plain gels [Si(OH)$_4$]. As evidenced by ^{29}Si nuclear magnetic resonance (NMR) analysis, the addition of 3.2–6.6% SMS results in a slight rise of Q^2 and Q^3 structures by 3–10% in the final AAMK, which can be ascribed to the gel rearrangement and organosilicon monomer structures [59]. Q^4 units linked to four silicon/aluminate tetrahedra are more difficult to synthesise in AAM as the initial gels and oligomers may have been grafted with SMS. Therefore, the incorporation of alkyl-organosilicons, often as terminal units, can disrupt the continuous development of tetrahedral linkage, leading to an increase in the face/chain gel structure and a decrease in the amorphous network structure [59,61]. Additionally, the addition of 3.9% PMS reduces the binding energy of Si-OH, Si-O-Si and Si-O-Na bonds by 0.152, 0.153 and 0.594 eV as confirmed by X-ray photoelectron spectroscopy (XPS) analysis, indicating a drop in bond strength and a reduced degree of polymerisation between constituent atoms within the final gels [67]. However, more gel products are generated in AAS with PMS and the Si-O-Si content goes up by 23.4%, attributed to the enhanced alkalinity and heat release (**Fig. 3**). Alkyl-organosilicons with hydrophobic structures can also bind to precursors and/or initial gels through physical adsorption or chemical bonding, leading to the formation of a protective hydrophobic film that can effectively impede the precursor dissolution and the initial gel rearrangement. It is also a main reason for these organosilicons to inhibit the degree of polymerisation of gels in AAM [66].

For organosilicons with organic functional groups like amino, epoxy, methacrylate and benzene (functional-organosilicons), the polarity of the molecular structure plays a crucial role in determining the development of gels in AAM. The incorporation of KH550 (with amino) and KH570 (with methacrylate) facilitates the polymerisation process of AAM, resulting in the formation of densely crosslinked gel networks [111,113-114,121]. KH570 notably exhibits a more pronounced enhancing

effect in formation of silicon tetrahedral structures with high degree of polymerisation in AAS, as the bridging silicon proportion of C-A-S-H gels increases by 75.18%, as estimated using XPS [121]. Amino and methacrylate groups are highly polar and hydrophilic, thus promoting the dispersion of precursors and initial gels. This can potentially explain why these functional-organosilicons can improve the degree of polymerisation. In contrast, there exist varying conjectures regarding the impact of KH560, bearing epoxy groups, on the degree of polymerisation. It was reported that KH560 slightly inhibits the polymerisation of C-A-S-H gels in AAS, due to the weaker hydroxyl polycondensation between epoxy groups and C-A-S-H gels [121]. Aforementioned organosilicon dosage, referring to a content of above 2%, noticeably suppresses the reaction and thus reduces the degree of polymerisation [114]. For the organic structures with functional groups, longer hydrocarbon chains introduce increased steric hindrance, which subsequently inhibits the rates of continuous hydrolysis and condensation of organosilicon [111,125]. Regarding hydrolysable functional groups, the hydrolysis rate of trimethoxy group is higher than that of triethoxy group, and thus the early polymerisation and adsorption of organosilicons with hydrolytic functional groups of low molecular weight are more intensive [41].

3.2. Phase assemblage and microstructure

Organic functional structures grafted on gels in AAM can typically be identified through various analytical techniques such as Fourier transform infrared (FTIR) spectroscopy, energy-dispersive X-ray spectroscopy (EDS), XPS, NMR and derivative thermal gravimetry (DTG)/thermal gravimetry (TG) [59-60,66-67]. **Fig. 4** presents some representative examples of ^{29}Si NMR and FTIR patterns of organic-grafted AAM, showing the detected organic structures. ^{29}Si NMR peaks at the chemical shift of −40 to −60 ppm are associated with Si atomic sites linked to a methyl, x tetrahedral units and $(3-x)$ hydroxyl groups from organosilicon SMS [59,126-127]. FTIR peaks denoting the vibration of Si-CH$_3$ and C-H bonds appear at wavelengths of around 775/1275cm^{-1} and 1440/2960 cm^{-1}, respectively [128-129]. These results indicate that the SMS molecules can be grafted on the gel structure of AAMK to form a modified gel system. Similar organic structures like alkyl-linked Si sites and chemical bonds can also be detected in AAS with PMS [67] and AAMK with MTMS [61].
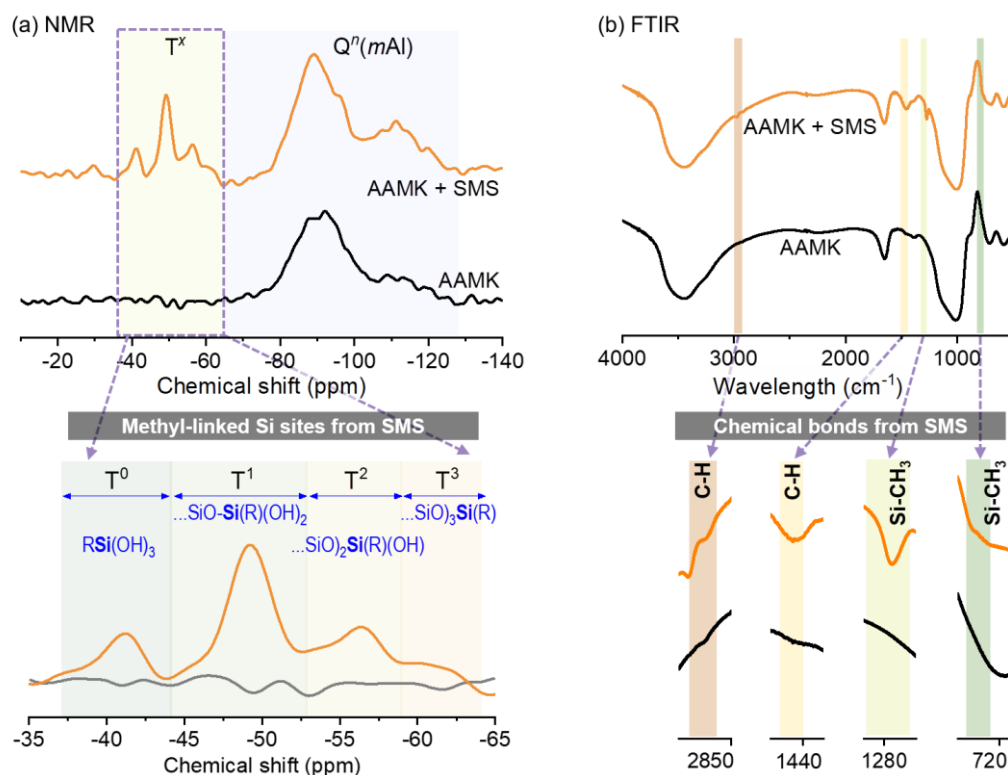
Fig. 4. (a) ^{29}Si NMR and (b) FTIR patterns of organic-grafted AAMK with SMS, indicating the detected methyl-linked Si sites and chemical bonds from SMS (adapted from [59,66]).

It is noteworthy that the thermal stability of these organic structures at elevated temperatures is significantly lower compared to that of aluminosilicate gels in AAM. When exposed to temperatures of approximately 350–550 °C, organosilicons undergo partial or complete decomposition, resulting in a loss of novel emerging properties [60,66,130-131]. Hence, it is imperative to account for the temperature and thermal radiation influences when implementing organosilicon-grafted AAM in practical engineering applications.

Owing to the low molecular weight of organosilicons, the morphology observed using scanning electron microscopy (SEM) or transmission electron microscopy (TEM) exhibit no notable distinctions or discernible novel products in organic-grafted AAM compared to plain AAM at micro-scale to nano-scale [66,68]. As seen in **Fig. 5**, the gel particles observed by TEM in AAMK with 6.6% SMS have smaller sizes than those in plain AAMK [66]. The result indicates that the chemical bonding of alkyl-organosilicons inhibits the reorganisation and growth of gel particles. As discussed in Section 3.1, SMS molecules are bound to the aluminosilicate oligomers or initial gels through physical adsorption and chemical bonding in the early-age reaction, reducing the bonding sites on the surface of the gel particles [59]. The alkyl groups on the organosilicons molecules also further hinder the initial gel binding and expansion due to steric hindrance, causing changes in the microstructure
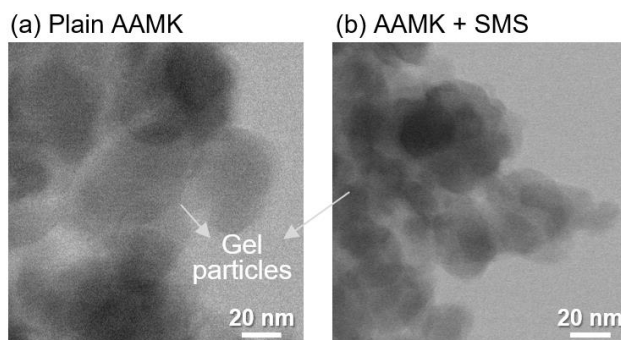
of gels in AAM.

Fig. 5 TEM images gel particles in (a) plain AAMK and (b) organic-grafted AAMK with 6.6% SMS (adapted from [66]).

Organosilicons with dosage of below 2% induces pore structure densification, whereas an excess of organosilicons fosters pore development [113-114]. The addition of 0.4–6.6% alkyl-organosilicons increases the porosity of gel pores with a diameter of <10 nm in AAMK containing SMS and AAFS containing S823 by 3–10% measured through the mercury intrusion porosimetry (MIP) test [60,66]. This consequently leads to a substantial augmentation in the surface area of AAM [114]. In contrast, organic-grafted AAM generally have lower capillary porosity (10–10,000 nm) compared to plain AAM [66,111,121]. Organosilicon exerts diverse regulatory influences on the pore structure of AAM. These effects can be categorised into both positive and negative impacts. On the positive side, organosilicons contribute to pore refinement by partially occupying pore space when bound to the pore wall. Additionally, different silane molecules form an inter-connected network through silicon-oxygen bonds, effectively filling the pores and stabilising the matrix. This also leads to a drop in volume fraction of micro-cracks and pores due to volume shrinkage. However, there are also negative effects to consider. Organosilicons adsorbed on precursors and initial gels may inhibit the gel polymerisation and promote pores in immature AAM. Furthermore, the self-condensation of organosilicons leads to the creation of numerous micropores, typically with the size of smaller than 10 nm [132].

3.3. Mechanical properties

As seen in **Fig. 6**a and b, the addition of 0–1.5% alkyl-organosilicons (S823, S1213, and SMS) generally weakens the compressive strength of organic-grafted AAM, mainly due to the reduced degree of polymerisation of the gel structure (see Section 3.2). When assessing the curing duration, 6.6% SMS accelerates the early-age reaction of AAMK so that its 1-d compressive strength

significantly increases by up to 195% [59]. However, organic-grafted AAM exhibit lower compressive strength (reduced by 90% with 0.75% S1213) compared to plain AAM after 3 d of curing, and the final strength (≥7 d) fluctuates between -48% and 97%. After 3 d, a substantial amount of loose initial gels, oligomers and unreacted raw materials exist in organic-grafted AAM, creating numerous sites for the adsorption and bonding of organosilicons [133-135]. This early-stage adsorption significantly inhibits the strength development of organic-grafted AAM. Upon the completion of the polymerisation and reorganisation reactions in all specimens, the reaction time of organic-grafted AAM is longer than plain AAM when the curing time extends to 7 or 28 d. Hence, the strength difference between organic-grafted and plain AAM becomes smaller after 3 d of curing [60]. The influence of alkyl-organosilicons on the final compressive strength of organic-grafted AAM is typically minor compared to that on initial strength (≤3 d), resulting in a strength variation within ±50%. Additionally, the compressive strength of organic-grafted AAM can be negatively affected by the grafted organosilicons, due to their lower elastic modulus compared to the inorganic gel matrix [122].

In contrast, the addition of 1–7% functional-organosilicons (KH550, KH560, KH570 and N-[3-(trimethoxysilyl)propyl]ethylenediamine, i.e., KH792) leads to a rise in compressive and flexural strengths of final AAM by up to 102%, indicating that these organosilicons can bond firmly with the matrix of AAM (**Fig. 6**c and d). Functional groups are the key components that can enhance the polarity, dissolution and dispersion of organosilicons, further facilitating the probability of organosilicons binding to aluminosilicate oligomers or gels [121,136-137]. Consequently, AAM containing functional-organosilicons can experience higher polymerisation with denser matrix. Different types of functional groups have varying impacts on the strength of AAM (**Fig. 6**c and d). KH570, featuring a methacrylate structure, exhibits the most substantial enhancement effect due to its carbon-carbon double bonds which can undergo cleavage, leading to the organosilicon self-condensation and the formation of a denser and stronger organic network [138]. Due to the weak physical and chemical interaction between epoxy groups and gels, the compressive strength of AAM can be barely affected by KH560 with epoxy groups (varying within ±20%) [121]. The addition of 4–6% KH560 rises the flexural strength by 10–47%. KH550 with amino groups can significantly enhance the strength of AAS by up to 93%, whereas its effect on the strength of AAMK can be negligible (varying within ±15%) [113,120-121]. The main reaction products of calcium-based AAM

include C-A-S-H gels which exhibit a disorder tobermorite-like structure, consisting of silicate chains held together by calcium oxide layers [1,139-140]. Compared with N-A-S-H gels with highly crosslinked disordered structure, C-A-S-H layered structure seems to be better coupled by silicone and thus its mechanical strength is improved.
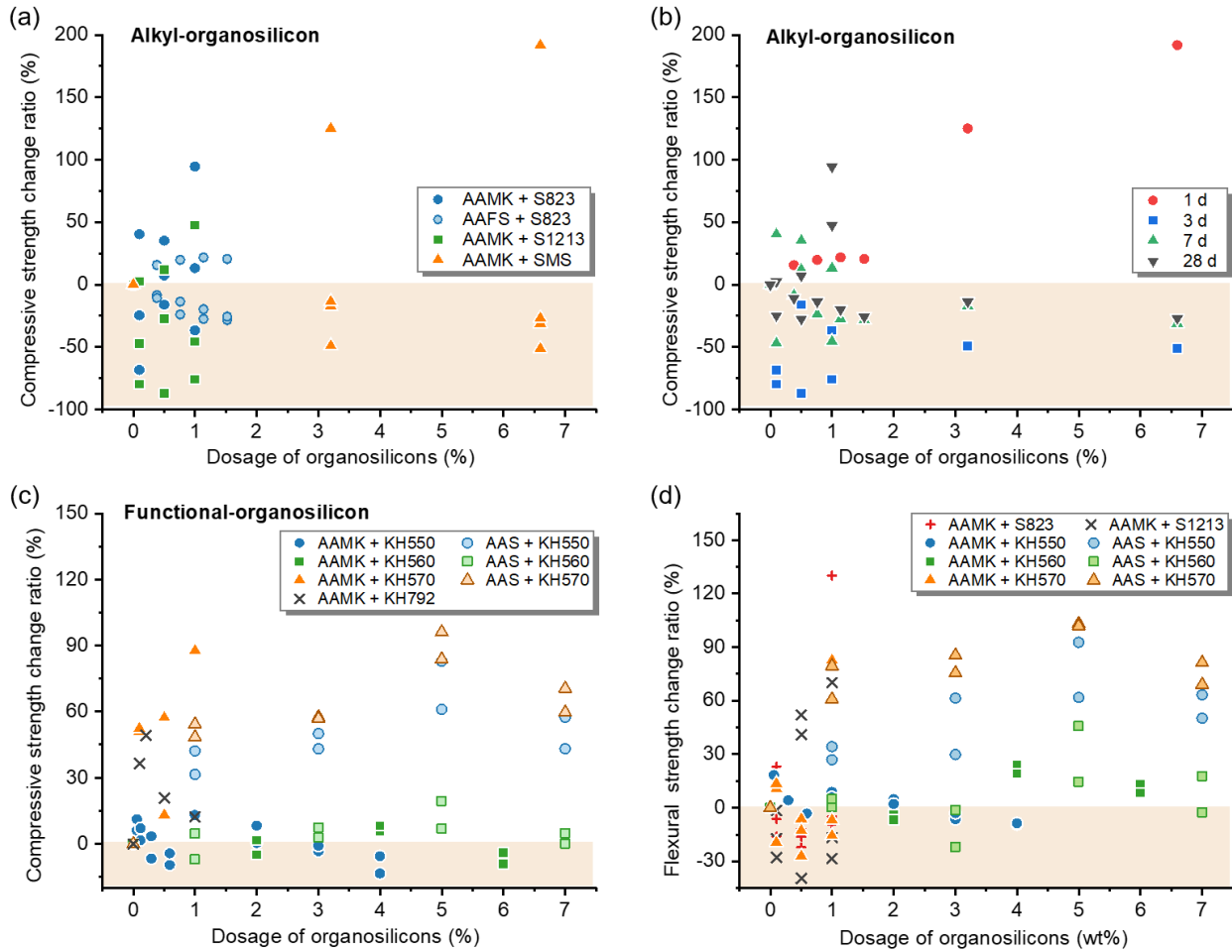

Fig. 6. Relative change in compressive strength of organic-grafted AAM incorporating alkyl-organosilicons with different (a) organosilicon type and (b) curing time, as well as (c) organic-grafted AAM with different functional-organosilicons. (d) Relative change in flexural strength of organic-grafted AAM incorporating different organosilicons [41,59,112-113,120-122,141].

3.4. Durability-related properties

3.4.1. Wettability

Hydrophobic and waterproof modification of organic-grafted AAM can be achieved by incorporating alkyl-organosilicons, including S823, S1213, MTMS, SMS and PMS. Water contact angle on a solid relies on the free energy and microstructure of the contact surface, indicating the equilibrium of surface tensions at the interface of solid-liquid-gas phases [142-143]. Plain AAM is highly hydrophilic with a water contact angle of below 40° (**Fig. 7**). The gel surface resulting from

the chemical condensation reaction contains numerous free hydrophilic hydroxyl groups, making AAM rapidly wetted by water [35]. As seen in **Fig. 7**, the addition of alkyl-organosilicons can hydrophobically modify AAM in an effective way [66-67]. When the organosilicon dosage exceeds 1%, the hydrophobic performance of organic-grafted AAM becomes more obvious with a water contact angel over 90° (grey points and shading in **Fig. 7**). The contact angle of organic-grafted AAM can reach a maximum value of approximately 140°, surpassing hydrophobic organic materials like epoxy, rubber and biofilm [144-145]. The alkyl-organosilicons are chemically bonded into the AAM through the reaction of the silanol structure with the hydroxyl groups on the gel surface. The alkyl groups and/or hydrocarbon chains from organosilicons can evenly attach to the AAM matrix, forming a continuous but not necessarily dense hydrophobic film [60]. The hydrophobicity of AAM is significantly enhanced when partially or fully covered with low-surface-energy organosilicons. However, due to the limited bonding sites on gels, there is a restricted capacity for bonding organosilicon molecules. The excessive organosilicon dosage (>1%) leads to the formation of a thicker hydrophobic film through organosilicon adsorption instead of increasing the proportion of hydrophobic areas, thus causing a retarded growth in hydrophobicity of organic-grafted AAM [146].
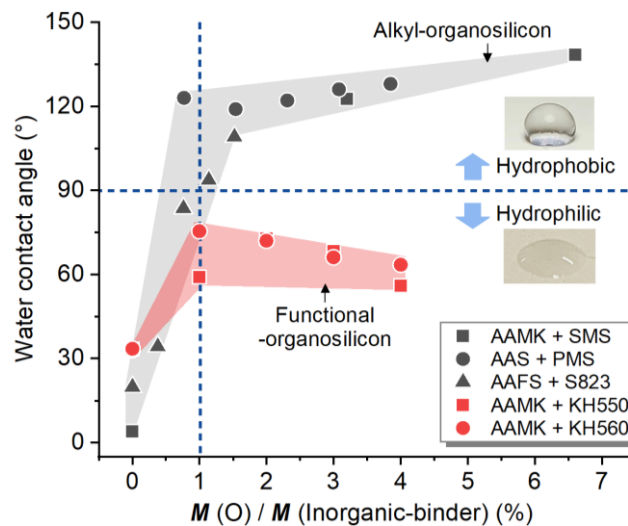

Fig. 7. Water contact angle of organic-grafted AAM containing organosilicons (grey dots and shading denote alkyl-organosilicon-grafted AAM; red dots and shading represent functional-organosilicon-grafted AAM) [60,66-67,114].

Functional-organosilicons can moderately deduct the hydrophilicity of AAM but cannot impart hydrophobic modification (red dots and shading in **Fig. 7**). The addition of KH550 or HK560 in AAMK increases the water contact angle, reaching a maximum point of approximately 75° with 1% dosage [114]. The typical organic structure of functional-organosilicons consists of

hydrocarbon/carbon-oxygen chains along with organic groups. Although the hydrocarbon chain and alkyl groups (e.g., -CH$_3$, -CH$_2$- and -CH=) are hydrophobic, organic functional groups (e.g., amino and ester groups) show strong hydrophilicity [147]. Therefore, the capability of functional-organosilicons to regulate the wettability of AAM is potentially related to the composition and polarity of their organic structures [148]. More than 1% functional-organosilicons can reduce the water contact angle of organic-grafted AAM, different from alkyl-organosilicon which can slightly increase it. When excessive functional-organosilicons are grafted on AAM matrix, the hydrophilic functional groups, typically endpoint groups, are more likely to exist on the surface of the organic membrane compared to hydrocarbon chains, thereby reducing the hydrophobicity of organic-grafted AAM [149-150].

3.4.2. *Water absorption and permeability resistance*

It was reported that the incorporation of 1.0–6.6% alkyl-organosilicons (S823, SMS and PMS) can substantially reduce the water absorption of AAM by up to 90% [60,66-67]. A schematic illustration of waterproofing mechanisms of organic-grafted AAM is given in **Fig. 8**. The driving force for water absorption is the tendency of liquids to spontaneously diffuse across solid surfaces, which is determined by the surface energy relationship at the solid-liquid-gas interface [151]. Alkyl-organosilicons effectively substitute hydrophilic hydroxyl groups, resulting in the creation of a hydrophobic film on the capillary wall characterised by low surface energy and a high water contact angle [152]. Consequently, the matrix fails to generate adequate upward suction for water, leading to a significant drop in the capillary absorption rate of organic-grafted AAM, thereby enhancing their waterproofing properties [60]. Furthermore, the reduction and optimisation of capillary structures is another significant reason contributing to decreased water absorption. The infiltration effect of organosilicon SMS can fill capillary pores with a size of 10–1000 nm, while blocking small mesopores and transition throats, effectively hindering the water diffusion and transport in organic-grafted AAM [66]. It is noteworthy that organic-grafted AAM still exhibits capillary adsorption capacity as the organosilicon hydrophobic film cannot inhibit the process of water vapor free diffusion [153]. Water vapour can enter the capillary pores under the action of moisture gradient, condense and adsorb on the inner pore wall or hydrophobic film layer [88,154]. Overall, the outstanding waterproof properties of organic-grafted AAM make it a compelling choice for further research and engineering applications.

Thanks to the outstanding capability on waterproof modification, the addition of alkyl-organosilicons has been employed to enhance the corrosion permeability resistance of AAM, particularly when mitigating chloride ingress into concrete structures exposed to marine environments [155-156]. The flexural strength loss of AAMK containing 1% organosilicons (S823, S1213 and KH570) after immersion in seawater is significantly slowed down compared to plain AAM [111]. The organic-grafted AAM have a dense microstructure and are resistant to microcrack formation during seawater corrosion due to the formation of an organic-inorganic 3D network, resulting in higher strength stability. Their flexural toughness is even improved with additional organosilicons. The bonding of organosilicons not only impedes the seawater penetration of but also enhances gel network density, thereby mitigating alkali ion leaching and material degradation [157]. PMS-grafted AAS can also serve as protective coating on concrete structures in aggressive chloride environments which can provide excellent and long-term corrosion protection for rebar [67]. Alkyl groups from PMS served as gel terminals, covering the transport pathways of the corrosive fluid and making it difficult for chloride to be adsorbed and chemically bound onto the gel structure in organic-grafted AAS. In addition, AAM containing KH550 of less than 0.2% dosage exhibit an enhanced resistance to sulphate corrosion and freeze-thaw damage, due to a more stable and denser matrix structure [113,120].
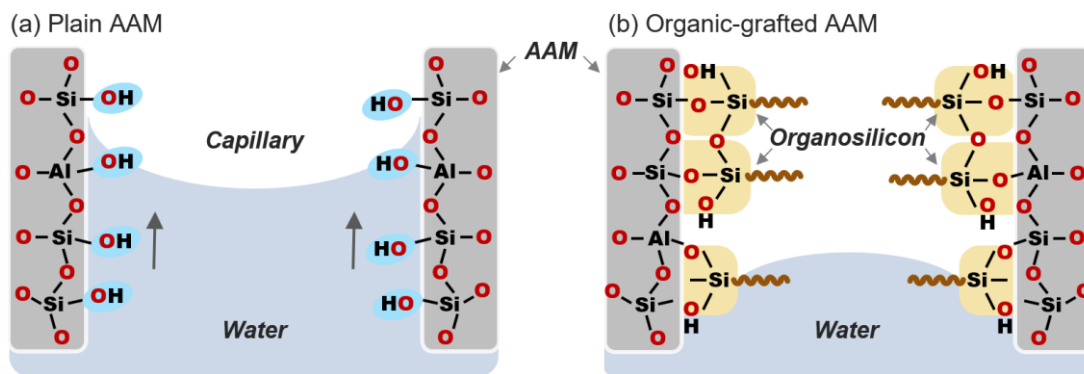

Fig. 8. Schematic illustration of transport channels and capillary water absorption behaviour in (a) plain AAM and (b) waterproof organic-grafted AAM.

3.4.3. Volume deformation

Compared to plain AAMK, the chemical and autogenous deformations of AAMK with alkyl-organosilicon SMS at 7d were found to drop by 27.0% and 91.1%, respectively [90]. The early-age volume deformation of AAM arises from the combined effect of mechanical properties of the gel matrix, pore structure, capillary stress and separation pressure [158-160]. During matrix hardening,

internal liquid depletion and redistribution result in the emergence of many liquid columns and menisci, inducing capillary stress that is recognised as the primary driver of autogenous shrinkage [161]. The results of internal water distribution obtained by low field ^{1}H NMR reveal that the proportions of free and capillary water in the final AAM containing 6.6% SMS go up by 2.0% and 1.6%, respectively, while the inter-gel water content drops due to the water redistribution caused by self-desiccation [90]. As shown in **Fig. 9**, in hydrophobic organic-grafted AAM, water tends to diffuse in the unsaturated pore network and be stored in large capillary pores rather than accumulating in narrow gel pores owing to the effect of meniscus surface tension [162]. The water in large pores causes much less stress on the AAM matrix than in small pores, which is the key reason for the sharp reduction in early-age autogenous shrinkage of hydrophobic organic-grafted AAM [90,163]. Furthermore, the meniscus curvature of the water column decreases with increasing hydrophobicity of the pore wall. In pores of the same size, the stress exerted by water on hydrophobic pore walls is much smaller than that on hydrophilic pore walls [27,164]. Moisture transport tendency of agglomeration mitigates dispersion of water column and liquid-vapor meniscus in organic-grafted AAM. Thus, hydrophobic organic-grafted AAM exhibit reduced susceptibility to volume deformation, in comparison with hydrophilic plain AAM.
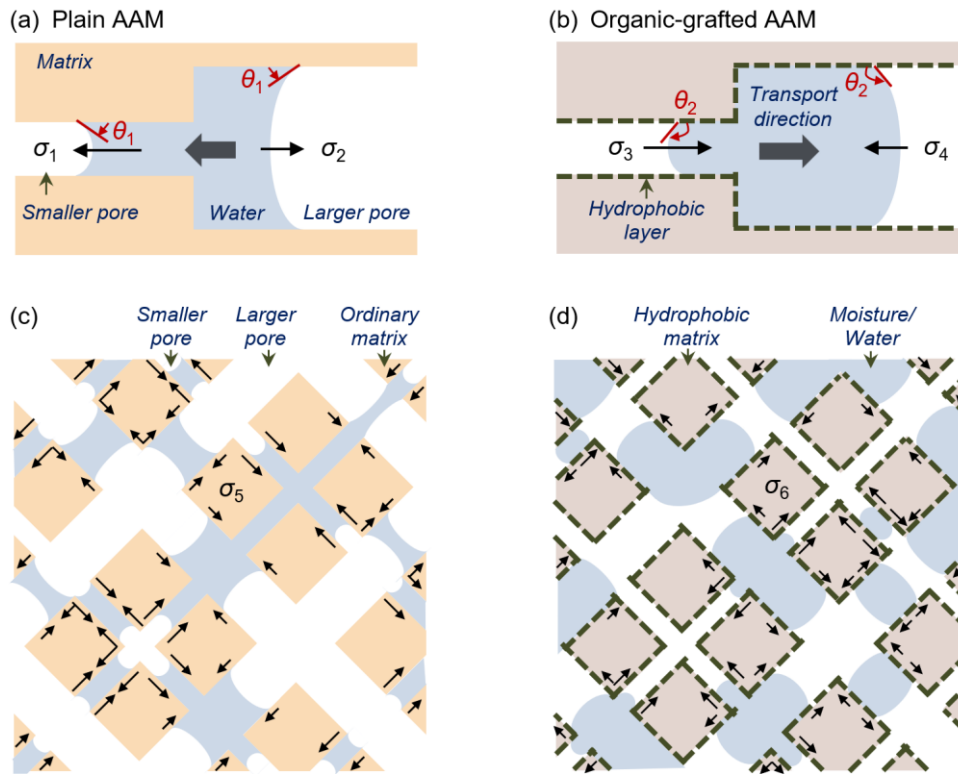

Fig. 9. Schematic illustration of water/moisture transport trend and possible distribution in pores of (a, c) hydrophilic plain AAM and (b, d) hydrophobic organic-grafted AAM (adapted from [90]).

The drying shrinkage of AAMK containing 0.1–1.0% alkyl-organosilicons S823 and S1213 also shows an obvious drop by approximately 25% [111]. Organosilicons can form covalent bonds with gels in AAM through condensation reaction, leading to an optimised gel structure which effectively mitigates the rapid water evaporation and drying shrinkage [68,165]. The rapid hardening can also decrease the plastic shrinkage rate of fresh organic-grafted AAM, while the inclusion of functional-organosilicon weakens the drying shrinkage of AAM with a minor impact [111-112].

4. Reaction, microstructure and properties of organic-adsorbed AAM

4.1. Reaction mechanisms

Surfactants regulate the synthesis reaction process and affect the degree of polymerisation by adsorbing on precursors and initial gels. They are partially adsorbed on gels in final AAM, while the remainder resides within the pore solution (**Fig. 2**) [166]. The effect of superplasticisers on the reaction heat evolution of AAM is relatively modest. The addition of 4% naphthalene superplasticisers (NS) or polycarboxylate superplasticisers (PS) can result in a slight reduction in both the synthesis reaction rate and intensity of AAFS, and the 72-h cumulative heat is reduced by 9.8–12.2% compared to plain AAFS [167]. In contrast, the incorporation of 0.8% NS, PS or aliphatic superplasticisers (AS) increases the formation rate of hydration products including N-A-S-H and C-A-S-H, as the occurrence of corresponding exothermic peak of organic-adsorbed AAM can be observed 1.5–3 h earlier than plain AAM [168]. Superplasticisers adsorbed on the precursor surface promotes the particle dispersion through steric hindrance and electrostatic repulsion, thereby raising the contact area between the precursor and the alkaline solution [44,169]. Moreover, superplasticisers can alter the charge distribution on the precursor surface, thus elevating the leaching of silicon and aluminium oligomers and promoting the reaction process [168].

The addition of alcohols can significantly prolong the synthesis reaction of AAM by up to 17 d, and the reaction intensity is weakened [21,145,170-173]. Alcohols with lower molecular weights exhibit a more pronounced effect [170,172,174]. **Fig. 10** illustrates the change of calorimetric response of AAS containing alcohols with dosages and molecular structures within 20 d of curing. The exothermic peak corresponding to the rapid polymerisation of gels in AAS with PEG200 (i.e., propylene glycol polymer with average molecular weight of 200) is postponed to about 10 d of curing, while the synthesis reaction of plain and other organic-adsorbed AAS containing EG monomers, PEG400, PEG1000 or PEG10000 is almost completed in the first 3 d. PG monomer also retards gel

polymerisation by about 6 d. EG/PG monomers and polymers with low molecular weight tend to quickly dissolve in alkaline solutions and interact with AAM in the initial reaction stage, e.g., adsorption on precursors. By contrast, high-molecular-weight polymers can exert a more extensive influence on the overall polymerisation process [170,173]. The addition of alcohols results in a lower surface tension of the pore solution and a slight hydrophobic modification of gels in AAM, thereby inhibiting the reaction between the precursor and the alkaline activator [21,171]. Thus, alcohols can lead to a diminished precursor reaction, ultimately yielding a reduced degree of polymerisation [174].
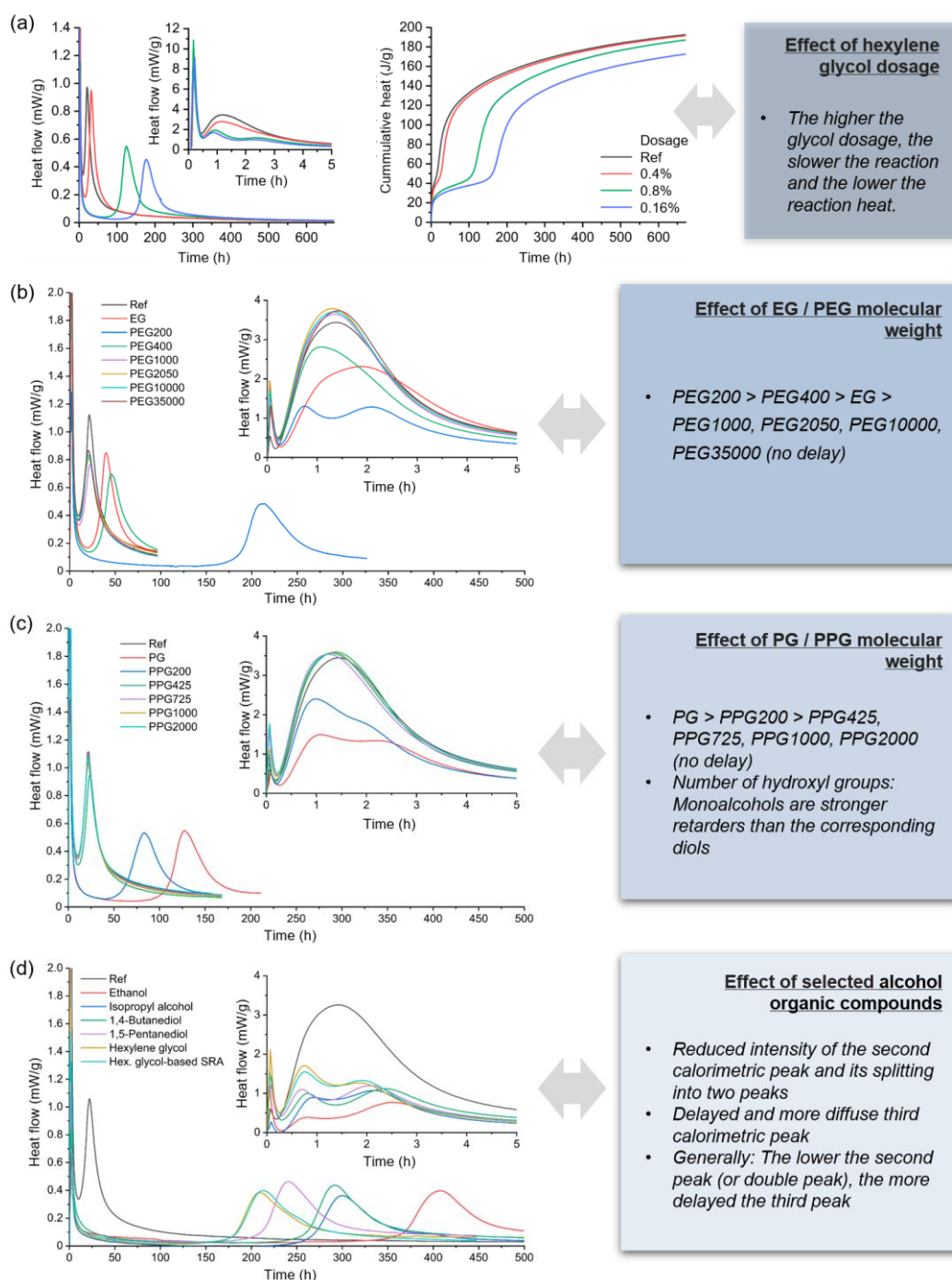

Fig. 10. Effects of (a) hexylene glycol dosage, molecular weight of (b) EG/PEG and (c) PG/PEG,

22

and (d) selected alcohols on the calorimetric response of AAS (adapted from [172]).

PDMS, as a representative of silicone oil, has little effect on reaction mechanisms. In the synthesis reaction of AAM, PDMS can be uniformly dispersed in fresh slurry through high stirring, and effectively adsorbed onto the aluminosilicate gel matrix [18,175]. The early adsorption behaviour of organic components blocks the further reaction of solid and liquid raw materials to a certain extent, which is a main reason for the decreased degree of polymerisation of PDMS-adsorbed AAM. The molar fraction of silicate structural units Q^3 and Q^4 slightly drops by about 10% in the final PDMS-adsorbed AAM, compared to plain AAM [18].

4.2. Phase assemblage and microstructure

The chemical composition and gel structure of organic-adsorbed AAM, prepared by incorporating surfactants, remain unchanged in comparison with plain AAM. These organics are primarily physical adsorbed onto the matrix rather than directly engaging gel formation [21,168,176]. As for morphology, similar to organosilicons, micromolecular surfactants and superplasticisers may not be directly distinguished from AAM by SEM and TEM. In contrast, alcohol monomers can further condense, resulting in the formation of distinguishable fibrous or flaky phases that are closely integrated with gels (**Fig. 11**a) [171,177]. Different morphologies appear in AAS with 0.16% hexylene glycol (**Fig. 11**b) [172]. The matrix and unreacted precursors are covered with a conspicuous organic film, which binds the inorganic phases together through adjacent surfaces. PDMS can not only be adsorbed on gels in AAM at nano-scale but also hybridise with the matrix to form micro-scale organic-inorganic hybrid particles with certain shapes (**Fig. 11**c) [18]. PDMS-AAMK hybrids mainly involved shapes of irregular blocks and long chains have a 13–26% higher carbon content, i.e., a higher proportion of organic PDMS, compared to the gels in PDMS-adsorbed AAM (approximately 5%). The hybridisation reaction is more pronounced at the end of PDMS molecules, with the main chain generally preserving their original structure [178-179]. Although the incorporation of PDMS enhances the formation of the hybrid particles, its effect on the aluminosilicate gel structure can be negligible [18,175].
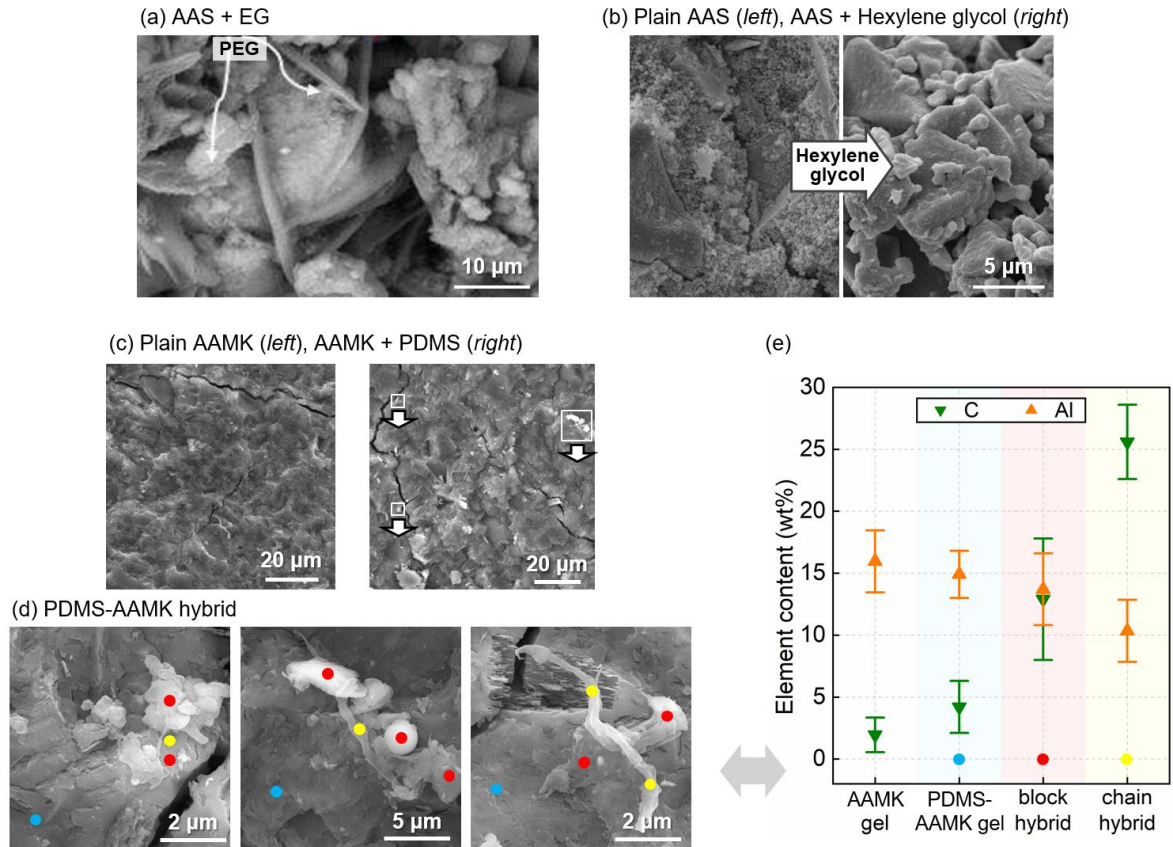
Fig. 11. Microstructure of (a) organic-adsorbed AAS with 5% EG and (b) 0.16% hexylene glycol, as well as that of (c) plain AAMK, AAMK with 5.4% PDMS and (d) PDMS-AAMK hybrids. (e) Chemical composition of gels in plain AAMK, gels in organic-adsorbed AAMK with 5.4% PDMS, and corresponding block/chain hybrids (adapted from [18,172,177]).

Regarding pore structure, as foam stabilisers in foamed AAM, micromolecular surfactants can adsorb onto air bubbles in fresh slurry to avoid bubbles merging through electrostatic repulsion and steric hindrance [79,81-82,180-182]. In non-foamed AAM, most micromolecular surfactants can also promote the development of pore structure. In particular, adding 1% sodium lauryl ether sulphate (SLES) enhances the total porosity of AAMK by 16.2%, while alkyl polyglycoside (APG), benzalkonium chloride (BAC) and sucrose fatty acid esters (SE) have a modest effect on the change of nano-pores [183]. The influence of micromolecular surfactants on nano-scale gel pores is primarily linked to the degree of polymerisation for gels, and there remains a research gap in this area. Organic-adsorbed AAM with superplasticisers generally have a refined pore structure. The addition of 0.44% PS, AS and NS reduces the porosity of alkali-activated red mud-slag by below 10%, and its micro-scale pores are refined [168]. The dispersion effect of superplasticisers weakens the bubble stability in fresh AAM, and a controlled superplasticiser dosage of no more than 1% can mitigate the formation

of large bubble pores [184]. However, superplasticisers with a dosage of more than 3% foster the formation of large pores (>100 μm) due to the agglomeration of numerous organic molecules into micelle structures and flocculates [69,168,185]. Although there exist inconsistent findings on the pore structure of alcohol-adsorbed AAM, most studies suggest that alcohols (0.72% PPG or 2% hexylene glycol) notably enhance porosity and pore size of AAS and AAF [22,174]. The impact is more pronounced with polymer alcohols of lower molecular weight [174]. Nevertheless, adding PPG with a dosage of less than 1.5% optimises the pore structure of AAS at various curing ages [21]. The effect of silicone oil, represented by PDMS, on the pore structure of AAM is modest [18,88,94]. PDMS with a low dosage of 0.5–4% reduces the total porosity of AAMK by 5.8–12.2% measured by MIP, while PDMS with a high dosage of above 4% notably promotes the transformation of small gel pores (<10 nm) into large capillary pores (>10 nm) [18]. PDMS also makes it easier to introduce air bubbles into fresh AAM, possibly due to increased slurry viscosity [94].

4.3. Mechanical properties

It was found that the incorporation of 1% micromolecular surfactants including SLES, APG, BAC and SE can reduce the final compressive strength of AAMK by 9–30%, due to the role of surfactants in introducing bubbles [183]. Current research on superplasticiser-adsorbed AAM predominantly is mainly focused on the compressive strength of AAS or AAFS, while the flexural strength and toughness of low-calcium AAM have been rarely explored. As illustrated in **Fig. 12**a, adding 1.5% lignosulfonate superplasticisers (LS) substantially reduces the compressive strength of AAM by around 75%, while the impact of incorporating 0.5–3% melamine superplasticisers (MS) is relatively less noticeable (with less than 20% change). Conversely, the inclusion of NS or AS by less than 1% into AAM can enhance the compressive strength by up to 60%, whereas higher dosages over 1% have negligible effects [186]. The incorporation of 0–4% PS can generally trigger the strength development of AAM (**Fig. 12**b). The compressive strength of AAM containing 2% PS goes up by 54%. Adsorbed superplasticisers improve the dispersion and dissolution of precursors through the electrostatic repulsion and steric hindrance, thereby promoting the development of gel structure in AAM [187]. Nonetheless, the decreased stability of certain SP in alkaline solution or the propensity to agglomerate into clusters can lead to increased defects in AAM matrix [167,188-189].
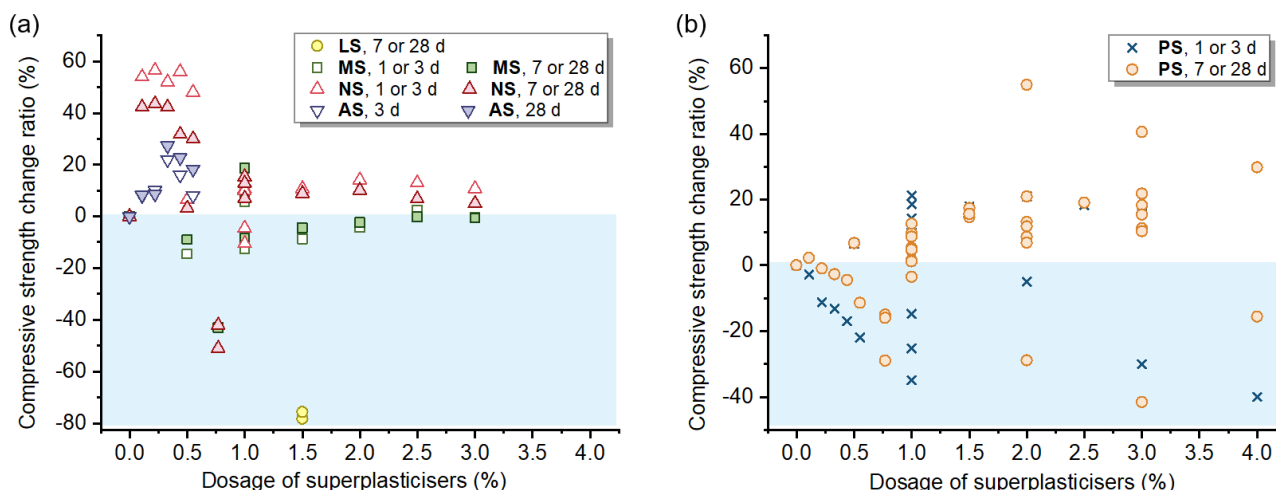
Fig. 12. Relative change in compressive strength of superplasticiser-adsorbed AAM with different superplasticiser types and curing time: (a) LS, MS, NS and AS and (b) PS [167-168,176,187-191].

As seen in **Fig. 13**, the addition of 0–9% alcohol on the strength and toughness (flexural/compressive strength ratio) of AAM is prone to exhibit more negative impacts. In early stage of curing (<3 d), the compressive strength of AAM is reduced by 95% with the addition of 10% EG alcohols, due to the delaying effect of alcohols on the synthesis reaction [177]. Besides, the incorporation of alcohols reduces the compressive and flexural strengths of AAS throughout its development, and a low dosage of no more than 2% shows an obvious effect (**Fig. 13**b and e). Alcohols, as shrinkage reducing agents, inhibit the drying shrinkage and crack propagation of AAM, thereby benefiting the strength growth [87,170]. On the other hand, the addition of alcohols may slow down the gel polymerisation and formation of large pores in AAM [174]. Furthermore, alcohols impact the gel strength development by altering the gel structure through the formation of weak hydrogen bonds, affecting both chemical reaction and microstructure [192]. As displayed in **Fig. 13**c and d, the molecular weight of alcohol polymers is an important factor that affects the strength levels [174,193]. AAM containing alcohol monomers or polymers with low molecular weights of below 1000 exhibit enhanced strengths over plain AAM [170,174]. The addition of alcohols with low molecular weights significantly inhibits the early-age reaction, indicating the superior solubility and activity in AAM, which can be ascribed to the improved hydrophilicity and hydroxyl value (i.e., hydroxyl concentration in a molecule, mgKOH/g) [194-195]. Moreover, the incorporation of alcohols enhances the water retention of AAM, potentially leading to remained high strength during the drying process [177]. Followed by heat treatment and drying, aluminosilicate gels in alcohol-adsorbed AAM exhibit a substantial rise in degree of polymerisation. The drying shrinkage, cracks and microdefects

caused by water loss in alcohol-adsorbed AAM are slight against plain AAM. The suppression of gel crystallinity due to the thickening effect of alcohols is also a main reason for maintaining the strength development of AAM [177].
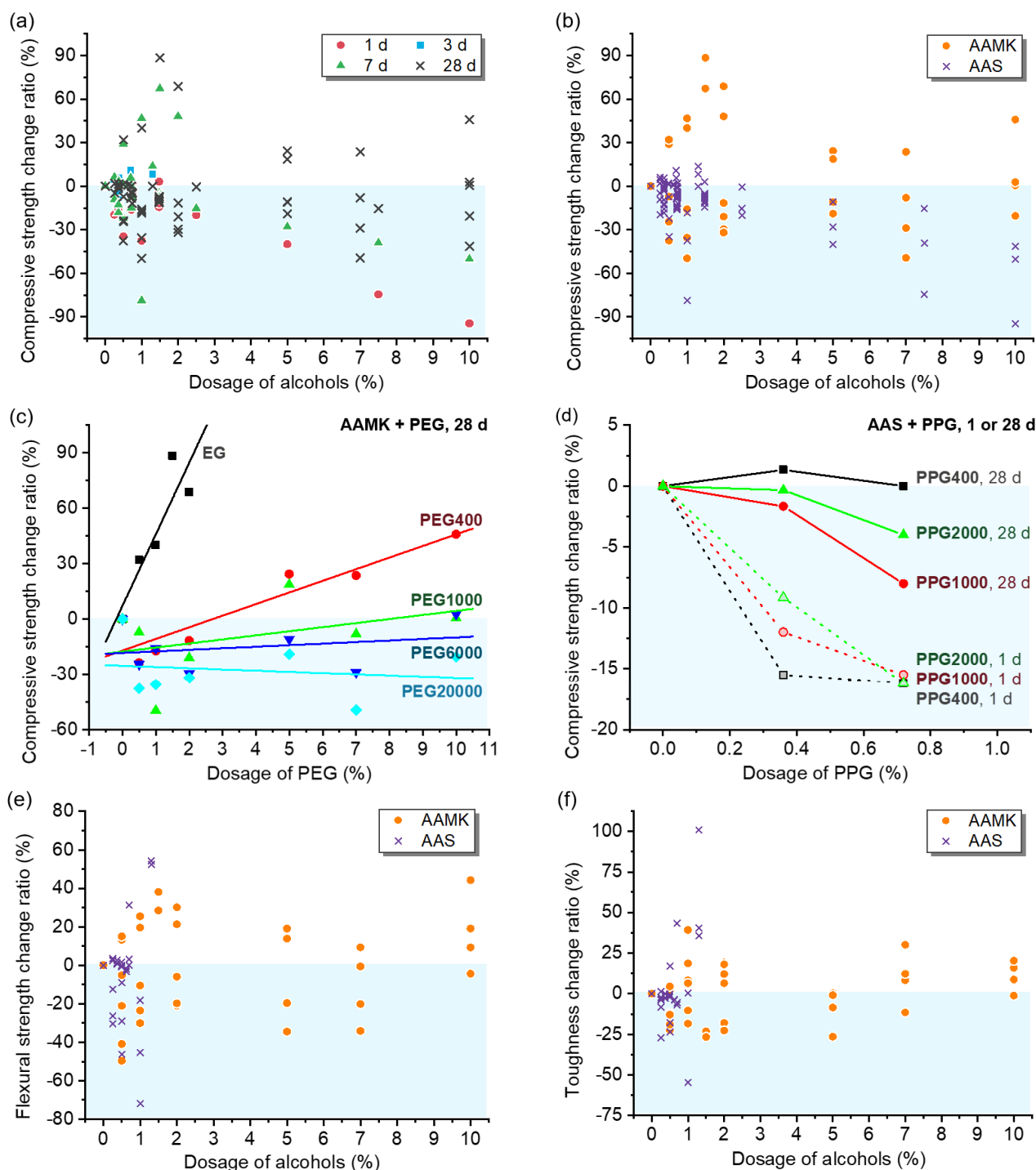

Fig. 13. Relative change in compressive strength of alcohol-adsorbed AAM with different (a) curing time and (b) AAM systems, as well as that of AAM incorporating (c) EG/PEG [193] and (d) PPG [174] with different molecular weight. Relative changes in (e) flexural strength and (f) toughness of alcohol-adsorbed AAMK and AAS [21,96,170,173,177,192,196].

In contrast, the strength of PDMS-adsorbed AAM goes up with rising dosage (<3%) of PDMS by

up to 25% but drops by 11–28% with an over-dosage (>3%) [18,94]. PDMS molecules can be dispersed, adsorbed and crosslinked in and with the AAM matrix, playing a similar role to nanometre fibres in reinforcing the gel matrix, and thus enhance the compressive strength. However, excessive PDMS leads to molecule agglomeration and cluster formation, inducing matrix defects and strength reduction [18].

4.4. Durability-related properties

4.4.1. Wettability and water absorption

Similar to alkyl-organosilicon-grafted AAM, AAM containing PDMS also exhibit excellent hydrophobicity with a water contact angle of around 130° [18,88]. The hydrophobic alkyl layer covering the matrix reduces the surface energy, and the micro-scale PDMS-AAM hybrid particles increase the surface roughness by 1.9 μm [18]. According to the Cassie-Baxter model, these changes in chemical composition and microstructure contribute to the formation of a solid-liquid-gas hydrophobic interface between PDMS-adsorbed AAM and water [197-198].

The capillary water absorption process in PDMS-adsorbed AAM exhibits a prolonged transition stage with an exceptionally slow water absorption rate lasting for up to 60 h [89,91]. The sorptivity for low-adsorption stage in AAM containing 1.6% PDMS goes down by 98% compared to that of plain AAM, which can be mainly ascribed to the effective and durable hydrophobic modification of AAM by sufficient PDMS [88]. The hydrophobic PDMS layer greatly reduces the capillary-induced upward force on water, preventing immediate wetting of AAM upon contact [199]. However, hydrophobic PDMS-adsorbed AAM still possess capillary adsorption capability as the PDMS layer cannot prevent the moisture diffusion. The low-adsorption stage ends when the PDMS layer is completely covered by condensed water. The water vapor adsorption test also proves that vapor absorption is the main physical process in the low-adsorption stage of PDMS-adsorbed AAM [88].

4.4.2. Volume deformation

Alcohols have a good mitigation effect on the autogenous shrinkage of AAM. The incorporation of 1.9% polyether drops the autogenous shrinkage of AAS by over 60% [145]. Alcohols can reduce the surface tension of pore solution and help AAM retaining a high internal humidity, thus leading to a reduction in capillary stress [145,166]. This is different from the shrinkage reducing mechanism of hydrophobic modification for alkyl-organosilicons. The addition of alcohols including EG, PEG, PPG, hexylene glycol, alkyl polyether, aminoethanol and propionamide with a dosage of over 3% can

reduce the drying shrinkage of AAM by 20–80%, while the addition of 2% alcohols can decrease the polarity and surface tension of distilled water by approximately 50% [22,145,166,170,174,177,200]. The improved hydroxyl ion concentration in pore solution accelerates such reduction in surface tension [201-202]. As per the Laplace-Kelvin law, the reduced surface tension of pore solution significantly weakens the shrinkage stress induced by capillary water. The separation pressure theory suggests that alcohols also weaken the attraction within the inorganic matrix and hinder shrinkage in space [170]. The extension of the reaction induction period caused by the addition of alcohols also contributes to reducing the collapse and reorganisation and maintaining the stability of gel phases, thereby reducing the internal micro-cracks [21]. In addition, the incorporation of alcohols enhances water evaporation in AAM, implying that drying shrinkage may not be solely dependent on water loss [145,166,200].

The influence of alcohols on drying shrinkage of AAM is affected by molecular weight and curing environment. As seen in **Fig. 14**a, PPG with low molecular weight (e.g., PPG400) of dosage 0.72% exhibits more superior shrinkage resistance than PPG with higher molecular weight (e.g., PPG1000 and PPG2000) in AAS [174]. However, another study reported that macro-molecular alcohols of PEG2000 and PEG10000 are slightly more effective in reducing shrinkage of AAS compared to EG monomers, PEG400 and PEG35000 (dosage: 0.74%, **Fig. 14**b) [170]. Alcohols with higher molecular weights can accelerate separation pressure reduction and increase resistance to leaching, while their limited solubility in alkaline solution declines the concentration of active ingredients, thereby weakening the shrinkage resistance. Hence, it is vital to select alcohols with a suitable molecular weight for reducing shrinkage of AAM. As for curing conditions, the incorporation of 0.72% PPG reduces the shrinkage of AAS by 50% when drying at a relative humanity (RH) of 43%, while its impact is negligible at 75% RH [174]. In AAM, the majority of alcohols are adsorbed onto pore surfaces of the matrix to decrease the surface tension, leaving only a limited proportion of alcohols in pore solution [203]. Higher RH levels (e.g., 75% RH) may reduce the presence of organic molecules at the liquid-air interface, potentially hinder their effectiveness in reducing shrinkage [166]. Rising alcohol dosages beyond their critical micelle concentration can partially mitigate this effect. Although this approach does not further reduce the surface tension of pore solution, it effectively expands the interfacial area through the use of micelles as buffers [204]. PDMS (1.6%) can also reduce the autogenous shrinkage of AAMK by approximately 40% [90]. Its shrinkage mitigation

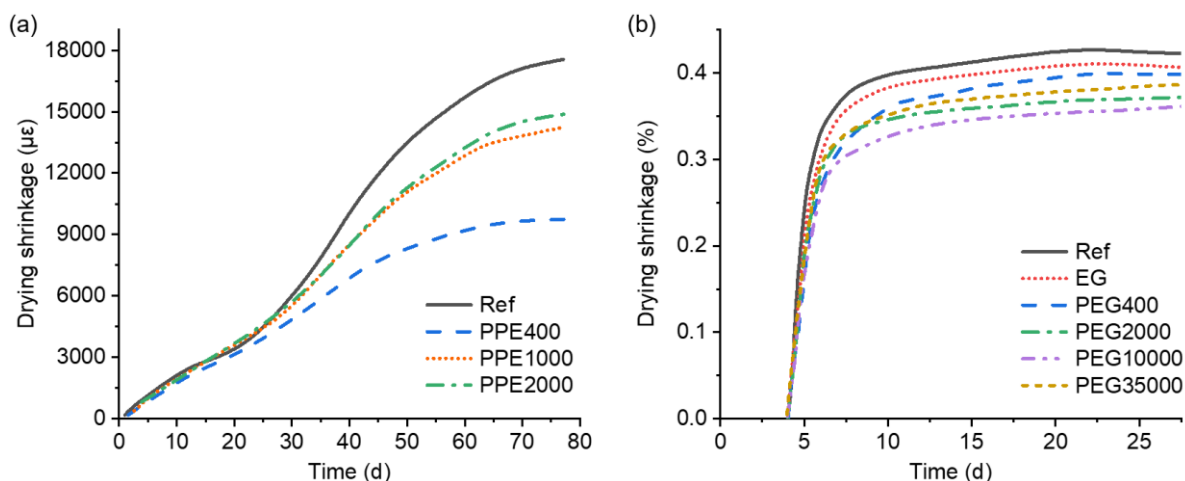mechanism is similar to that of alkyl-organosilicon (see Section 3.4.4).

Fig. 14. Drying shrinkage of alcohol-adsorbed AAS incorporating (a) 0.72% PPE or (b) 0.74% EG/PEG with different molecular weight (adapted from [170,174]).

5. Reaction, microstructure and properties of phase-crosslinked AAM

5.1. Reaction mechanisms

Organic polymers (or their constituent monomers, emulsions or latexes) typically engage in reactions to synthesise phase-crosslinked AAM at various stages (**Fig. 2**). Initially, organic polymer particles dispersed in the aqueous phase exhibit a preference for adsorption onto precursors and/or the initial gels of AAM [205]. As the exothermic reaction and internal water loss proceed, organic polymers further condense into an organic film that encapsulates the gels, resulting in the establishment of a crosslinked network with the gel skeleton in AAM as a whole [206-207]. The molecular structures such as ester and ether in organic polymers can effectively enhance their affinity with the inorganic matrix via hydrogen bonds [97,208]. Polymers with reactive functional groups like carboxyl can potentially undergo chemical condensation reactions when interacting with gels in AAM [208-209].

Organic polymers can hinder the workability of fresh AAM and delay their polymerisation and hardening process [121,208,210]. The presence of organic polymers adsorbed onto or enveloping the precursors tend to form clusters which may inhibit the reaction of solid-liquid raw materials, and thereby impeding the formation of gel products [121,211]. The addition of polymer emulsion also reduces the alkalinity of fresh AAM slurry, and thus slows down the synthesis reaction rate [208,210]. The addition of 3–12% styrene-acrylic (SA) emulsion declines the content and degree of polymerisation of aluminosilicate gel in final AAS by up to 31% [208]. The poly(acrylic acid) (PAA)

emulsion promotes the transformation of silicon tetrahedrons Q^4 and layered silicon tetrahedrons Q^3 into chain structures Q^2 and end structures Q^1 in AAMK, thus the gel structure may become more disordered [209]. The carboxyl group in PAA can also form chemical bonds with the initial gel, thereby occupying the site on the gels that extends the binding silicon or aluminium tetrahedral structures [121,212].

5.2. Phase assemblage and microstructure

Similar to other organics, the addition of water-soluble polymers or their emulsions does not alter the type of mineral phases and gel products in AAM [138,208]. Compared with organic-grafted and organic-adsorbed AAM, the microstructure of phase-crosslinked AAM presents a uniform phase with a larger spatial scale. In other words, organic polymers, inorganic gel and their interfaces within the phase-crosslinked AAM can be distinguished by SEM (**Fig. 15**). Organic polymers develop into an extensive spatial organic network through the breakage and reorganisation of carbon-carbon double bonds, and its volume is significantly larger than organic molecules such as organosilicons and surfactants. In addition, although the organic components in AAM are protected by the crosslinked gels, they still decompose at high temperatures. The styrene-acrylic (SA) emulsion and styrene-butadiene rubber (SBR) latex in AAS begin to decompose when the exposure temperature exceeds 300 °C [208,211]. Adding 0.5–3.0% SA emulsion slightly increases the total porosity of AAMK and facilitates the transformation of gel pores (<10 nm) into capillary pores (10–50 nm) [138]. Although the hydrogen bond generated rises the density of gels, the polymer network disrupts the matrix continuity in AAM, promoting the generation of micro-pores. The addition of excessive SA emulsion (>10%) sharply increases the harmful pores with size of more than 100 nm in phase-crosslinked AAM due to the reduction in fluidity of fresh slurry [208].
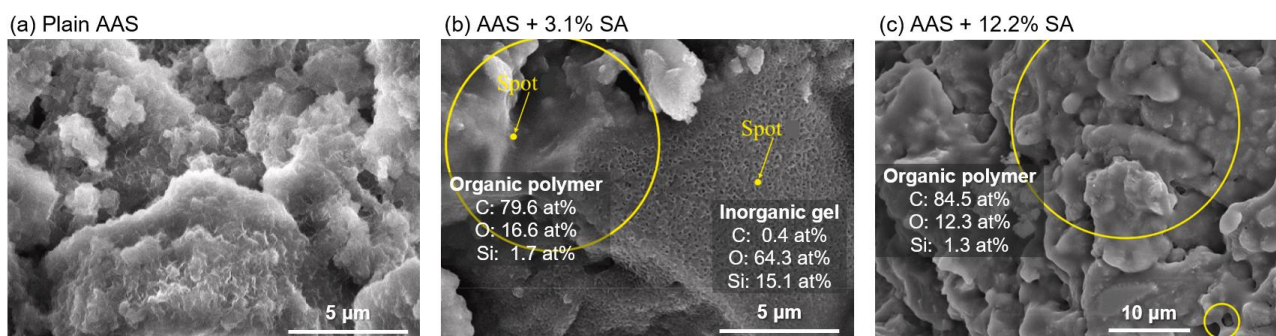

Fig. 15. SEM images of (a) plain AAS, as well as distinguishable organic polymer and inorganic gel in phase-crosslinked AAS with (b) 3.1% and (c) 12.2% SA emulsion (adapted from [208,213]).

5.3. Mechanical properties

Various organic polymers (dosage: 0.5–11%) such as PAA, sodium polyacrylate (PAAS), polyethylene co-vinyl acetate (PVA), acrylate (AE) and SBR can improve the compressive strength by up to 60% (**Fig. 16**a). The optimum mechanical performance can be achieved when the polymer dosage is around 4%, while the strength-enhancement effect diminishes gradually weakened after exceeding this critical dosage [121,209]. It is worth noting that the organic polymers have a more significant effect on improving the flexural strength, toughness and ductility. As seen in **Fig. 16**b and c, almost all organic polymers offer a substantial enhancement in flexural strength by up to 78% for AAM [214]. In contrast, the incorporation of 1.8–12.2% SA leads to a drop in compressive strength by 0–60% but significantly boosts the toughness by up to 190%, which can be ascribed to the steric hindrance of benzene ring group [138,208]. In the phase-crosslinked AAM, a resilient organic polymer network with high ductility and toughness is formed through self-condensation. Organic network integrates and interlaces with the inorganic gel network, and these two phases are closely connected through hydrogen bonds and a few covalent bonds (e.g., Si-O-C bonds) [208,212]. Organic polymers can also enhance the bond between matrix and aggregates while minimising the micro-cracks in the matrix by optimising the ITZ [215-216]. Therefore, the mechanical properties of phase-crosslinked AAM are significantly improved. In contrast, polymers with an over-dosage (generally >4%) may compromise the mechanical properties of AAM through hindering the gel synthesis reaction, introducing macro-pores by increasing the viscosity of fresh slurry, and increasing organic impurities synthesised by self-condensation [215].

Adding silane coupling agents can further promote the crosslinking and bonding between organic polymers and inorganic gels [121,212]. The 28-d flexural strength of AAS with multi organics of 5% PAAS and 5% KH550/KH560/KH570 is 23.1–103.8% higher than those with 5% PAAS alone, and they also exhibit improved fracture toughness and elastic modulus [212]. As discussed in Section 3.1, these silane coupling agents undergo hydrolysis in alkaline solutions and generate multiple active hydroxyl groups. These organosilicons not only bridge organic polymers and inorganic gels but also self-condensate into a silane network, further reinforcing the entire multi-component AAM structure.
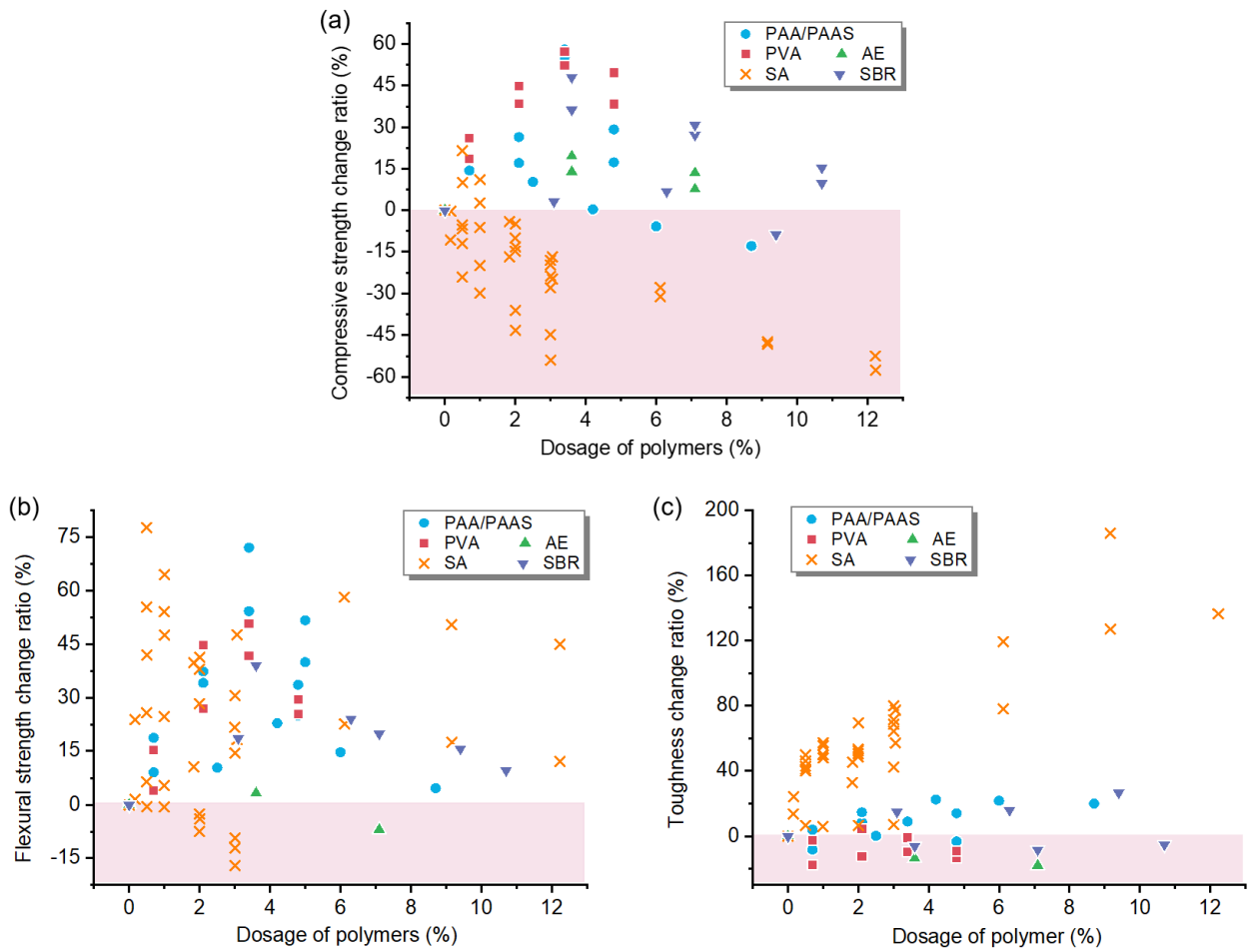
Fig. 16. Relative changes in (a) compressive strength, (b) flexural strength and (c) toughness of phase-crosslinked AAM with different types of water-soluble polymers or organic emulsions [121,138,208-209,211-212,215].

5.4. Durability-related properties

The addition of SBR latex with an appropriate dosage inhibits the water absorption of AAFS mortar. The organic polymer fills some small pores and transitional channels during the interpenetration process with the matrix, effectively reducing the moisture transport pathways [215,217]. Furthermore, the organic polymer adhered to the capillary wall may introduce a mild hydrophobic effect, despite its lower alkyl group and hydrocarbon chain density compared to alkyl-organosilicon and PDMS [217]. Due to the reduction in capillary absorption, the chloride-induced corrosion resistance of AAFS mortar with SBR latex is also improved, while sulphate ions can interact with SBR to weaken the interface strength, so that phase-crosslinked AAM may not be suitable for applications in sulphate-corrosive environments [217]. It is interesting to note that the change in pore structure of phase-crosslinked AAM with excessive polymer can increase its capillary absorption [138,215].

With regard to volume deformation, the incorporation of organic polymers such as SBR latex, AE latex and SA emulsion can reduce the moisture movement and drying shrinkage of AAM by up to 55% [208,211,217]. The micro-pore filling and sealing effects of the polymer are the primary factors resisting moisture escape [138,218]. The slow and gradual accumulation of polymerisation products due to the reduced reaction rate in AAM also lead to the drop in drying shrinkage of phase-crosslinked AAM.

6. Reaction, microstructure and properties of phase-separated AAM

6.1. Reaction mechanisms

The formation of epoxy resin-AAM composite involves a multifaceted chemical reaction process, including resin curing reaction, AAM synthesis, and organic-inorganic hybridisation (**Fig. 2**). The pre-mixing of liquid epoxy resin and curing agent first initiates the ring structure opening within the epoxy resin molecules [109,111]. A substantial quantity of active hydroxyl and ether groups are then generated on resin molecules, resulting in enhanced dispersion within the fresh AAM suspension [219]. As the reaction proceeds, a large proportion of resin molecules first undergo self-polymerisation. The curing reaction of epoxy resin is much faster compared to the synthesis of AAM. The operational time of epoxy resin depends on different factors such as material composition and curing temperature, typically falling within around 1 h [220-221]. Upon surpassing the designated operational time limit, the resin experiences a swift viscosity escalation, ultimately culminating in complete hardening within a period of 5–7 h [219]. In contrast, the synthesis reaction of AAM is gentler but more complex, involving simultaneous processes of precursor dissolution, gelation, reorganisation and polycondensation within the first 3 d [222-223]. Afterwards, the polymerisation and hardening dominate the formation of amorphous gels with higher density [224].

AAM with 30% epoxy resin exhibits a final setting time approximately 38% shorter than plain AAM [111]. The curing reaction characteristics of epoxy resin also cause a drop in the frequency of collisions between components in the mixed suspension, resulting in heterogeneous products with phase separation [110]. Consequently, a larger proportion of resin solidifies before AAM hardens, leading to the formation of a phase-separated composite. The phase-separated epoxy resin is connected with AAM matrix primarily through hydrogen bonds with a cohesive integration [111,225]. A minor proportion of chain resin molecules can experience condensation with hydroxyl groups presented on aluminosilicate oligomers or initial gels, and potentially participate in the formation of

continuous hybrid gels [109-110]. Certain resin molecules feature a minor presence of uncondensed active silicon-oxygen structures (R_m-Si(O$^-$)$_n$), facilitating their chemical bonding with the gel network in AAM [107,226]. Hydroxyl groups on resin can also impede the water evaporation by adsorbing and stabilising water molecules, thereby promoting the polymerisation reaction of AAM [111]. The curing and hybridisation of epoxy resin significantly accelerate the exothermic peak of AAM from 650 min to 100 min post-mixing, inducing a shortened setting time [226].

6.2. Phase assemblage and microstructure

Phase-separated AAM containing epoxy resin are a system of multiple coexisting phases, including AAM matrix, hardened epoxy resin, hybrid regions, unreacted precursors, pores, and cracks. The main matrix contains a highly crosslinked amorphous aluminosilicate gels and xonotlite crystals, surrounding the hardened epoxy particles [1,227-229]. The dosage of epoxy resin in composites is generally less than 30% (Table 7), the addition of which does not alter the mineral phase and chemical composition in AAM but slightly affects the arrangement and polymerisation of silicon-oxygen and aluminium-oxygen tetrahedra in gels [219,227].

Fig. 17 displays the microscopic morphology of composite AAM with various precursors and epoxy resin at different dosages obtained through SEM and energy dispersive X-ray spectrometer (EDS) techniques. Within the dosage range of 10–30%, hardened epoxy resin usually exists in the AAM matrix as discontinuous spherical, crescent-shaped and basin-shaped solids with a diameter of 1–20 μm [41,107-108,227]. The morphology and distribution of hardened epoxy resin are typically independent of the specific inorganic materials used but are closely related to the wettability and dosage of organic additives. As seen in Fig. 17d, the hardened epoxy resin is matte and porous, attributed to the utilisation of a hydrophilic curing agent [226]. In aqueous fresh AAM, this resin demonstrates a propensity to form small and non-spherical aggregates with a random distribution. Water-based epoxy resins and curing agents tend to have greater compatibility with AAM compared to their oil-based counterparts. The epoxy resin dosage also significantly affects the uniformity of the matrix [226]. When the mass ratio of organic additives to inorganic binder is equal to 1 (dosage: 100%), the continuity of the AAM matrix is disrupted. In this ratio, the hardened epoxy resin forms independent intertwined networks with AAM in 3D space, which is a dominant factor influencing the macroscopic properties of composites.

The epoxy resin particles exhibit tight interlocking within the AAM matrix, displaying an

improved ITZ devoid of visible micro-cracks (**Fig. 17**) [41,107]. The thickness of the ITZ between AAM and epoxy resins is generally less than 1 μm, much smaller than the size of hardened epoxy particles [107]. The commendable binding affinity of epoxy resin with gels in AAM features a notable level of nano-scale hybridisation that enhances the adhesion between organic and inorganic components [227]. The ITZ in phase-separated AAM exhibits more superior nano hardness and elastic modulus in comparison with epoxy resin or AAM [41,111,219]. The addition of 5% epoxy resin improves the crack resistance of the matrix [230], while the uniformity of the ITZ is limited, confirming that the nano-scale hybridisation of epoxy resin and gels in AAM is relatively limited and uncertain [41].
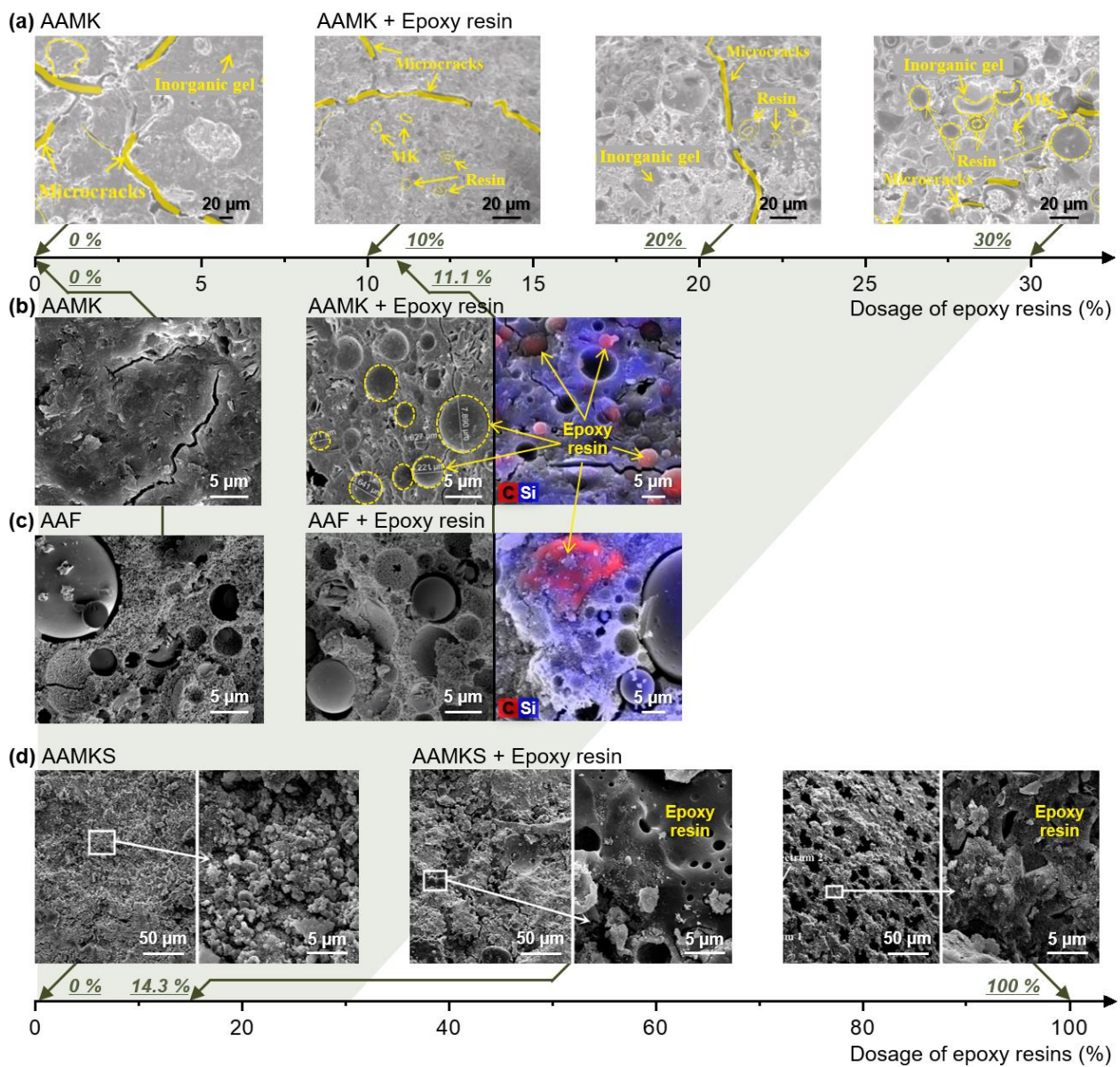

Fig. 17. Morphology images of phase-separated AAM with various precursors and epoxy resins at different dosages obtained through SEM and EDS techniques (adapted from [219,226-227]).

In terms of pore structure, adding epoxy resin with a dosage of less than 30% can reduce the volume fraction of air pores (>10 μm) in composite AAM while increasing the volume fraction of capillary pores (<10 μm) [111,227]. The total porosity of composite AAM drops as the micro-sized hardened epoxy resin can fill a proportion of pores, while excess epoxy resin increases the viscosity of fresh AAM, thus introducing air bubbles into composites [110]. For engineering applications, the preparation of composite AAM requires a judicious selection of epoxy resin dosage to achieve a balance of filling and air-entrainment effects resulting from the incorporation of organics.

6.3. Mechanical properties

For low-calcium AAM the main precursor of metakaolin or fly ash, the addition of epoxy resin has a positive effect on the compressive strength development (**Fig. 18**a and b). The compressive strength of composite AAMK with an epoxy resin dosage of 10–30% in short-term (1 d) and long-term (≥7 d) of curing is increased by up to 60% [110,219]. Epoxy resin can effectively mitigate defects, e.g., micro-cracks, without compromising the structural integrity of N-A-S-H gels, which can be attributed to the strong bonding between organic and inorganic phases and the reduced drying shrinkage within composites [230]. The presence of organic resin as a reinforcement can absorb partial load through crack deflection mechanism and plastic deformation [40,219]. The heat released by the self-polycondensation of epoxy resin also contributes to enhancing both the extent and rate of the synthesis reaction, so that the AAM containing a high dosage (>30%) of epoxy resin still maintains high strength [226]. In contrast, the compressive strength of phase-separated AAMK at 3 d closely approximates that of the plain one (**Fig. 18**a). The rise in fresh slurry viscosity caused by the epoxy resin incorporation leads to a drop in the uniformity of hardened composite, which is a potential cause for strength reduction [219]. In addition, epoxy resin has a positive effect on the compressive strength of AAF (approximately twice that of AAMK), due to the presence of more defects and unreacted precursors in AAF (**Fig. 18**b) [231]. Hardened epoxy resin can fill more cracks and pores in the matrix of AAF and bind otherwise separated inorganic phases such as gels and unreacted fly ash.

For high-calcium AAM with slag, the addition of 0.5–3% epoxy resin brings a modest enhancement in compressive strength by up to 30%, followed by a significant drop by up to 70% with a dosage of more than 3% (**Fig. 18**c) [109,230]. Incorporating epoxy resin can negatively influence the C-A-S-H gel layered structure compared to its effect on N-A-S-H gels with highly crosslinked disordered structure, mainly due to the competitive reactions with organic and AAM, as well as

binding sites of resin molecules with C-A-S-H gels during reaction process. The use of epoxy resin exerts a more pronounced adverse impact on the compressive strength of initial AAS composites cured for 1 d and 3 d when contrasted with the final composites. This finding indicates that resin molecules can impede the formation of C-A-S-H gels which also disrupt the structural integrity of calcium oxide layers and dreierketten silicate chains [1,37]. Additionally, AAS containing 2.8% epoxy resin and 0.3–0.6% silane coupling agent (KH560) exhibit superior compressive strength compared to those with only epoxy resin [230]. Silane coupling agents can act as bridge between different phases and promote the interface bonding from electrostatic adsorption and mechanical bonding to covalent bond between the hardened epoxy resin and the gel structure in AAS [232]. Thus, the synergistic effects of epoxy resin and silane coupling agent result in the improved mechanical properties of AAS.
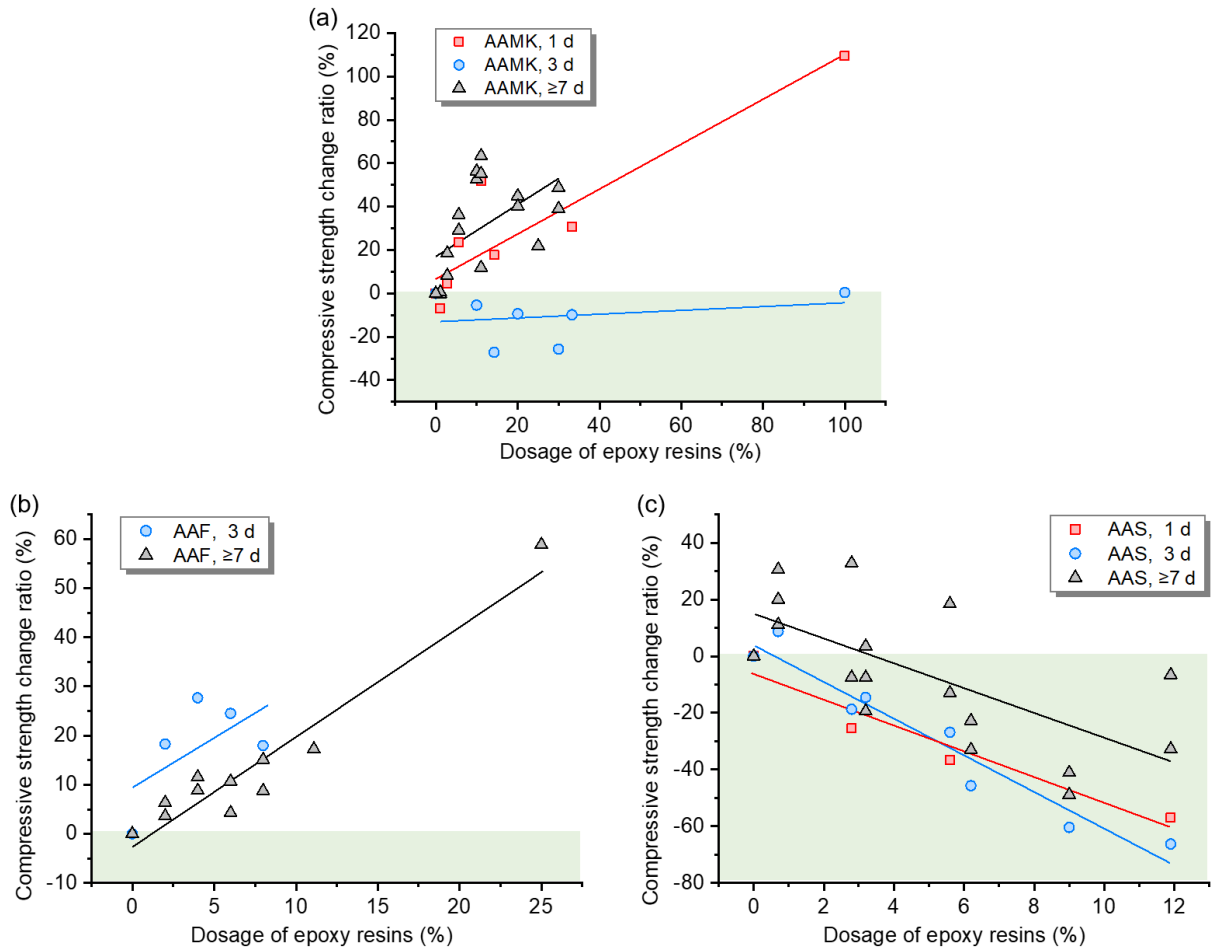

Fig. 18. Relative change in compressive strength of epoxy phase-separated AAM with the main precursor of (a) metakaolin, (b) fly ash and (c) slag cured for 1, 3 and ≥7 d [41,109-110,219,226-227,230,233].

As seen in **Fig. 19**a–c, the effect of epoxy resin addition on the flexural strength of phase-separated

AAM with a certain precursor is similar to that on the compressive strength, especially for AAS. For low-calcium AAM, the flexural strength first goes up rapidly and then retains a fluctuation balance as the epoxy resin dosage increases. The critical dosages of epoxy resin for AAMK and AAFA composites are about 10% and 4%, respectively [41,227]. The inclusion of 0–30% epoxy resin enhances the long-term toughness of AAMK and AAS by around 40%, in contrast to its limited effect on that of AAF with fluctuation of no more than 20% (**Fig. 19**d–f). Organic epoxy resin with excellent ductility and adhesive properties can be tightly bound to the matrix of AAM with high brittleness and rigidity [234]. The hardened epoxy resin can also take part of the load via plastic deformation, thereby further improving the toughness [40,235]. It is worth noting that epoxy resin shows a greater influence on the toughness of AAM with short-term of curing. During the early-age stages of formation, the rapid hardening of epoxy resin outpaces the polymerisation of AAM, making the hardened epoxy resin as the primary load-bearing phase.
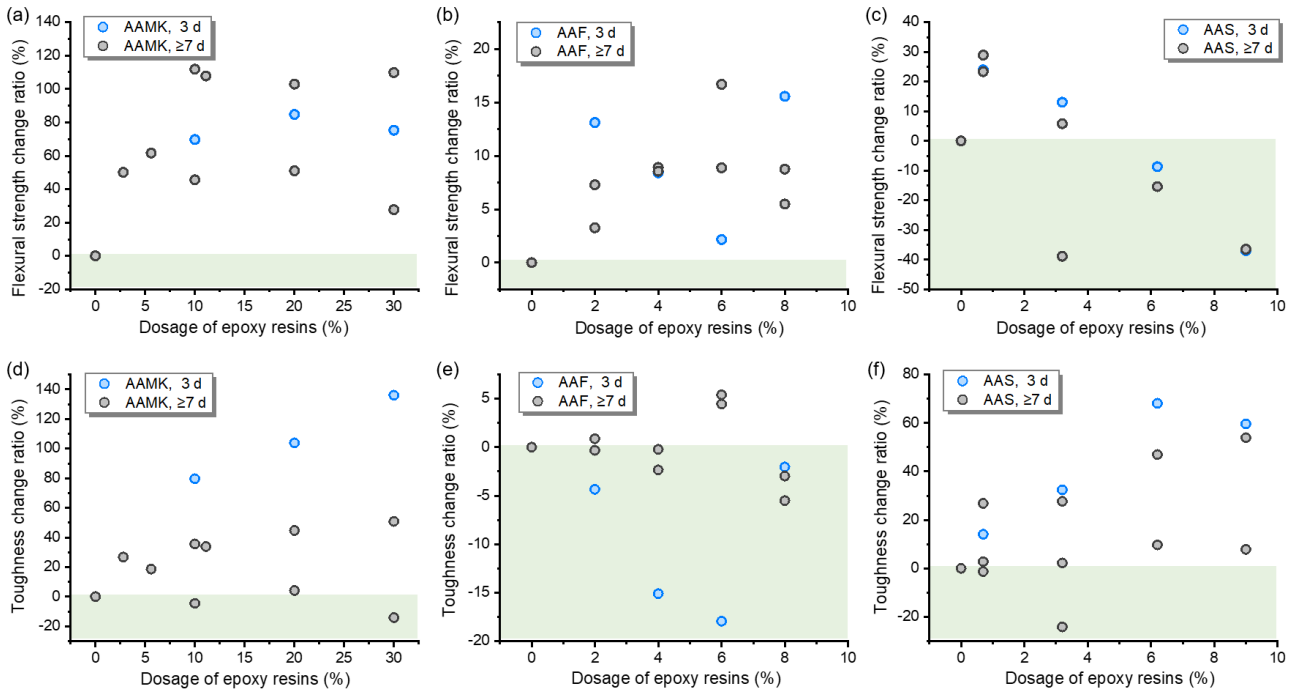

Fig. 19. Relative changes in (a–c) flexural strength and (d–f) toughness of phase-separated AAM with the main precursor of (a, d) metakaolin, (b, e) fly ash and (c, f) slag cured for 1, 3 and ≥7 d [41,109-110,227,233].

As a potential repair material, the bond strength of AAM to other substrates is an important index for evaluation, which depends primarily on the adhesion and mechanical bite of the interface involving cohesive bonding [6,236]. Compared to plain AAM, the bond strength between phase-separated AAM and concrete indicates a notable enhancement (with an about 35% rise), mainly due

to the following reasons [111,227]. First, the reduced porosity and increased reactivity help optimise the microstructure of the repair interface [227]. The drop in shrinkage and micro-cracks also declines the deformation of composites relative to the old substrate [237]. Moreover, more hydroxyl groups from epoxy resin and curing agent can be coupled with old substrate via chemical condensation or hydrogen bonding, enhancing the bonding properties and durability of AAM [238].

6.4. Durability-related properties

The capillary water absorption of phase-separated AAFS exhibits an initial rise, followed by a subsequent decline with the increasing epoxy resin dosage (from 2% to 8%) [227]. The water absorption coefficient of AAFS containing 6% epoxy resin is the highest, which is about three times that of plain AAFS, ascribed to the increased capillary porosity and inter-connected pores exiting in the ITZ [227]. In contrast, adding a large quantity of epoxy resin (8%) diminishes the proportion of porous matrix within AAM, consequently leading to a drop of approximately 25% in water absorption [227]. Phase-separated AAM shows better chloride resistance than plain AAM thanks to the improved microstructure with the addition of epoxy resin [111]. The curing agent can further strengthen the interaction between epoxy resin and inorganic gels, stabilising the 3D aluminosilicate network that can effectively adsorb chloride ions to prevent chloride penetration [239-240]. Moreover, the addition of 30% epoxy resin can reduce the drying shrinkage of AAMK by 37% [111]. Following the ring-opening reaction, numerous hydrogen bonds exist among epoxy resin, water molecules and gels in AAM, which can help stabilise the unbound water within the matrix, consequently mitigating the drying-induced shrinkage [40,109].

Fig. 20 presents the TG analysis results of thermal stability in terms of weight residue and decomposition temperature of phase-separated and plain AAM. All AAM exhibit rapid mass loss due to water evaporation and dehydration in the temperature range of 50–200 °C [241-242]. At this stage, free and adsorbed water in the capillary pores of AAM, as well as structural water in the gel network and hydroxyl groups are removed [243-244]. Dehydration reactions also occur in hardened epoxy resin [245]. The addition of epoxy resin rises the hydrogen bond content and moisture/hydroxyl stability, so that the dehydration temperature of phase-separated AAM is slightly higher than plain AAM [110]. Epoxy resin experiences degradation when subjected to temperatures above 250 °C. The polyamine chain and carbon scaffold of epoxy resin undergo rapid thermal fracture at around 280 °C, while aromatic hydrocarbons begin to decompose after 400 °C [245-246]. The phase-separated

AAMK after heat treatment at 800 °C exhibits a highly continuous network of pores and cavities. The presence of the matrix within the AAM provides a protective barrier, effectively preventing complete degradation of the organic phases [110]. The addition of 1% and 5% epoxy resin can improve the thermal stability of the inorganic structure in AAM and reduce the strength loss under high temperatures (up to 850 ℃) [233], since organic epoxy resin can be inserted into the gaps of the gel network in AAM as an active filler, and further condense with the matrix through dehydration to form continuous gels at high temperatures. Overall, the thermal stability of AAM can be relatively improved by adding epoxy resin, due to the coupling effect of the organic and inorganic phases.
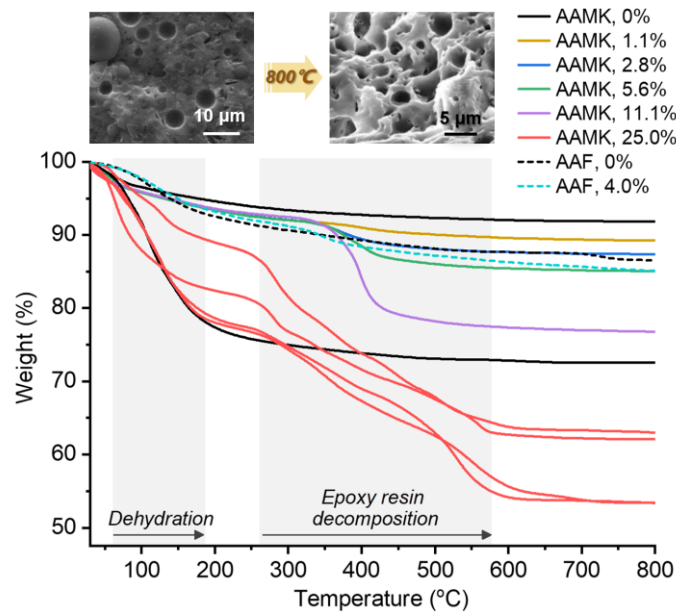

Fig. 20. TG curves of plain and phase-separated AAM, as well as morphology of phase-separated AAMK before and after heat treatment at 800 °C [39,107,110,227].

7. Potential applications and challenges

7.1. Potential applications

Organic-containing AAM with improved performance and new functions open up a range of potential applications, which can be categorised into following three distinct areas (**Fig. 21**):

(1) High-performance building materials: phase-crosslinked AAM with water-soluble polymers and phase-separated AAM with epoxy resin always demonstrate superior mechanical properties and thus can be adopted to produce high-performance concrete for civil engineering applications [97,227]. A study reported that AAFS with 4% epoxy resin exhibits a dense microstructure and excellent bonding performance, which can be used to strengthen or repair structures as the 28-d compressive and flexural strengths can reach over 65 and 7 MPa, respectively [227]. It was also found that the

microscopic fracture toughness of a phase-crosslinked AAS with 2% PAAS and 7% KH570 went up by 104% compared to traditional AAS [247]. Besides, adding superplasticisers can enhance the workability of fresh AAM, enabling the production of high-performance AAM with reduced water content and superior mechanical properties [44]. The incorporation of these organics effectively addresses the limitations of traditional AAM such as high brittleness, poor toughness and susceptibility to cracking, thereby expanding their applications in various environments.

(2) Corrosion-resistant materials for wet environments: As alkyl-organosilicon-grafted AAM and PDMS-adsorbed AAM exhibit superior hydrophobicity, waterproof performance and corrosion resistance, they can be used as coatings or binding materials for civil infrastructure in corrosive environments such as underground engineering, water conservancy engineering, marine and coastal engineering [67,248]. These organic-containing AAM with hydrophobic surface even exhibit excellent anti-fouling, self-cleaning, anti-icing and anti-biological adhesion, and are considered the most effective strategy to reduce corrosion [249-250]. For instance, a hydrophobic PMS-grafted AAS possesses significantly enhanced water and chloride resistance, leading to a remarkable 97% reduction in corrosion rate, thereby effectively protecting steel bars [67]. Phase-crosslinked AAM and phase-separated AAM, despite lacking hydrophobic modifications, offer desired corrosion resistance owing to the well-defined structures and dense microstructures.

(3) Functional organics in AAM systems: Organics introduced into AAM systems can impart unique functionalities, e.g., coupling agents, dispersants, stabilisers and shrinkage reducing agents. Functional-organosilicons can not only directly modify the AAM matrix, but also serve as coupling agents to enhance the interfacial bond between organic and inorganic phases [251]. Admixtures of epoxy, organic polymers, fibres and rubber particles can form stronger bonds with AAM through functional-organosilicon bridges (e.g., KH550, KH560, KH670 and KH792), resulting in the formation of final products with superior performance [41,121,138,252]. These reinforced AAM composite can serve in real-world construction projects for better durability. Additionally, micromolecular surfactants and superplasticisers are commonly used as dispersants for solid raw materials and stabilisers for bubbles or oily liquids in fresh AAM. These organics promote the formation of homogeneous composite systems [48,180]. Organic-adsorbed AAM containing appropriate superplasticisers can be used as raw materials for 3D printing in construction, as these fresh AAM possess good pumpability, extrudability, printability and buildability available for use in
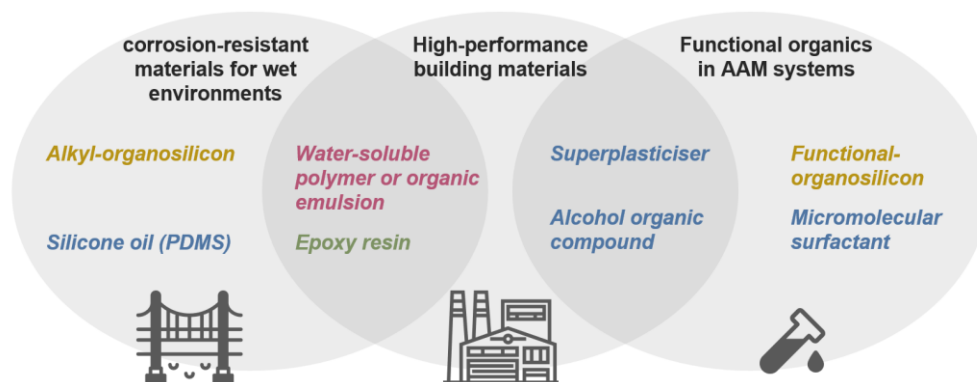
practical operations [16,45].

Fig. 21. Potential applications of AAM with organics.

7.2. Challenges

Although AAM have been acknowledged for their potentials to significantly reduce CO_2 emissions and energy consumption compared to traditional cementitious materials, the integration of organics within AAM introduces complexity in assessing their environmental benefits. Firstly, the incorporation of organics can affect the leachability of AAM, leading to potential release of organics into the environment and thus would cause risks to water sources and ecosystems, challenging the "green" reputation of AAM [253]. The stability of organics such as silicone oil and surfactants embedded in AAM is generally relatively lower compared to those that are grafted, like organosilicons. Some surfactants (e.g., superplasticisers) contain phthalates or other substances that can adversely impact environmental health [254]. When used in wading projects, the organic components of AAM may leach out slowly, contaminating the environment and possibly harming wildlife and human health [255]. Additionally, over the course of their service life, organic-containing AAM would degrade slowly, releasing volatile organic compounds and other hazardous by-products, especially from organosilicons and alcohol organic compounds [256]. The degradation of epoxy resin in phase-separated AAM may also result in the release of harmful components such as bisphenol A and epichlorohydrin into ecosystems, which can lead to air and water pollution [257]. Moreover, it is important to note that most AAM with organics are unsuitable for high-temperature applications. They are effective up to temperatures of 300 °C but beyond this, heat can cause the decomposition of organic phases, resulting in the loss of functional properties and increased CO_2 emissions [66].

Overall, although AAM with organics offer substantial advantages for sustainable development, their widespread adoption must be approached with caution. Rigorous environmental and health assessments are required to fully understand and mitigate potential risks associated with these

materials. Ongoing research is needed to gain a good understanding of their behaviour under different environmental conditions, developing safer and more stable formulations and establishing clear guidelines for their use to protect environmental and public health.

8. Conclusions and perspectives

8.1. Conclusions

As a novel class of building materials, AAM with organics exhibit highly homogenous microstructure and improved properties. This paper presents a systematic review of organic-containing AAM in terms of hybridisation modes, reaction mechanisms, phase assemblage, microstructure, mechanical properties, durability and potential applications (Table 8). The main conclusions can be drawn as follows:

(1) Hybridisation of organics and AAM can be achieved through various bonding mechanisms, including chemical bonds, hydrogen bonds, physical adsorption, electrostatic attraction and phase crosslinking. Based on the specific hybridisation modes, the AAM with organics can be categorised into four distinct types: organic-grafted, organic-adsorbed, phase-crosslinked and phase-separated AAM.

(2) Organic-grafted AAM, synthesised by the reaction of organosilicons grafted with active silanols with AAM, exhibit uniform microstructure and notable improved early-age strength, toughness and resistance to corrosion and volume deformation. The incorporation of alkyl-organosilicons with hydrophobic hydrocarbon chains or alkyl groups also significantly improves the hydrophobicity and water resistance of organic-grafted AAM, thereby bolstering the suitability for applications in wet environments.

(3) In organic-adsorbed AAM, various organics like surfactants (micromolecular surfactants, superplasticisers and alcohol organic compounds) and silicone oil (PDMS) exhibit a propensity for physical adsorption onto solid precursors, initial gel particles and final gel networks. Superplasticisers primarily affect the macroscopic properties of final AAM by improving fresh properties, while alcohols can mitigate the volume deformation. PDMS has comparable effect of waterproof modification to alkyl-organosilicons for AAM.

(4) In phase-crosslinked AAM, the organic network formed by self-condensation of water-soluble polymers interpenetrates and crosslinks with the gel skeleton in AAM. The toughness and corrosion resistance of them are greatly improved, with a broader range of potential applications.

(5) The combination of AAM and epoxy resin results in a phase-separated composite due to discernible hardened resin particles (1−20 μm). The interfaces between organic and inorganic phases possess dense microstructure and exceptional strength, toughness and bonding properties. The mechanical properties of epoxy resin-AAM composites, prepared with low- and high-calcium precursors, exhibit distinct variations due to their gel structures.

8.2. Perspectives

Given the great potential of AAM with organics in practical applications and the current research gaps, the following aspects can be considered for future research.
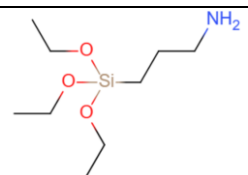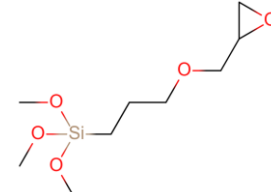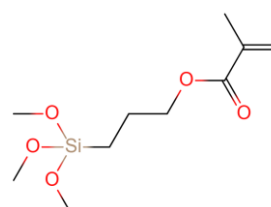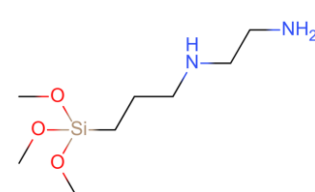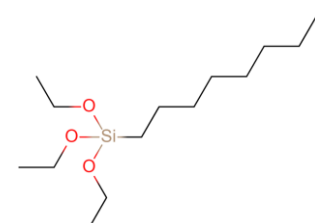
(1) Since there exist distinct preferences and limitations in the selection of AAM systems within certain types of organic-containing AAM in literature, a thorough investigation into both low- and high-calcium AAM with organics is required, as well as alcohol-adsorbed AAM due to significant discrepancies in findings among existing studies.

(2) It is vital to further explore the significance of organic functional groups such as amino, methacrylate, epoxy, ether, ester and hydroxyl in AAM with organics. These functional groups play a crucial role in the chemical bonding and adsorption behaviour between organic and inorganic components, and their coupling effects may lead to new hybridisation techniques.

(3) The influence of environmental conditions such as temperature, humidity and CO_2 presence on the reaction mechanisms of organic-containing AAM needs to be further explored. It helps understand how these conditions alter the hydrolysis, adsorption and condensation reactions or introduce new pathways to produce high-performance AAM.

(4) Although micromolecular surfactants and water-soluble polymers are widely employed in cement systems, AAM with these organics have been rarely studied. Due to the difference in AAM and Portland cement, further research is required to better understand the interaction between AAM and these organics as well as the overall performance of the resultant AAM.

(5) More studies are required to better understand the durability of organic-containing AAM such as corrosion resistance, efflorescence and thermal stability, which help evaluate their potential applications in real-world construction projects.

(6) It is necessary to understand the expending roles of organics in AAM systems. In addition to serving as organic additions, some alkaline organics, e.g., alkali-citrates, have demonstrated potential as alkaline activators for fabricating novel AAM [258-259]. For instance, tri-potassium

citrate can be used to produce alkali-activated slag pastes with high compressive strength (up to 75 MPa at 28 d) and low porosity [258]. Thus, the binding modes of organics as alkaline activators with gel structures and mineral phases in AAM deserve investigation.

Acknowledgements

Table 1 Parameters for organosilicons used to synthesise organic-grafted AAM.

Organosilicon	Abbreviation	Functional groups	Molecular formula	Molecular weight (g/mol)	Chemical structure
3-aminopropyltriethoxysilane	KH550	Amino	$C_9H_{23}NO_3Si$	221	
[(2,3-epoxypropoxy)propyl]trimethoxysilane	KH560	Epoxy	$C_9H_{20}O_5Si$	246	
3-methacryloxypropyltrimethoxysilane	KH570	Methacrylate	$C_{10}H_{20}O_5Si$	258	
N-[3-(trimethoxysilyl)propyl]ethylenediamine	KH792	Amino	$C_8H_{22}N_2O_3Si$	222	
Triethoxyoctylsilane	S823	Hydrocarbon chain (C8)	$C_{14}H_{32}O_3Si$	276	
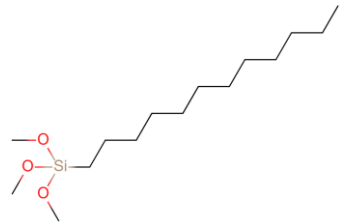
Dodecyltrimethoxysilane	S1213	Hydrocarbon chain (C12)	$C_{15}H_{34}O_3Si$	291	
N-[3-(trimethoxysilyl)propyl]aniline	PAMS	Amino, benzene ring	$C_{12}H_{21}NO_3Si$	255	
Methyltrimethoxysilane	MTMS	Methyl	$C_4H_{12}O_3Si$	136	
Sodium methyl siliconate	SMS	Methyl	$CH_3Na_3O_3Si$	160	
Potassium methyl siliconate	PMS	Methyl	$CH_3K_3O_3Si$	208	

Table 2 A summary of existing studies on organic-grafted AAM synthesised using organosilicon as one of the raw materials.

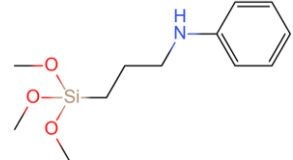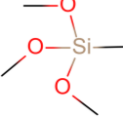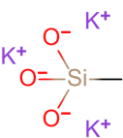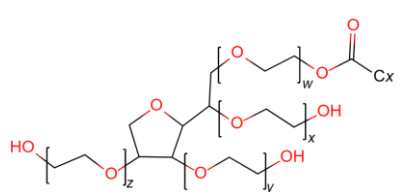| Reference	Precursor	Alkaline activator	Organic	Dosage	Specimen type	Processing route	Curing condition	Characterisation
[61]	MK	Na_2SiO_3 + NaOH	MTMS	/	Paste	Mixing organosilicon with fresh AAM paste	Room temperature	Reaction mechanisms, chemical composition, microstructure, mechanical properties, wettability
[60]	FA + S (1:1)	Na_2SiO_3 + NaOH	S823	0.38%, 0.76%, 1.14%, 1.52%	Paste	Mixing organosilicon with fresh AAM paste	20 °C, >95% RH	Reaction mechanisms, chemical composition, microstructure, pore structure, mechanical properties, wettability, water absorption
[41]	MK	Na_2SiO_3 + NaOH	S823, S1213, KH570	0.1%, 0.5%, 1.0%	Mortar	Mixing organosilicon with fresh AAM paste	25 °C, 75% RH	Reaction mechanisms, chemical composition, microstructure, interface performance, mechanical properties
[212]	S	Na_2SiO_3 + NaOH	KH550, KH560, KH570	5%	Paste	1) Mixing all liquid materials including organosilicon; 2) Mixing all liquid and solid materials	24 h steam curing at 80 °C and room temperature for 6 d	Microstructure, mechanical properties
[66]	MK	Na_2SiO_3 + NaOH	SMS	3.2%, 6.6%	Paste	1) Mixing AA including organosilicon; 2) Mixing the pre-mixed solution from 1) with solid precursor	25±2 °C, water conservation	Chemical composition, microstructure, pore structure, wettability, water absorption, corrosion resistance, thermal stability
[59]	MK	Na_2SiO_3 + NaOH	SMS	3.2%, 6.6%	Paste	1) Mixing AA including organosilicon; 2)	25±2 °C, water conservation	Reaction mechanisms, chemical composition, microstructure, fresh properties, mechanical properties

49

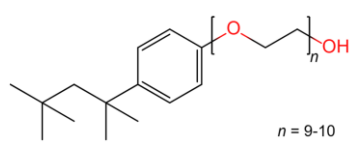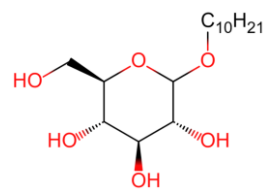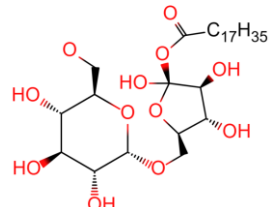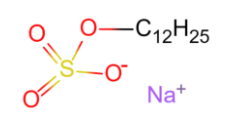|							
[90]	MK	Na_2SiO_3 + NaOH	SMS	0.32%, 1.60%	Paste	Mixing the pre-mixed solution from 1) with solid precursor 1) Mixing organic additive and AA solution; 2) Mixing pre-mixed liquid solution from 1) with solid raw materials	25±2 °C, water conservation	Pore structure, wettability, water absorption, volume deformation, moisture movement
[111]	MK	Na_2SiO_3 + NaOH	S823, S1213, KH570	1.0%	Mortar	Mixing organosilicon with fresh AAM paste	25 °C, 75% RH	Chemical composition, microstructure, pore structure, fresh properties, mechanical properties, volume deformation, chloride penetration, thermal stability, wear resistance, anti-carbonation performance
[121]	S	Na_2SiO_3 + NaOH	KH550, KH560, KH570	1%, 3%, 5%, 7%	Paste	1) Mixing all liquid materials including organosilicon; 2) Mixing all liquid and solid materials	80 °C for 4 h and then cured at 25 °C	Chemical composition, microstructure, pore structure, mechanical properties, fresh properties
[114]	MK + cement (6:4)	Na_2SiO_3 + NaOH	KH550, KH560	1%, 2%, 3%, 4%	Mortar	Mixing organosilicon (hydrolysate) with fresh AAM mortar	/	Pore structure, wettability, water absorption, water resistance
[113]	MK	Na_2SiO_3 + NaOH	KH550	0.06%, 0.12%, 0.29%, 0.59%	Paste	Mixing organosilicon with fresh AAM paste	20±2 °C, ≥95% RH	Chemical composition, pore structure, microstructure, fresh properties, mechanical properties, corrosion resistance
[120]	MK +	Na_2SiO_3	KH550	1%, 2%,	Mortar	Mixing organosilicon	20±2 °C, 95% RH	Chemical composition,
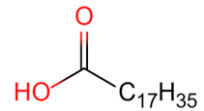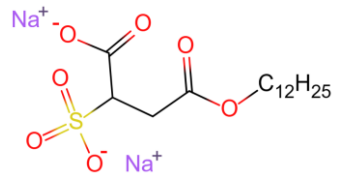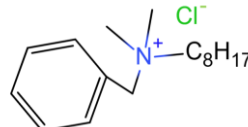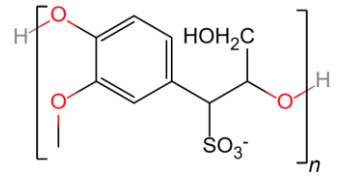
Ref.	Precursor	Activator	Silane	Dosage	Form	Mixing method	Curing condition	Properties
	cement (6:4)	+ NaOH		3%, 4%		(hydrolysate) with fresh AAM paste		microstructure, pore structure, fresh properties, mechanical properties, corrosion resistance
[67]	S	Na_2SiO_3	PMS	0.08%, 1.54%, 2.31%, 3.08%, 3.85%	Mortar	Mixing all raw materials	/	Chemical composition, microstructure, mechanical properties, mechanical properties, water resistance, corrosion resistance
[141]	MK	Na_2SiO_3 + NaOH	KH550	0.06%, 0.12%, 0.29%, 0.59%	Paste	Mixing silane with fresh AAM paste	20±2°C, ≥95 RH	Chemical composition, microstructure, pore structure, fresh properties, mechanical properties
[112]	MK	Na_2SiO_3 + NaOH	KH792	0.1%, 0.2%, 0.5%, 1.0%	Paste	Mixing organosilicon (hydrolysate) with fresh AAM paste	20 °C, ≥90 RH (seal curing for 24 h); 20 °C, 99% RH (after demoulding)	Chemical composition, pore structure, properties, volume stability
[122]	Ultrafine MK	Na_2SiO_3 + NaOH	KH560	2%, 4%, 6%	Paste	Mixing all raw materials	/	Chemical composition, microstructure, pore structure, fresh properties, mechanical properties
[68]	MK	Na_2SiO_3 + NaOH	KH550	0.2%, 0.4%, 0.6%, 0.8%	/	Mixing organosilicon (hydrolysate) with fresh AAM paste	20±2 °C, >95±5% RH	Reaction mechanisms, chemical composition, microstructure
[260]	MK	Na_2SiO_3 + NaOH	KH570, KH550, PAMS	/	/	/	/	Reaction mechanisms, microstructure, pore structure, mechanical properties, volume stability
[261]	MK	Na_2SiO_3	KH570	7.2%	/	1) Mixing	25 °C	Chemical composition,
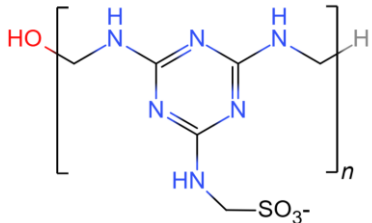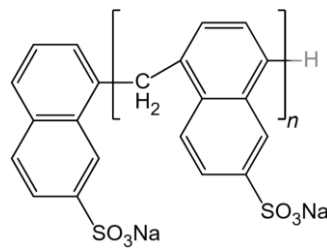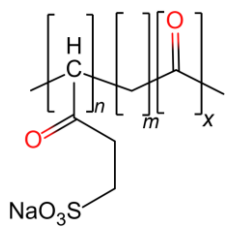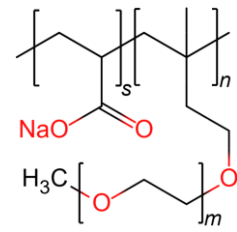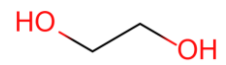
| | + NaOH | and/or KH550, PAMS | | organosilicon with MK; 2) Mixing mixture from 1) with AA | microstructure, bond performance |

Notes: (1) Dosage is the mass ratio of organic to inorganic binder; (2) MK, FA and S denote metakaolin, fly ash and slag, respectively; (3) AA is alkaline activator; (4) RH is relative humidity; (5) The arrangement is made according to the chronological order of publications, from the most recent to the furthest in time.

Table 3 Parameters for surfactants and silicone oil used to synthesise organic-adsorbed AAM.

Organic	Abbreviation	Functional groups	Molecular weight (g/mol)	Molecular formula	Chemical structure
Micromolecular surfactant					
Tween 20 (non-ionic)	/		/	/	
Tween 60 (non-ionic)	/	Hydrocarbon chain, epoxy, ether, ester, hydroxyl	/	/	
Tween 80 (non-ionic)	/		/	/	
Triton X-100 (non-ionic)	/	Benzene ring, ester, hydroxyl, methyl	/	/	
Alkyl polyglycoside (non-ionic)	APG	Hydrocarbon chain, epoxy, ether, hydroxyl	320	$C_{16}H_{32}O_6$	
Sucrose fatty acid esters (non-ionic)	SE	Hydrocarbon chain, epoxy, ether, ester, hydroxyl	609	$C_{30}H_{56}O_{12}$	
Sodium dodecyl sulphate (anionic)	SDS	Sulphate group, hydrocarbon chain	288	$C_{12}H_{25}NaO_4S$	

Name	Abbr.	Functional groups	Molecular weight	Molecular formula	Structure
Sodium lauryl ether sulphate (anionic)	SLES	Sulphate group, hydrocarbon chain	328	$C_{12}H_{26}Na_2O_5S$	
Stearic acid (anionic)	STA	Hydrocarbon chain, carboxyl	284	$C_{18}H_{36}O_2$	
Disodium laureth sulfosuccinate (anionic)	DLS	Sulphate group, hydrocarbon chain, ester	414	$C_{16}H_{28}Na_2O_7S$	
Cetyltrimethylammonium bromide (cationic)	CTAB	Amino, hydrocarbon chain, methyl	364	$C_{19}H_{42}BrN$	
Benzalkonium chloride (cationic)	BAC	Amino, benzene ring, hydrocarbon chain, methyl	284	$C_{17}H_{30}ClN$	
Superplasticiser					
Lignosulfonate superplasticiser	LS	Sulphate group, hydrocarbon chain, benzene ring, hydroxyl, methyl	/	/	

Melamine superplasticiser	MS	Sulphate group, amino, benzene ring, hydroxyl	/	/	
Naphthalene superplasticiser	NS	Sulphate group, naphthalene	/	/	
Aliphatic superplasticiser	AS	Sulphate group, hydrocarbon chain, carbonyl	/	/	
Polycarboxylate superplasticiser	PS	Hydrocarbon chain, ether, carboxy, methyl	/	/	
Vinyl copolymer superplasticiser	VCS	Hydrocarbon chain, C=C	/	/	/
Alcohol organic compound					
Ethylene glycol monomer	EG monomer	Hydroxyl	62	$C_2H_6O_2$	
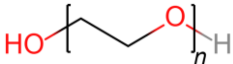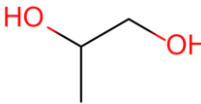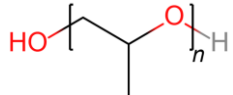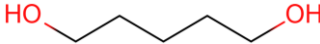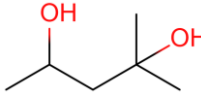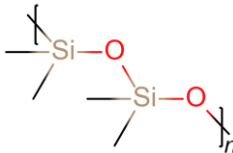
Polyethylene glycol	PEG	Hydroxyl	/	/	
Propylene glycol monomer	PG monomer	Hydroxyl, methyl	76	$C_3H_8O_2$	
Polypropylene glycol	PPG	Hydroxyl, methyl	/	/	
Pentylene glycol	/	Hydroxyl	104.15	$C_5H_{12}O_2$	
Hexylene glycol	/	Hydroxyl, methyl	118	$C_6H_{14}O_2$	
Silicone oil					
Polydimethylsiloxane	PDMS	Si-O, methyl	/	/	

Table 4 A summary of existing studies on organic-adsorbed AAM synthesised using surfactant or silicone oil as one of the raw materials.

Reference	Precursor	Alkaline activator	Organic	Dosage	Specimen type	Processing route	Curing condition	Characterisation
Micromolecular surfactant								
[81]	FA	K_2SiO_3 + KOH	Tween 60 (non-ionic), Triton X-100 (non-ionic), SDS (anionic), CTAB (cationic)	0.2% Triton X-100 or 0.1 Tween 60 + 0.005% CTAB or 0.2% SDS	Foamed paste	Mixing surfactant and foaming agent with fresh AAM paste	Room temperature for 24 h, 45 °C for 4 h, then room temperature and water retention	Chemical composition, pore structure, fresh properties, mechanical properties, gas permeability, heat conduction
[82]	MK	K_2SiO_3 + KOH	SDS (anionic)	1.80%	Foamed paste	Mixing surfactant and foaming agent with fresh AAM paste	/	Pore structure, mechanical properties, heat conduction, fire resistance
[180]	FA	Na_2SiO_3 + NaOH	SDS (anionic), SLES (anionic)	<0.1%	Foamed paste and mortar	/	90 °C for 24 h, and then room temperature for 6 d	Chemical composition, microstructure, pore structure, mechanical properties, fresh properties, thermal stability
[183]	MK	Na_2SiO_3 + NaOH	SLES (anionic), APG (non-ionic), BAC (cationic), SE (non-ionic), STA (anionic)	1%	Paste	1) Mixing surfactant and AA; 2) Mixing pre-mixed solution from 1) with solid precursors	20±1 °C and > 99% RH for 7 d, 20±1 °C and 50±5 % RH for 21 d	Microstructure, pore structure, fresh properties, water absorption, mechanical properties
[181]	FA + S	Na_2SiO_3 + NaOH	Washing liquid (anionic)	0.1%, 0.3%, 0.5%	Foamed paste	1) Mixing surfactant and AA; 2) Mixing pre-mixed solution from 1) with solid precursors	Room temperature	Pore structure, mechanical properties, fresh properties, thermal stability, heat conduction, fire resistance

[83]	S	Na$_2$SiO$_3$ + NaOH	SDS (anionic), SLES (anionic), DLS (anionic)	0.5%, 1%, 1.5%, 2%, 2.5%	Foamed paste	Mixing surfactant and foaming agent with fresh AAM paste	70 °C for 24 h, and then room temperature for 7 d	Chemical composition, microstructure, pore structure, mechanical properties
[182]	MK	Na$_2$SiO$_3$ + NaOH	Pluronic L35 (non-ionic), Tween 80 (non-ionic), Triton X100 (non-ionic), SDS (anionic), CTAB (cationic)	/	Foamed paste	Mixing all raw materials	Room temperature for 10 h, and then 60 °C for 24 h	Microstructure, pore structure, mechanical properties
[262]	MK	K$_2$SiO$_3$ + KOH	Egg white	/	Foamed paste	Mixing surfactant and foaming agent with fresh AAM paste	1) Room temperature; 2) 75 °C for 24 h	Reaction mechanisms, pore structure, thermal stability
Superplasticiser								
[187]	FA + S (1.83:1)	Na$_2$SiO$_3$ + NaOH	Sulphonated MS, NS, PS	0.5%, 1%, 1.5%, 2%, 2.5%, 3%	Mortar	1) Mixing superplasticiser and AA; 2) Mixing pre-mixed solution from 1) with solid precursors	Water conservation for 1 d, and then room environment	Fresh properties, mechanical properties
[186]	FA + S (3:1)	Na$_2$SiO$_3$ + NaOH	Sulphonated NS	0.5%, 1%, 1.5%, 2%	Concrete	/	Ambient-cured or oven-cured	Fresh properties, mechanical properties, thermal stability
[168]	Red mud + S (1:1)	NaOH	PS, AS, NS	0.11%, 0.22%, 0.33%, 0.44%, 0.55%	Paste	1) Mixing superplasticiser and AA; 2) Mixing pre-mixed	21±1 °C and water	Chemical composition, microstructure, pore structure, fresh properties

Ref	Precursor	Activator	SP type	Dosage	Form	Mixing procedure	Curing	Properties
						solution from 1) with solid precursors		
[190]	S or FA + S (1:1)	Na$_2$SiO$_3$ + NaOH	PS	1%, 2%, 3%	Concrete	/	/	Mechanical properties, water absorption
[185]	Lunar regolith simulant	NaOH	NS, PS	3%	Paste	Mixing all raw materials	80 ℃ for 6 h	Chemical composition, microstructure, fresh properties, mechanical properties, freeze-thaw cycle
[191]	FA + S (1:1)	Na$_2$SiO$_3$	NS, MS, PS	1%, 3%	Paste	1) Diluting SP; 2) Mixing diluted superplasticiser and fresh AAM paste	Water conservation	Reaction mechanisms, chemical composition, pore structure, fresh properties, mechanical properties
[263]	FA + S (1:1)	Na$_2$SiO$_3$	NS, MS, PS	1%	Paste	1) Diluting SP; 2) Mixing diluted superplasticiser and fresh AAM paste	Water conservation	Fresh properties, mechanical properties
[188]	FA + S (1:1)	Na$_2$SiO$_3$	Three types of PS and two types of NS	1%	Paste	1) Mixing all solid raw materials; 2) Mixing pre-mixed materials from 1) with water	60 ℃ for 24 h, 23±3 ℃	Fresh properties, mechanical properties
[264]	S	Na$_2$SiO$_3$ + NaOH	PS	1.2%, 1.8%, 2.4%, 3.0%, 3.6%	Concrete	1) Mixing all solid raw materials except SP; 2) Mixing pre-mixed materials from 1) with AA solution; 3) Mixing SP, water, and pre-mixed materials from 2)	22–25±2 ℃	Fresh properties, mechanical properties

Ref	Precursor	Activator	Superplasticiser	Dosage	Matrix	Mixing procedure	Curing	Properties
[265]	S + Micro silica	NaOH	LS, sulfonated MS, sulfonated NS, PS, AS	0.50%	Mortar	/	/	Chemical composition, microstructure, fresh properties, mechanical properties
[176]	FA + S (17:3)	Na_2SiO_3	PS, sodium and calcium LS, sodium triphosphate, sodium gluconate	~1.5%	Paste	1) Mixing all solid raw materials; 2) Mixing pre-mixed materials from 1) with water	20±2 °C, 70±10% RH	Chemical composition, microstructure, fresh properties, mechanical properties
[184]	FA	Na_2SiO_3 + NaOH	LS, NS, MS, PS, VCS	0.4%, 0.67%	Mortar	Mixing superplasticiser with fresh AAM mortar	23±2 °C, water conservation	Chemical composition, pore structure, fresh properties, mechanical properties, water absorption
[266]	Palm oil fuel ash	Na_2SiO_3 + NaOH	Sulphonated NS	3.1%, 7.2%	Mortar	Mixing superplasticiser with fresh AAM mortar	25 °C for 1 d, 60±5 °C for 1 d, and then room temperature, water conservation	Chemical composition, microstructure, mechanical properties
[267]	FA and/or Kaolin	Na_2SiO_3 + NaOH or Na_2SiO_3 + KOH	NS, MS, PS	~0.7%	Concrete	1) Mixing superplasticiser with AA solution; 2) Mixing pre-mixed solution from 1) with solid raw materials	Room temperature	Chemical composition, microstructure, mechanical properties
[268]	FA	Na_2SiO_3 + NaOH	/	<11.5%	Concrete	Mixing superplasticiser with fresh AAM concrete	23 °C or 70 °C for 24 h, and then	Fresh properties, mechanical properties

[189]	FA	Na$_2$SiO$_3$ + NaOH or NaOH	PS, NS, MS	0.77%	Paste	Mixing superplasticiser with fresh AAM paste	/	Fresh properties, mechanical properties
[167]	FA + S	Na$_2$SiO$_3$ + NaOH	PS, NS	1%, 2%, 3%, 4%	Paste	/	Room temperature	Reaction mechanisms, chemical composition, microstructure, fresh properties
[269]	FA	Na$_2$SiO$_3$ + NaOH	PS	3%, 4%, 5%, 6% 7%	Concrete	1) Mixing all solid raw materials; 2) Mixing pre-mixed materials from 1) with all liquid materials	70 °C for 48 h, then at outdoor environment	Microstructure, fresh properties, mechanical properties
[270]	MK	Na$_2$SiO$_3$ + NaOH	/	1%, 2%, 3%	Mortar	1) Mixing all solid raw materials; 2) Mixing pre-mixed materials from 1) with all liquid materials	20 °C	Fresh properties, mechanical properties
[271]	FA	Na$_2$SiO$_3$ + NaOH	PS	3%, 4%, 5%, 6%, 7%	Concrete	1) Mixing all solid raw materials; 2) Mixing pre-mixed materials from 1) with all liquid materials	70 °C for 48 h, then at outdoor environment	Fresh properties, mechanical properties
[272]	FA	Na$_2$SiO$_3$ + NaOH	PS	3%, 4%, 5%, 6%, 7%	Concrete	1) Mixing all solid raw materials; 2) Mixing pre-mixed materials from 1) with all liquid materials	70 °C for 48 h, then at outdoor environment	Microstructure, fresh properties, mechanical properties
[273]	S	Na$_2$SiO$_3$ + NaOH	PS, MS, NS, VCS	0.3%, 0.5%, 1.0%, 1.5%,	Paste and mortar	/	/	Fresh properties

				2.0%				
[274]	FA	Na$_2$SiO$_3$ + NaOH	MS	~2–8%	Mortar	1) Mixing all solid raw materials; 2) Mixing pre-mixed materials from 1) with all liquid materials	25–28 °C	Fresh properties
[95]	S	NaOH or Na$_2$SiO$_3$	NS, PS, VCS, MS	1%	Paste and mortar	/	20±2 °C, 99% RH	Fresh properties, mechanical properties
Alcohol organic compounds								
[172]	S	Na$_2$SiO$_3$	Hexylene glycol, EG, PEG, PG, PPG	0.4%, 0.8%, 0.16%	Paste	1) Mixing organic additive and AA solution; 2) Mixing pre-mixed liquid solution from 1) with solid raw materials	25 °C	Reaction mechanisms, chemical composition, pore structure, microstructure, fresh properties
[192]	MK	Orthophosphoric acid (AR grade 85%, 10 M)	PEG	1%, 2%, 3%	Paste	1) Mixing organic additive and AA solution; 2) Mixing pre-mixed liquid solution from 1) with solid raw materials	Room temperature	Chemical composition, microstructure, mechanical properties
[200]	S and coal gangue calcined at 700℃ (1:1)	Na$_2$SiO$_3$ + NaOH	Alkyl polyether	1%, 2%, 3%	Mortar and concrete	/	20±2 °C, 95±1% RH	Microstructure, pore structure, mechanical properties, chloride resistance, sulphate corrosion resistance, freeze-thaw cycle, volume deformation
[96]	MK	Na$_2$SiO$_3$	EG	0.5%, 1%,	Paste	/	Ambient	Chemical composition,
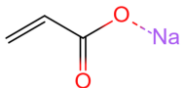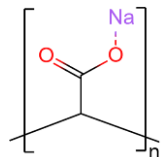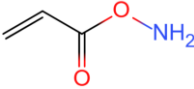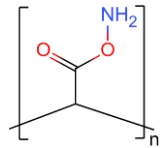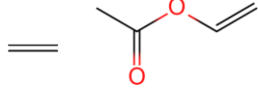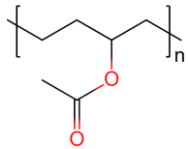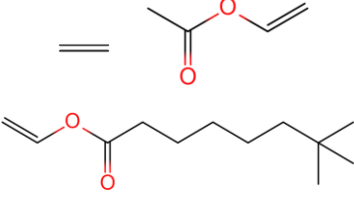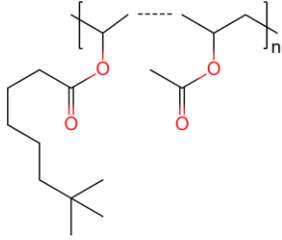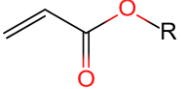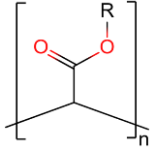
							temperature for 24 h, and then 40 °C, 100% RH	microstructure, mechanical properties, thermal stability
1.5%, 2%								
[174]	S	NaOH	PPG	0.36%, 0.72%	Paste	/	20±0.5 °C, 100% RH	Pore structure, fresh properties, mechanical properties, volume deformation
[166]	S	Na$_2$SiO$_3$	Aminoethanol, propionamide	<0.5%	Paste	/	25 °C	Reaction mechanisms, pore structure, mechanical properties, surface tension
[145]	S	Na$_2$SiO$_3$ + NaOH	Polyether	1.9%	Paste	1) Mixing organic additive and AA solution; 2) Mixing pre-mixed liquid solution from 1) with solid raw materials	20 °C, 50% RH	Reaction mechanisms, chemical composition, water absorption, internal humidity, volume deformation
[171]	S	Na$_2$SiO$_3$ + NaOH	PEG	2.5%	Mortar and concrete	/	22±2 °C, 50±4% RH	Reaction mechanisms, chemical composition, microstructure, volume deformation
[22]	FA	Na$_2$SiO$_3$ + NaOH	Hexylene glycol	2%	Paste	/	50±2 °C, 55% RH	Pore structure, fresh properties, mechanical properties, volume deformation
[170]	S	Na$_2$SiO$_3$ + NaOH	PEG	0.74%, 1.48%	Paste and mortar	1) Mixing organic additive, water, and AA solution; 2) Mixing pre-	/	Reaction mechanisms, pore structure, fresh properties, mechanical properties, surface

Ref	Precursor	Activator	Additive	Dosage	Sample	Procedure	Curing	Properties
						mixed liquid solution from 1) with solid raw materials		tension, volume deformation
[196]	S	Na₂SiO₃ + KOH	PEG	0.25%, 0.37%, 0.49%, 0.62%	Mortar	1) Mixing organic additive and AA solution; 2) Mixing pre-mixed liquid solution from 1) with solid raw materials	Room temperature, 90±5% RH	Chemical composition, microstructure, pore structure, mechanical properties
[193]	MK	Na₂SiO₃	PEG	0.5%, 1%, 2%, 5%, 7% and 10% (by MK)	Mortar	1) Mixing organic additive and AA solution; 2) Mixing pre-mixed liquid solution from 1) with solid raw materials	40 °C, 45±5% RH	Microstructure, pore structure, density, mechanical properties
[173]	S	Na₂SiO₃ + NaOH	Pentylene glycol	0.25%, 0.50%, 1.0%	Paste and mortar	1) Mixing organic additive and AA solution; 2) Mixing pre-mixed liquid solution from 1) with solid raw materials	Laboratory temperature	Reaction mechanisms, microstructure, pore structure, mechanical properties, volume deformation
[177]	S	NaOH	EG	2.5%, 5%, 7.5%, 10%	Paste	1) Mixing organic additive and AA solution; 2) Mixing pre-mixed liquid solution from 1) with solid raw materials	Room temperature, 100% RH	Chemical composition, microstructure, fresh properties, mechanical properties, volume deformation
[275]	MK	Na₂SiO₃ + NaOH	PEG	3%, 6%	Paste	1) Mixing organic additive and AA solution; 2) Mixing pre-mixed	45 °C for 24 h, and then room temperature	Chemical composition, microstructure, mechanical properties

Ref	Precursor	Activator	Organic additive	Dosage	Type	Preparation	Curing condition	Properties
						liquid solution from 1) with solid raw materials		
[21]	S	Na$_2$SiO$_3$	PPG	~0.7%, ~1.3%	Mortar	Mixing all raw materials	20±2 °C, 99% or 50% RH	Chemical composition, microstructure, mechanical properties, pore structure, volume deformation
[95]	S	Na$_2$SiO$_3$ or NaOH	PPG	1%	Paste and mortar	/	20±2 °C, 99% RH	Fresh properties, mechanical properties
[276]	Kaolinite	Na$_2$SiO$_3$ + NaOH	PEG	0.2%, 0.4%, 0.6%, 0.8%, 1%, 1.2%	Paste	Mixing all raw materials	40–90 °C, 99% RH	Fresh properties, mechanical properties
Silicone oil								
[90]	MK	Na$_2$SiO$_3$ + NaOH	PDMS	0.32%, 1.60%	Paste	1) Mixing organic additive and AA solution; 2) Mixing pre-mixed liquid solution from 1) with solid raw materials	25±2 °C, water conservation	Pore structure, wettability, water absorption, volume deformation, moisture movement
[94]	FA + S (3:2)	Na$_2$SiO$_3$ + NaOH	PDMS	0.31%, 0.63%, 0.94%, 1.25%, 1.56%, 1.88%	Paste	1) Mixing organic additive and AA solution; 2) Mixing pre-mixed liquid solution from 1) with solid raw materials	20±2 °C, 95±3%R H	Microstructure, chemical composition, pore structure, mechanical properties, wettability, water absorption
[88]	MK	Na$_2$SiO$_3$ + NaOH	PDMS	0.16%, 0.32%, 0.80%, 1.60%	Paste	1) Mixing organic additive and AA solution; 2) Mixing pre-mixed liquid solution from 1)	25±2 °C	Microstructure, pore structure, wettability, water absorption, moisture absorption

[18]	MK	Na_2SiO_3 + NaOH	PDMS	0.54%, 1.35%, 2.70%, 4.06%, 5.40%, 8.12%, 10.80%	Paste	with solid raw materials 1) Mixing organic additive and AA solution; 2) Mixing pre-mixed liquid solution from 1) with solid raw materials	25±2 °C, 60±5% RH	Microstructure, chemical composition, pore structure, mechanical properties, wettability, roughness
[277]	Silica fume	Na_2SiO_3 + KOH	PDMS	1.50%	Paste	1) Mixing organic additive and AA solution; 2) Mixing pre-mixed liquid solution from 1) with solid raw materials	/	Chemical composition, microstructure, fire resistance
[175]	MK	Na_2SiO_3 + NaOH	PDMS	5%, 10%, 15%	Paste	Mixing organic additive with fresh AAM paste	Room temperature, >95 % RH	Microstructure, chemical composition, pore structure, mechanical properties, fire resistance
[93]	MK	Na_2SiO_3+ KOH	Sol-gel synthesis of the hydrophobic alkoxysilane	/	Paste	Sol-gel synthesis	/	Reaction mechanism, chemical composition, microstructure, pore structure

Table 5 Parameters for water-soluble polymer and organic emulsion used to synthesise phase-crosslinked AAM.

Organic	Abbreviation	Functional groups	Main components	Chemical structure of monomers	Chemical structure of copolymer
Sodium polyacrylate	PAAS	Carboxyl	/		
Polyacrylamide	PAM	Amino, carbonyl	/		
Polyethylene co-vinyl acetate	PVA	Methyl, ester group	/		
Ethylene-vinyl acetate-vinyl neodecanoate	EVA-VN	Methyl, hydrocarbon chain (~7C), ester group	/		
Acrylate latex	AE latex	Ester group, C=C	Acrylate		
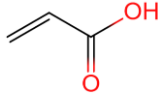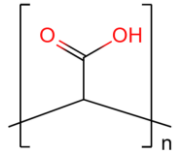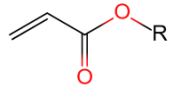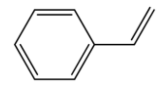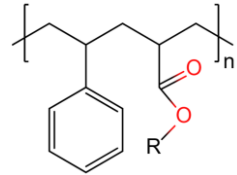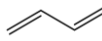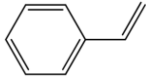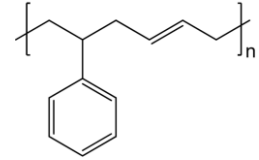
Poly(acrylic acid) emulsion	PAA emulsion	Carboxyl	Poly(acrylic acid)		
Styrene-acrylic emulsion	SA emulsion	Alkyl, benzene ring, ester group	Acrylate and Styrene		
Styrene-butadiene rubber latex	SBR latex	Benzene ring, C=C	1,3-Butadiene and Styrene		

Table 6 A summary of existing studies on phase-crosslinked AAM synthesised using water-soluble polymer or organic emulsion as one of the raw materials.

Reference	Precursor	Alkaline activator	Organic	Dosage	Specimen type	Processing route	Curing condition	Characterisation
					Water-soluble polymer			
[212]	S	Na_2SiO_3 + NaOH	PAAS	5%	Paste	1) Mixing all liquid materials including polymer; 2) Mixing all liquid and solid materials	24-h steam cure at 80 °C, room temperature for 6 d	Microstructure, mechanical properties, adhesive properties
[121]	S	Na_2SiO_3 + NaOH	PAAS, PVA	0.7%, 2.1%, 3.4%, 4.8%	Paste	1) Mixing all liquid materials including polymer; 2) Mixing all liquid and solid materials	80 °C for 4 h and then cured at 25 °C	Chemical composition, degree of polymerisation, microstructure, pore structure, fresh properties, mechanical properties
[278]	S	Na_2SiO_3 or K_2SiO_3	SA	1.6%, 3.1%, 6.3%	Paste	Three method: pre-addition, normal addition, and delayed addition	20 °C, 100% RH	Chemical composition, microstructure, pore structure, mechanical properties
[279]	S	Na_2SiO_3	SA, EVA, EVA-VN	/	Colloid	/	/	Stability of colloid
[280]	FA	Na_2SiO_3	PVA	0.69%	Mortar	/	70 °C, 80 °C, or 90 °C	Pore structure, mechanical properties
					Organic emulsion			
[138]	MK	Na_2SiO_3 + NaOH	SA emulsion	0.5%, 1.0%, 2.0%, 3.0%	Paste	1) Mixing all organic raw materials to prepare an organic emulsion; 2) Mixing pre-mixed	20±2 °C, >90% RH	Chemical composition, microstructure, pore structure, mechanical properties, thermal stability

					emulsion from 1) with fresh AAM paste within 60 min		
[215]	FA + S (3:2)	Na_2SiO_3 + NaOH	SBR latex	3.1%, 6.3%, 9.4%	Mortar	Mixing organic latex with fresh AAM mortar	29±3 °C, 70±10% RH	Chemical composition, microstructure, fresh properties, mechanical properties, durability (water absorption, volume deformation, chloride ion permeability, acid resistance, sulphate resistance), thermal stability
[208]	S	Na_2SiO_3 + NaOH	SA emulsion	0.16%, 1.83%, 3.05%, 6.11%, 9.16%, 12.22%	Paste	Mixing all raw materials including organic emulsion	20±1 °C, 95±5% RH	Chemical composition, pore structure, fresh properties, mechanical properties, volume deformation, thermal stability
[209]	MK	Na_2SiO_3 + NaOH	PAA emulsion	2.5%, 4.2%, 6.0%, 8.7%	Mortar	Mixing all raw materials including organic emulsion	40 °C for 6 h; 20 °C and 95% RH for 28 d	Chemical composition, pore structure, mechanical properties
[211]	S	Na_2SiO_3 + NaOH	SBR latex or AE latex	3.6%, 7.1%, 10.7% (SBR); 3.6%, 7.1% (AE)	Mortar	/	30 °C or 60 °C	Microstructure, mechanical properties, fresh properties, volume deformation
[210]	FA + S (3:2)	Na_2SiO_3 + NaOH	SBR latex	5%, 10%, 20%	Mortar	Mixing all raw materials including organic latex	20 °C, 90% RH	Fresh properties, mechanical properties, adhesive properties

Table 7 A summary of existing studies on phase-separated AAM synthesised using epoxy resin as one of the raw materials.

Reference	Precursor	Alkaline activator	Organic	Dosage	Specimen type	Processing route	Curing condition	Characterisation
[41]	MK	Na₂SiO₃ + NaOH	Epoxy resin (E51) and curing agent (Q17)	10%, 20%, 30%	Mortar	1) Mixing epoxy resin and curing agent (5:3); 2) Mixing pre-mixed epoxy resin with fresh AAM paste	25 °C, 75% RH	Reaction mechanisms, chemical composition, microstructure, interface performance, mechanical properties
[227]	FA + S (7:3)	Na₂SiO₃ + NaOH	Epoxy resin (waterborne epoxy emulsion) and curing agent (2:1)	2%, 4%, 6%, 8%	Mortar	1) Mixing epoxy resin and curing agent for 2 min; 2) Mixing pre-mixed epoxy resin with precursors and AA	20±3 °C, 90% RH	Microstructure, mechanical properties, water absorption, thermal stability
[111]	MK	Na₂SiO₃ + NaOH	Epoxy resin (E51) and curing agent (Q17)	10%, 20%, 30%	Mortar	1) Mixing epoxy resin and curing agent (5:3); 2) Mixing pre-mixed epoxy resin with fresh AAM paste	Ambient condition (about 25 °C, 75% RH)	Chemical composition, microstructure, pore structure, fresh properties, mechanical properties, volume deformation, chloride penetration, thermal stability, wear resistance, anti-carbonation performance
[110]	MK	Na₂SiO₃ + NaOH	Solid epoxy resin (diglycidyl ether of bisphenol A) and solid curing agent (dicyandiamide) (10:1)	1.1%, 2.8%, 5.6%, 11.1%	Paste	1) Grinding the mix of precursors, solid epoxy resin, and solid curing agent at 400 rpm for 5 min (10–100 μm); 2) Mixing	Heat cured (220 °C, water conservation for 2 h) + ambient condition (27 °C,	Chemical composition, microstructure, mechanical properties, thermal stability

Ref	Precursor	Activator	Polymer	Dosage	Type	Preparation	Curing	Characterization
						solid materials from 1) with AA	99% RH)	
[281]	FA + S (11:9)	Na$_2$SiO$_3$ + NaOH	Epoxy resin (bisphenol F)	0.7%, 1.6%	Paste	Mixing epoxy resin with precursors and AA	70 °C for 24 h + 20 °C until test, water conservation	Microstructure, mechanical properties, thermal stability, alkaline dissolution behaviour
[282]	Glass wool waste with epoxy resin	Na$_2$SiO$_3$	/	/	Paste	/	1) room temperature; 2) 40 °C on the first d, followed by room temperature; 3) 60 °C on the first d, followed by room temperature.	Reaction mechanisms, chemical composition, microstructure, fresh properties, mechanical properties, thermal stability
[106]	S	Na$_2$SiO$_3$ or NaOH	Epoxy resin (bisphenol A, E-51) and curing agent (polyamide resin) (1:1)	/	Mortar	1) Mixing epoxy resin and curing agent; 2) Mixing pre-mixed epoxy resin with fresh AAM paste	/	Chemical composition, microstructure, mechanical properties
[230]	S	NaOH	Epoxy resin (bisphenol A) and curing agent (sulfonyldianiline) (1:1.2)	2.8%, 5.6%, 11.9%	Paste	1) Mixing epoxy resin and curing agent; 2) Mixing pre-mixed epoxy resin with fresh AAM paste	7 °C, 10 °C, or 15 °C	Reaction mechanisms, chemical composition, microstructure, fresh properties, mechanical properties, thermal stability
[226]	MK + S (5:1)	NaOH	Epoxy resin (bisphenol A) and curing agent (waterborne polyamine) (2:3)	14.3 %, 33.3 %, 100 %	Paste	1) Mixing epoxy resin and curing agent; 2) Mixing pre-mixed epoxy resin with fresh AAM paste	7 °C	Reaction mechanisms, microstructure, fresh properties, mechanical properties

Ref	Precursor	Activator	Polymer	Dosage	Form	Preparation	Curing condition	Characterization
[219]	FA or MK	Na$_2$SiO$_3$ + NaOH	Epoxy resin (Epojet, two-component epoxy adhesive)	11.1%, 25%	Paste	1) Mixing epoxy resin and curing agent; 2) Pre-mixed resins being cured at room temperature for 10 min; 3) Mixing pre-mixed epoxy resin with fresh AAM paste	25 °C, >95% RH	Microstructure, mechanical properties, thermal stability
[107]	MK	Na$_2$SiO$_3$ + NaOH	Epoxy resin (N,N-diglycidyl-4-glycidyloxyaniline) and curing agent (melamine) (6:1, 3:1)	5.3%, 11.1%, 17.6%, 25%, 33.3%	Paste	1) Mixing epoxy resin and curing agent; 2) Pre-mixed resins being cured at 60 °C for 20 min; 3) Mixing pre-mixed epoxy resin with fresh AAM paste	60 °C for 24 h + room temperature for 6 d (>95 % RH), room temperature and humidity for 21 d	Chemical composition, microstructure, pore structure, mechanical properties, thermal stability
[39]	MK	Na$_2$SiO$_3$ + NaOH	1) Epoxy resin (N,N-diglycidyl-4-glycidyl-oxyaniline, 82.0 wt.%) and curing agent (bis-(2-aminoethyl)amine, 18.0 wt.%) 2) Epoxy resin (N,N-diglycidyl-4-glycidyl-oxyaniline, 79.6 wt.%) and curing agent (bis-(2-aminoethyl)amine, 4.4 wt.%; 2,4-diamino-toluene, 16.0 wt.%)	25%	Paste	1) Mixing epoxy resin and curing agent; 2) Pre-mixed resins being cured for 45 min at room temperature before complete crosslinking and hardening; 3) Mixing pre-mixed epoxy resin with fresh AAM paste	Room temperature, 99 % RH	Chemical composition, microstructure, mechanical properties, thermal stability

[40]	MK	Na$_2$SiO$_3$ + NaOH	Epoxy resin (Epojet and EpojetLV, two-component epoxy adhesive)	25%	Paste	1) Mixing epoxy resin and curing agent; 2) Mixing pre-mixed epoxy resin with fresh AAM paste	25 °C, >95% RH	Chemical composition, microstructure, mechanical properties, thermal stability
[233]	MK + S (1:4)	Na$_2$SiO$_3$	Resin powder (polyvinyl acetate) and resin emulsion (acrylic acid butyl acrylate)	0.7%, 3.2%	Paste	Mixing resin with precursors and AA	20 °C, 99% RH for 24 h + room temperature	Chemical composition, microstructure, mechanical properties, thermal stability
[109]	MK + S (1:4)	Na$_2$SiO$_3$	Resin powder (polyvinyl acetate) and resin emulsion (acrylic acid butyl acrylate)	0.7%, 3.2%, 6.2%, 9.0%	Paste	Mixing resin with fresh AAM paste	20 °C, 99% RH	Chemical composition, mechanical properties, thermal stability
[38]	Kaolin	K$_2$SiO$_3$ + KOH	Epoxy resin (diglycidyl ether of bisphenol-A)	400%	Paste	Mixing epoxy resin and curing agent with fresh AAM paste	60 °C for 6 h + 180 °C for 2 h	Thermal stability

Table 8 A summary of basic systems, reaction, microstructure, properties and potential applications of AAM with organics.

Type	Organic	Dosage	Primary AAM system	Bonding mode	Reaction process	Degree of polymerisation	Chemical composition	Morphology	Pore structure	Mechanical properties	Water absorption	Corrosion resistance	Volume deformation	Thermal stability	Potential applications
Organic-grafted AAM	Alkyl-organosilicon	Mainly: <2%, Generally: <7%	AAMK (>75%)	Chemical bonds, van der Waals forces, hydrogen bonds, electrostatic attraction	Promoted in early-age reaction	Decreased	Grafted with organic structures	Similar to plain AAM	Increased in porosity of gel pores (<10 nm)	Increased in early-age strength and slightly decreased in final strength	Significantly decreased; being hydrophobic	Significantly improved	Significantly decreased in early-age deformation and drying shrinkage	Organic structures decomposing at 350–550 °C	Corrosion-resistant materials for wet environments
	Functional-organosilicon					Increased in most studies			Decreased in porosity of capillary pores (10-10,000 nm)	Increased in strength	N/A	Improved	Slightly decreased in drying shrinkage		Coupling agents

Category	Type	Dosage	Suitable AAM	Interaction mechanism	Setting	Workability		Microstructure	Pore structure	Strength			Shrinkage		Application
Organic-adsorbed AAM	Micromolecular surfactant	N/A	Foamed AAM	Van der Waals forces, hydrogen bonds, electrostatic attraction	N/A	Increased	No change	Similar to plain AAM	Promoted in development of pore structure	Deceased with most surfactants in strength	N/A	N/A	N/A	N/A	Dispersants; foam/oil stabilizer
	Superplasticiser	Mainly: <1%, Generally: <4%	AAFA, AAS or AAFS (>85%)	Van der Waals forces, hydrogen bonds, electrostatic attraction	Slightly promoted	Increased		Similar to plain AAM	Refined in pore structure	LS: Decreased in strength; MS: Slightly affected; NS and AS: Increased with low-dosage in strength; PS: Increased in strength in most studies	N/A		N/A		Dispersants; high-performance building materials
	Alcohol organic compound	Mainly: <3%, Generally: <10%	AAS (>65%)	Van der Waals forces, hydrogen bonds	Significantly delayed	Inconsistent		Fibrous or flaky organic phase; organic film	Inconsistent	Inconsistent	N/A		Significantly decreased in autogenous and drying shrinkage		Shrinkage reducing agents
	Silicone oil (PDMS)	Generally: <15%	AAMK (>70%)	Van der Waals forces, hydrogen bonds	N/A	Can be ignored		Micron-scale hybrid particles with shapes of irregular blocks and long chains	Slightly affected	Increased with a proper-dosage and decreased with an over-dosage	Significantly decreased; an induction stage with low sorptivity; being hydrophobic		Decreased in early-age deformation		Corrosion-resistant materials for wet environments
Phase-crosslinked AAM	Water-soluble polymer or organic emulsion	Mainly: <5%, Generally: <13%	AAS or AAFS (>80%)	Phase crosslinking, van der Waals forces, hydrogen	Delayed in polymerisation	Decreased	No change	Differentiable organic and inorganic phases at the micron-scale	Inconsistent	Decreased with SA but increased with others in compressive	Decreased with a proper-dosage and increased with an	Enhanced in chloride resistance; Impaired in sulfate resistance	Slightly decreased in drying shrinkage	Organic structures beginning to decompose at 300 °C	High-performance building materials; corrosion-resistant

Phase-separated AAM															
			bonds							strength; Significantly increased in flexural strength and toughness	over-dosage				materials for wet environments
Phase-separated AAM	Epoxy resin	Mainly: <12%, Generally: <40%	AAMK (>55%)	Hydrogen bonds, van der Waals forces, chemical bonds	Promoted	Slightly affected in gel network	N/A	Separated organic and inorganic phases; dense hybrid interface	Decreased in air pores and increased in capillary pores	Deceased with most surfactants in strength	Decreased with a proper-dosage	Enhanced in chloride resistance	Decreased in drying shrinkage	Improved in thermal stability of composites; Organic structures decomposing at 250–550 °C	High-performance building materials; corrosion-resistant materials for wet environments; used in thermal environments

References

[1] J.L. Provis, Geopolymers and other alkali activated materials: why, how, and what? Materials and Structures 47(2014) 11-25.

[2] C. Shi, A.F. Jiménez and A. Palomo, New cements for the 21st century: the pursuit of an alternative to portland cement, Cement and Concrete Research 41(2011) 750-763.

[3] B.C. McLellan, R.P. Williams, J. Lay, A. van Riessen and G.D. Corder, Costs and carbon emissions for geopolymer pastes in comparison to ordinary Portland cement, Journal of Cleaner Production 19(2011) 1080-1090.

[4] M. Amran, S. Debbarma and T. Ozbakkaloglu, Fly ash-based eco-friendly geopolymer concrete: a critical review of the long-term durability properties, Construction and Building Materials 270(2021) 121857.

[5] P. Cong and Y. Cheng, Advances in geopolymer materials: a comprehensive review, Journal of Traffic and Transportation Engineering (English Edition) 8(2021) 283-314.

[6] P. Zhang, K. Wang, Q. Li, J. Wang and Y. Ling, Fabrication and engineering properties of concretes based on geopolymers/alkali-activated binders-a review, Journal of Cleaner Production 258(2020) 120896.

[7] S. Nie, J. Zhou, F. Yang, M. Lan, J. Li, Z. Zhang, Z. Chen, M. Xu, H. Li and J.G. Sanjayan, Analysis of theoretical carbon dioxide emissions from cement production: methodology and application, Journal of Cleaner Production 334(2022) 130270.

[8] L. Poudyal and K. Adhikari, Environmental sustainability in cement industry: an integrated approach for green and economical cement production, Resources, Environment and Sustainability 4(2021) 100024.

[9] K. Yang, J. Song and K. Song, Assessment of co2 reduction of alkali-activated concrete, Journal of Cleaner Production 39(2013) 265-272.

[10] W. Huang and H. Wang, Multi-aspect engineering properties and sustainability impacts of geopolymer pervious concrete, Composites Part B: Engineering 242(2022) 110035.

[11] I. Garcia-Lodeiro, A. Palomo and A. Fernández-Jiménez, 2-an overview of the chemistry of alkali-activated cement-based binders, Handbook of Alkali-Activated Cements, Mortars and Concretes, Woodhead Publishing, Oxford, 2015, pp. 19-47.

[12] B. Walkley, R. San Nicolas, M. Sani, G.J. Rees, J.V. Hanna, J.S.J. van Deventer and J.L. Provis, Phase evolution of C-(N)-A-S-H/N-A-S-H gel blends investigated via alkali-activation of synthetic calcium aluminosilicate precursors, Cement and Concrete Research 89(2016) 120-135.

[13] W. Tu and M. Zhang, Behaviour of alkali-activated concrete at elevated temperatures: a critical review, Cement and Concrete Composites 138(2023) 104961.

[14] Y. Wu, B. Lu, T. Bai, H. Wang, F. Du, Y. Zhang, L. Cai, C. Jiang and W. Wang, Geopolymer, green alkali activated cementitious material: synthesis, applications and challenges, Construction and Building Materials 224(2019) 930-949.

[15] H. Zhong and M. Zhang, Engineered geopolymer composites: a state-of-the-art review, Cement and Concrete Composites 135(2023) 104850.

[16] Y. Peng and C. Unluer, Development of alternative cementitious binders for 3D printing applications: a critical review of progress, advantages and challenges, Composites Part B: Engineering 252(2023) 110492.

[17] S. Chen, S. Ruan, Q. Zeng, Y. Liu, M. Zhang, Y. Tian and D. Yan, Pore structure of geopolymer materials and its correlations to engineering properties: a review, Construction and Building Materials 328(2022) 127064.

[18] S. Ruan, S. Chen, X. Zhu, Q. Zeng, Y. Liu, J. Lai and D. Yan, Matrix wettability and mechanical properties of geopolymer cement-polydimethylsiloxane (PDMS) hybrids, Cement and Concrete Composites 124(2021) 104268.

[19] M. Babaee and A. Castel, Water vapor sorption isotherms, pore structure, and moisture transport characteristics of alkali-activated and Portland cement-based binders, Cement and Concrete Research 113(2018) 99-120.

[20] A.A. Melo Neto, M.A. Cincotto and W. Repette, Drying and autogenous shrinkage of pastes and mortars with activated slag cement, Cement and Concrete Research 38(2008) 565-574.

[21] M. Palacios and F. Puertas, Effect of shrinkage-reducing admixtures on the properties of alkali-activated slag mortars and pastes, Cement and Concrete Research 37(2007) 691-702.

[22] Y. Ling, K. Wang and C. Fu, Shrinkage behavior of fly ash based geopolymer pastes with and without shrinkage reducing admixture, Cement and Concrete Composites 98(2019) 74-82.

[23] Z. Zhang, J.L. Provis, A. Reid and H. Wang, Fly ash-based geopolymers: the relationship between composition, pore structure and efflorescence, Cement and Concrete Research 64(2014) 30-41.

[24] M.A. Longhi, E.D. Rodríguez, B. Walkley, Z. Zhang and A.P. Kirchheim, Metakaolin-based geopolymers: relation between formulation, physicochemical properties and efflorescence formation, Composites Part B: Engineering 182(2020) 107671.

[25] Q. Li, K. Yang and C. Yang, An alternative admixture to reduce sorptivity of alkali-activated slag cement by optimising pore structure and introducing hydrophobic film, Cement and Concrete Composites 95(2019) 183-192.

[26] K. Sagoe Crentsil, T. Brown and S.Q. Yan, Medium to long term engineering properties and performance of high-strength geopolymers for structural applications, Advances in Science and Technology 69(2011) 135-142.

[27] M. Mastali, P. Kinnunen, A. Dalvand, R. Mohammadi Firouz and M. Illikainen, Drying shrinkage in alkali-activated binders - a critical review, Construction and Building Materials 190(2018) 533-550.

[28] F. Collins and J.G. Sanjayan, Effect of pore size distribution on drying shrinking of alkali-activated slag concrete, Cement and Concrete Research 30(2000) 1401-1406.

[29] G. Fang, W.K. Ho, W. Tu and M. Zhang, Workability and mechanical properties of alkali-

activated fly ash-slag concrete cured at ambient temperature, Construction and Building Materials 172(2018) 476-487.

[30] N. Ranjbar and M. Zhang, Fiber-reinforced geopolymer composites: a review, Cement and Concrete Composites 107(2020) 103498.

[31] J.V. Alemán, A.V. Chadwick, J. He, M. Hess, K. Horie, R.G. Jones, P. Kratochvíl, I. Meisel, I. Mita, G. Moad, S. Penczek and R.F.T. Stepto, Definitions of terms relating to the structure and processing of sols, gels, networks, and inorganic-organic hybrid materials (IUPAC recommendations 2007), Pure and Applied Chemistry 79(2007) 1801-1829.

[32] P. Gómez-Romero and C. Sanchez, Functional hybrid materials, John Wiley & Sons2006.

[33] C. Reeb, C. Pierlot, C. Davy and D. Lambertin, Incorporation of organic liquids into geopolymer materials - a review of processing, properties and applications, Ceramics International 47(2021) 7369-7385.

[34] C. Reeb, C.A. Davy, M. De Campos, J. Hosdez, C. Pierlot, C. Albert-Mercier and D. Lambertin, How are alkali-activated materials impacted by incorporating low viscosity organic liquids? Materials and Structures 56(2023) 11.

[35] P. Duxson, A. Fernández-Jiménez, J.L. Provis, G.C. Lukey, A. Palomo and J.S.J. van Deventer, Geopolymer technology: the current state of the art, Journal of Materials Science 42(2007) 2917-2933.

[36] K.M.L. Alventosa and C.E. White, The effects of calcium hydroxide and activator chemistry on alkali-activated metakaolin pastes, Cement and Concrete Research 145(2021) 106453.

[37] J.L. Provis and S.A. Bernal, Geopolymers and related alkali-activated materials, Annual Review of Materials Research 44(2014) 299-327.

[38] M. Hussain, R. Varely, Y.B. Cheng, Z. Mathys and G.P. Simon, Synthesis and thermal behavior of inorganic–organic hybrid geopolymer composites, Journal of Applied Polymer Science 96(2005) 112-121.

[39] C. Ferone, G. Roviello, F. Colangelo, R. Cioffi and O. Tarallo, Novel hybrid organic-geopolymer materials, Applied Clay Science 73(2013) 42-50.

[40] G. Roviello, L. Ricciotti, C. Ferone, F. Colangelo, R. Cioffi and O. Tarallo, Synthesis and characterization of novel epoxy geopolymer hybrid composites, Materials 6(2013) 3943-3962.

[41] M. Zhang, H. Xu, A.L.P. Zeze and J. Zhang, Metakaolin-based geopolymer composites modified by epoxy resin and silane: mechanical properties and organic-inorganic interaction mechanism, Applied Clay Science 232(2023) 106767.

[42] L. Bergamonti, R. Taurino, L. Cattani, D. Ferretti and F. Bondioli, Lightweight hybrid organic-inorganic geopolymers obtained using polyurethane waste, Construction and Building Materials 185(2018) 285-292.

[43] S.S. Amritphale, D. Mishra, M. Mudgal, R.K. Chouhan and N. Chandra, A novel green approach for making hybrid inorganic-organic geopolymeric cementitious material utilizing fly ash and rice husk, Journal of Environmental Chemical Engineering 4(2016) 3856-3865.

[44] T. Su, Y. Zhou and Q. Wang, Recent advances in chemical admixtures for improving the workability of alkali-activated slag-based material systems, Construction and Building Materials 272(2021) 121647.

[45] C. Lu, Z. Zhang, C. Shi, N. Li, D. Jiao and Q. Yuan, Rheology of alkali-activated materials: a review, Cement and Concrete Composites 121(2021) 104061.

[46] J. Sidhu and P. Kumar, Development of hydrophobicity in geopolymer composites-progress and perspectives, Construction and Building Materials 396(2023) 132344.

[47] V. Růžek, J. Novosád and K.E. Buczkowska, Geopolymer antimicrobial and hydrophobic modifications: a review, Ceramics 6(2023) 1749-1764.

[48] Y. Ettahiri, B. Bouargane, K. Fritah, B. Akhsassi, L. Pérez-Villarejo, A. Aziz, L. Bouna, A. Benlhachemi and R.M. Novais, A state-of-the-art review of recent advances in porous geopolymer: applications in adsorption of inorganic and organic contaminants in water, Construction and Building Materials 395(2023) 132269.

[49] M. El Alouani, B. Aouan, Y. Rachdi, S. Alehyen, E.H. El Herradi, H. Saufi, J. Mabrouki and N. Barka, Porous geopolymers as innovative adsorbents for the removal of organic and inorganic hazardous substances: a mini-review, International Journal of Environmental Analytical Chemistry (2022) 1-13.

[50] M. El Alouani, H. Saufi, G. Moutaoukil, S. Alehyen, B. Nematollahi, W. Belmaghraoui and M.H. Taibi, Application of geopolymers for treatment of water contaminated with organic and inorganic pollutants: state-of-the-art review, Journal of Environmental Chemical Engineering 9(2021) 105095.

[51] J. Zhao, L. Tong, B. Li, T. Chen, C. Wang, G. Yang and Y. Zheng, Eco-friendly geopolymer materials: a review of performance improvement, potential application and sustainability assessment, Journal of Cleaner Production 307(2021) 127085.

[52] M. Rajendran, K. Bakthavatchalam and S.M. Leela Bharathi, Review on the hybridized application of natural fiber in the development of geopolymer concrete, Journal of Natural Fibers 20(2023).

[53] J. Liu, N. Farzadnia and C. Shi, Microstructural and micromechanical characteristics of ultra-high performance concrete with superabsorbent polymer (sap), Cement and Concrete Research 149(2021) 106560.

[54] S.K. Kaliappan, A.A. Siyal, Z. Man, M. Lay and R. Shamsuddin, Effect of pore forming agents on geopolymer porosity and mechanical properties, AIP Conference Proceedings 2016(2018) 20066.

[55] Z. Wang and D. Lu, Study on the effect of emulsifiers on the pore structures of geopolymer prepared by emulsion templating, Materials Research Express 7(2020) 55508.

[56] D. Medpelli, J. Seo and D. Seo, Geopolymer with hierarchically meso-/macroporous structures from reactive emulsion templating, Journal of the American Ceramic Society 97(2014) 70-73.

[57] V. Cantarel, F. Nouaille, A. Rooses, D. Lambertin, A. Poulesquen and F. Frizon,

Solidification/stabilisation of liquid oil waste in metakaolin-based geopolymer, Journal of Nuclear Materials 464(2015) 16-19.

[58] C.A. Davy, G. Hauss, B. Planel and D. Lambertin, 3D structure of oil droplets in hardened geopolymer emulsions, Journal of the American Ceramic Society 102(2019) 949-954.

[59] S. Ruan, Y. Qiu, R. Gao, S. Chen, H. Qian, Y. Liu and D. Yan, Effect of organosilicone on the reaction process of functionalized geopolymers, Journal of Building Engineering 76(2023) 107348.

[60] Y. She, Y. Chen, L. Li, L. Xue and Q. Yu, Understanding the generation and evolution of hydrophobicity of silane modified fly ash/slag based geopolymers, Cement and Concrete Composites 142(2023) 105206.

[61] D. Wang, L. He, Y. Wu, Y. Li, W. Hu, T. Ma, S. Luo, J. Song, W. Sun and G. Zhang, Alkali-activated organogeopolymers with volumetric superhydrophobicity, Cement and Concrete Composites 145(2024) 105336.

[62] S. Sterman and J.G. Marsden, Silane coupling agents, Industrial & Engineering Chemistry 58(1966) 33-37.

[63] T. Aziz, A. Ullah, H. Fan, M.I. Jamil, F.U. Khan, R. Ullah, M. Iqbal, A. Ali and B. Ullah, Recent progress in silane coupling agent with its emerging applications, Journal of Polymers and the Environment 29(2021) 3427-3443.

[64] X. Wang, S. Zhai and T. Xie, Mechanism behind the improvement of coupling agent in interface bonding performance between organic transparent resin and inorganic cement matrix, Construction and Building Materials 143(2017) 138-146.

[65] T. Hooshmand, J.P. Matinlinna, A. Keshvad, S. Eskandarion and F. Zamani, Bond strength of a dental leucite-based glass ceramic to a resin cement using different silane coupling agents, Journal of the Mechanical Behavior of Biomedical Materials 17(2013) 327-332.

[66] S. Ruan, S. Chen, Y. Zhang, J. Mao, D. Yan, Y. Liu, X. Liu and H. Hosono, Molecular-level hybridized hydrophobic geopolymer ceramics for corrosion protection, Chemistry of Materials 35(2023) 1735-1744.

[67] X. Lv, Y. Qin, H. Liang, Y. Han, J. Li, Y. He and X. Cui, Potassium methyl silicate (CH_5SiO_3Na) assisted activation and modification of alkali-activated-slag-based drying powder coating for protecting cement concrete, Construction and Building Materials 326(2022) 126858.

[68] C. Zhang, Z. Hu, H. Zhu, X. Wang and J. Gao, Effects of silane on reaction process and microstructure of metakaolin-based geopolymer composites, Journal of Building Engineering 32(2020) 101695.

[69] Y. Tian, Q. Yuan, C. Yang, K. Yang, L. Yu, M. Zhang and X. Zhu, Insights into the efficiency loss of naphthalene superplasticizer in alkali-activated slag pastes, Journal of Building Engineering 68(2023) 106176.

[70] A.A. Siyal, M.R. Shamsuddin and A. Low, Fly ash based geopolymer for the adsorption of cationic and nonionic surfactants from aqueous solution - a feasibility study, Materials Letters

283(2021) 128758.

[71] D. Myers, Surfactant science and technology, John Wiley & Sons2020.

[72] B. Zhu and T. Gu, Surfactant adsorption at solid-liquid interfaces, Advances in Colloid and Interface Science 37(1991) 1-32.

[73] T. Dong, S. Xie, J. Wang, G. Zhao and Q. Song, Solidification and stabilization of spent TBP/OK organic liquids in a phosphate acid-based geopolymer, Science and Technology of Nuclear Installations 2020(2020) 1-7.

[74] A.J.N. MacLeod, F.G. Collins, W. Duan and W.P. Gates, Quantitative microstructural characterisation of portland cement-carbon nanotube composites using electron and X-ray microscopy, Cement and Concrete Research 123(2019) 105767.

[75] L. Zhao, X. Guo, Y. Liu, C. Ge, Z. Chen, L. Guo, X. Shu and J. Liu, Investigation of dispersion behavior of go modified by different water reducing agents in cement pore solution, Carbon 127(2018) 255-269.

[76] S. Parveen, S. Rana, R. Fangueiro and M.C. Paiva, Microstructure and mechanical properties of carbon nanotube reinforced cementitious composites developed using a novel dispersion technique, Cement and Concrete Research 73(2015) 215-227.

[77] W. Baomin and D. Shuang, Effect and mechanism of graphene nanoplatelets on hydration reaction, mechanical properties and microstructure of cement composites, Construction and Building Materials 228(2019) 116720.

[78] K. Walbrück, F. Maeting, S. Witzleben and D. Stephan, Natural fiber-stabilized geopolymer foams-a review, Materials 13(2020) 3198.

[79] R.M. Novais, R.C. Pullar and J.A. Labrincha, Geopolymer foams: an overview of recent advancements, Progress in Materials Science 109(2020) 100621.

[80] N.B. Singh, Foamed geopolymer concrete, Materials Today: Proceedings 5(2018) 15243-15252.

[81] K.M. Klima, C.H. Koh, H.J.H. Brouwers and Q. Yu, Synergistic effect of surfactants in porous geopolymer: tailoring pore size and pore connectivity, Cement and Concrete Composites 134(2022) 104774.

[82] K.W. Kim, H.M. Lim, S. Yoon and H. Ko, Fast-curing geopolymer foams with an enhanced pore homogeneity derived by hydrogen peroxide and sodium dodecyl sulfate surfactant, Minerals 12(2022).

[83] Z. Ji, M. Li, L. Su and Y. Pei, Porosity, mechanical strength and structure of waste-based geopolymer foams by different stabilizing agents, Construction and Building Materials 258(2020) 119555.

[84] V.S. Ramachandran and V.M. Malhotra, 7 - superplasticizers, Concrete Admixtures Handbook (Second Edition), William Andrew Publishing, Park Ridge, NJ, 1996, pp. 410-517.

[85] K. Yamada, T. Takahashi, S. Hanehara and M. Matsuhisa, Effects of the chemical structure on the properties of polycarboxylate-type superplasticizer, Cement and Concrete Research 30(2000) 197-207.

[86] P. Zhan and Z. He, Application of shrinkage reducing admixture in concrete: a review, Construction and Building Materials 201(2019) 676-690.

[87] B. Zhang, H. Zhu, P. Feng and P. Zhang, A review on shrinkage-reducing methods and mechanisms of alkali-activated/geopolymer systems: effects of chemical additives, Journal of Building Engineering 49(2022) 104056.

[88] S. Ruan, D. Yan, S. Chen, F. Jiang and W. Shi, Process and mechanisms of multi-stage water sorptivity in hydrophobic geopolymers incorporating polydimethylsiloxane, Cement and Concrete Composites 128(2022) 104460.

[89] S. Ruan, S. Chen, J. Lu, Q. Zeng, Y. Liu and D. Yan, Waterproof geopolymer composites modified by hydrophobic particles and polydimethylsiloxane, Composites Part B: Engineering 237(2022) 109865.

[90] S. Ruan, S. Chen, Y. Liu, Y. Zhang, D. Yan and M. Zhang, Early-age deformation of hydrophobized metakaolin-based geopolymers, Cement and Concrete Research 169(2023) 107168.

[91] S. Ruan, S. Chen, Y. Liu, D. Yan and Z. Sun, Investigation on the effect of fiber wettability on water absorption kinetics of geopolymer composites, Ceramics International 48(2022) 36678-36689.

[92] C. Peng, Z. Chen and M.K. Tiwari, All-organic superhydrophobic coatings with mechanochemical robustness and liquid impalement resistance, Nature Materials 17(2018) 355-360.

[93] B.E. Glad, W.M. Kriven, P. Colombo and P. Colombo, Highly porous geopolymers through templating and surface interactions, Journal of the American Ceramic Society 98(2015) 2052-2059.

[94] D. Zhang, H. Zhu, Q. Wu, T. Yang, Z. Yin and L. Tian, Investigation of the hydrophobicity and microstructure of fly ash-slag geopolymer modified by polydimethylsiloxane, Construction and Building Materials 369(2023) 130540.

[95] M. Palacios and F. Puertas, Effect of superplasticizer and shrinkage-reducing admixtures on alkali-activated slag pastes and mortars, Cement and Concrete Research 35(2005) 1358-1367.

[96] H.M. Khater and A. El Naggar, Combination between organic polymer and geopolymer for production of eco-friendly metakaolin composite, Journal of the Australian Ceramic Society 56(2020) 599-608.

[97] X. Zhang, M. Du, H. Fang, M. Shi, C. Zhang and F. Wang, Polymer-modified cement mortars: their enhanced properties, applications, prospects, and challenges, Construction and Building Materials 299(2021) 124290.

[98] L.K. Aggarwal, P.C. Thapliyal and S.R. Karade, Properties of polymer-modified mortars using epoxy and acrylic emulsions, Construction and Building Materials 21(2007) 379-383.

[99] J. Rottstegge, M. Arnold, L. Herschke, G. Glasser, M. Wilhelm, H.W. Spiess and W.D. Hergeth, Solid state NMR and LVSEM studies on the hardening of latex modified tile mortar systems,

Cement and Concrete Research 35(2005) 2233-2243.

[100] R. Wang, P. Wang and X. Li, Physical and mechanical properties of styrene-butadiene rubber emulsion modified cement mortars, Cement and Concrete Research 35(2005) 900-906.

[101] P. Łukowski and D. Dębska, Effect of polymer addition on performance of portland cement mortar exposed to sulphate attack, Materials 13(2019) 71.

[102] Y. Peng, G. Zhao, Y. Qi and Q. Zeng, In-situ assessment of the water-penetration resistance of polymer modified cement mortars by μ-XCT, SEM and EDS, Cement and Concrete Composites 114(2020) 103821.

[103] K.A. Khan, I. Ahmad and M. Alam, Effect of ethylene vinyl acetate (EVA) on the setting time of cement at different temperatures as well as on the mechanical strength of concrete, Arabian Journal for Science and Engineering 44(2019) 4075-4084.

[104] R. Wang and L. Zhang, Mechanism and durability of repair systems in polymer-modified cement mortars, Advances in Materials Science and Engineering 2015(2015).

[105] S.H. Song, F.T. Liu and Y.B. Huang, Effect of polymer latex and fiber on properties of sulpho aluminate cement mortar, Advanced Materials Research 450(2012) 402-406.

[106] S. Guo, Y. Lu, X. Wan, F. Wu, T. Zhao and C. Shen, Preparation, characterization of highly dispersed reduced graphene oxide/epoxy resin and its application in alkali-activated slag composites, Cement and Concrete Composites 105(2020) 103424.

[107] G. Roviello, L. Ricciotti, C. Ferone, F. Colangelo and O. Tarallo, Fire resistant melamine based organic-geopolymer hybrid composites, Cement and Concrete Composites 59(2015) 89-99.

[108] M. Hussain, R.J. Varley, Y.B. Cheng and G.P. Simon, Investigation of thermal and fire performance of novel hybrid geopolymer composites, Journal of Materials Science 39(2004) 4721-4726.

[109] Y.J. Zhang, Y.C. Wang, D.L. Xu and S. Li, Mechanical performance and hydration mechanism of geopolymer composite reinforced by resin, Materials Science and Engineering: A 527(2010) 6574-6580.

[110] R. Singla, M. Senna, T. Mishra, T.C. Alex and S. Kumar, High strength metakaolin/epoxy hybrid geopolymers: synthesis, characterization and mechanical properties, Applied Clay Science 221(2022) 106459.

[111] M. Zhang, H. Xu, A.L. Phalé Zeze, X. Liu and M. Tao, Coating performance, durability and anti-corrosion mechanism of organic modified geopolymer composite for marine concrete protection, Cement and Concrete Composites 129(2022) 104495.

[112] X. Wang, C. Zhang, Q. Wu, H. Zhu and Y. Liu, Thermal properties of metakaolin-based geopolymer modified by the silane coupling agent, Materials Chemistry and Physics 267(2021) 124655.

[113] C. Zhang, M. Wei, Z. Hu, T. Yang, B. Jiao, H. Zhu, N. Sun and H. Lv, Sulphate resistance of silane coupling agent reinforced metakaolin geopolymer composites, Ceramics International 48(2022) 25254-25266.

[114] B. Feng, J. Liu, Y. Chen, X. Tan, M. Zhang and Z. Sun, Properties and microstructure of self-waterproof metakaolin geopolymer with silane coupling agents, Construction and Building Materials 342(2022) 128045.

[115] J. Yang, W. She, W. Zuo, K. Lyu and Q. Zhang, Rational application of nano-sio2 in cement paste incorporated with silane: counterbalancing and synergistic effects, Cement and Concrete Composites 118(2021) 103959.

[116] Z. Zhang, J.L. Provis, H. Wang, F. Bullen and A. Reid, Quantitative kinetic and structural analysis of geopolymers. Part 2. Thermodynamics of sodium silicate activation of metakaolin, Thermochimica Acta 565(2013) 163-171.

[117] Y. Zuo, M. Nedeljković and G. Ye, Coupled thermodynamic modelling and experimental study of sodium hydroxide activated slag, Construction and Building Materials 188(2018) 262-279.

[118] A.R. Brough and A. Atkinson, Sodium silicate-based, alkali-activated slag mortars: part i. Strength, hydration and microstructure, Cement and Concrete Research 32(2002) 865-879.

[119] L.E. Prevette, T.E. Kodger, T.M. Reineke and M.L. Lynch, Deciphering the role of hydrogen bonding in enhancing pdna−polycation interactions, Langmuir 23(2007) 9773-9784.

[120] B. Feng, J. Liu, Y. Chen, M. Zhang and X. Tan, Investigation on basic properties and durability of metakaolin based geopolymer modified with silane, Polymer Composites 43(2022) 5500-5510.

[121] X. Xing, J. Wei, W. Xu, B. Wang, S. Luo and Q. Yu, Effect of organic polymers on mechanical property and toughening mechanism of slag geopolymer matrix, Polymers 14(2022).

[122] G. Ouyang, L. Wu, C. Ye, J. Wang and T. Dong, Effect of silane coupling agent on the rheological and mechanical properties of alkali-activated ultrafine metakaolin based geopolymers, Construction and Building Materials 290(2021) 123223.

[123] J. Zhao, M. Milanova, M.M.C.G. Warmoeskerken and V. Dutschk, Surface modification of tio2 nanoparticles with silane coupling agents, Colloids and Surfaces a: Physicochemical and Engineering Aspects 413(2012) 273-279.

[124] X. Ma, N. Lee, H. Oh, S. Jung, W. Lee and S. Kim, Morphology control of hexagonal boron nitride by a silane coupling agent, Journal of Crystal Growth 316(2011) 185-190.

[125] Y. Xie, C.A.S. Hill, Z. Xiao, H. Militz and C. Mai, Silane coupling agents used for natural fiber/polymer composites: a review, Composites Part a: Applied Science and Manufacturing 41(2010) 806-819.

[126] R.J. Hook, A 29si nmr study of the sol-gel polymerisation rates of substituted ethoxysilanes, Journal of Non-Crystalline Solids 195(1996) 1-15.

[127] G. Trimmel, R. Badheka, F. Babonneau, J. Latournerie, P. Dempsey, D. Bahloul-Houlier, J. Parmentier and G.D. Soraru, Solid state NMR and TG/MS study on the transformation of methyl groups during pyrolysis of preceramic precursors to SiOC glasses, Journal of Sol-Gel Science and Technology 26(2003) 279-283.

[128] A.P. Rao, A.V. Rao and G.M. Pajonk, Hydrophobic and physical properties of the ambient

pressure dried silica aerogels with sodium silicate precursor using various surface modification agents, Applied Surface Science 253(2007) 6032-6040.

[129] C.A. Hepburn, P. Vale, A.S. Brown, N.J. Simms and E.J. McAdam, Development of on-line ftir spectroscopy for siloxane detection in biogas to enhance carbon contactor management, Talanta 141(2015) 128-136.

[130] D.J. Skrovanik and C.K. Schöff, Thermal mechanical analysis of organic coatings, Progress in Organic Coatings 16(1988) 135-163.

[131] P. Liu, J. Song, L. He, X. Liang, H. Ding and Q. Li, Alkoxysilane functionalized polycaprolactone/polysiloxane modified epoxy resin through sol–gel process, European Polymer Journal 44(2008) 940-951.

[132] W. Werner and I. Halasz, Pore structure of chemically modified silica gels determined by exclusion chromatography, Journal of Chromatographic Science 18(1980) 277-283.

[133] P. Duan, C. Yan and W. Luo, A novel waterproof, fast setting and high early strength repair material derived from metakaolin geopolymer, Construction and Building Materials 124(2016) 69-73.

[134] P. Nath and P.K. Sarker, Effect of GGBFS on setting, workability and early strength properties of fly ash geopolymer concrete cured in ambient condition, Construction and Building Materials 66(2014) 163-171.

[135] J. Davidovits, Properties of geopolymer cements, in: First international conference on alkaline cements and concretes, Kiev State Technical University Kiev, Ukraine, 1994,131-149.

[136] J. Zhu, X. Ou, J. Su and J. Li, The impacts of surface polarity on the solubility of nanoparticle, The Journal of Chemical Physics 145(2016) 44504.

[137] J. Zhu, E. Zhao, C. Xu, Q. Peng, X. Li and J. Su, The influences of surface polar unit density on the water dispersity of nanoparticles, Journal of Molecular Liquids 325(2021) 115241.

[138] C. Zhang, W. Ming, Y. Li, Q. Wu and H. Zhu, Influence of organic emulsion on the structure and properties of geopolymer, Journal of Materials in Civil Engineering 35(2023) 4022398.

[139] X. Wan, D. Hou, T. Zhao and L. Wang, Insights on molecular structure and micro-properties of alkali-activated slag materials: a reactive molecular dynamics study, Construction and Building Materials 139(2017) 430-437.

[140] S. Puligilla and P. Mondal, Role of slag in microstructural development and hardening of fly ash-slag geopolymer, Cement and Concrete Research 43(2013) 70-80.

[141] C. Zhang, X. Wang, Z. Hu, Q. Wu, H. Zhu and J. Lu, Long-term performance of silane coupling agent/metakaolin based geopolymer, Journal of Building Engineering 36(2021) 102091.

[142] D. Chandler, Hydrophobicity: two faces of water, Nature 417(2002) 491.

[143] N. Giovambattista, P.G. Debenedetti and P.J. Rossky, Effect of surface polarity on water contact angle and interfacial hydration structure, The Journal of Physical Chemistry B 111(2007) 9581-9587.

[144] A. Syakur and H. Sutanto, Determination of hydrophobic contact angle of epoxy resin

compound silicon rubber and silica, in: IOP Publishing, 2017,12025.

[145] Z.Y. Qu, Q. Yu, Y.D. Ji, F. Gauvin and I.K. Voets, Mitigating shrinkage of alkali activated slag with biofilm, Cement and Concrete Research 138(2020) 106234.

[146] G. Xiong, B. Luo, X. Wu, G. Li and L. Chen, Influence of silane coupling agent on quality of interfacial transition zone between concrete substrate and repair materials, Cement and Concrete Composites 28(2006) 97-101.

[147] J.T. Davies, A quantitative kinetic theory of emulsion type, i. Physical chemistry of the emulsifying agent, in: Proceedings of 2nd International Congress Surface Activity, Citeseer, 1957,426-438.

[148] V. Purcar, O. Cinteza, M. Ghiurea, A. Balan, S. Caprarescu and D. Donescu, Influence of hydrophobic characteristic of organo-modified precursor on wettability of silica film, Bulletin of Materials Science 37(2014) 107-115.

[149] O.N. Tretinnikov, Wettability and microstructure of polymer surfaces: stereochemical and conformational aspects, Journal of Adhesion Science and Technology 13(1999) 1085-1102.

[150] S. Standal, J. Haavik, A.M. Blokhus and A. Skauge, Effect of polar organic components on wettability as studied by adsorption and contact angles, Journal of Petroleum Science and Engineering 24(1999) 131-144.

[151] C. Hall and W.D. Hoff, Water transport in brick, stone and concrete, CRC Press2011.

[152] F. Li, L. Liu, K. Liu, A. Zheng and J. Liu, Investigation on waterproof mechanism and micro-structure of cement mortar incorporated with silicane, Construction and Building Materials 239(2020) 117865.

[153] V. Soulios, E. de Place Hansen and H. Janssen., Hygric properties of hydrophobized building materials, in: 4th Central European Symposium on Building Physics (CESBP 2019), 2019,6.

[154] A. Johansson, M. Janz, J. Silfwerbrand and J. Trägårdh, Protection of concrete with water repellent agents–what is required to achieve a sufficient penetration depth? Concrete Repair, Rehabilitation and Retrofitting (2009) 763-768.

[155] C. Gong, L. Jianzhong, C. Cuicui, L. Changfeng and S. Liang, Study on silane impregnation for protection of high performance concrete, Procedia Engineering 27(2012) 301-307.

[156] S. Li, W. Zhang, J. Liu, D. Hou, Y. Geng, X. Chen, Y. Gao, Z. Jin and B. Yin, Protective mechanism of silane on concrete upon marine exposure, Coatings 9(2019) 558.

[157] X. Li, F. Rao, S. Song and Q. Ma, Deterioration in the microstructure of metakaolin-based geopolymers in marine environment, Journal of Materials Research and Technology 8(2019) 2747-2752.

[158] Z. Li, Y. Chen, J.L. Provis, Ö. Cizer and G. Ye, Autogenous shrinkage of alkali-activated slag: a critical review, Cement and Concrete Research 172(2023) 107244.

[159] O.M. Jensen and P.F. Hansen, Autogenous deformation and rh-change in perspective, Cement and Concrete Research 31(2001) 1859-1865.

[160] Z. Li, T. Lu, X. Liang, H. Dong and G. Ye, Mechanisms of autogenous shrinkage of alkali-

activated slag and fly ash pastes, Cement and Concrete Research 135(2020) 106107.

[161] P. Lura, Autogenous deformation and internal curing of concrete., 2003.

[162] Y. Song, Z. Li, J. Zhang, Y. Tang, Y. Ge and X. Cui, A low-cost biomimetic heterostructured multilayer membrane with geopolymer microparticles for broad-spectrum water purification, Acs Applied Materials & Interfaces 12(2020) 12133-12142.

[163] S. Tang, D. Huang and Z. He, A review of autogenous shrinkage models of concrete, Journal of Building Engineering 44(2021) 103412.

[164] N. Shahidzadeh-Bonn, A. Azouni and P. Coussot, Effect of wetting properties on the kinetics of drying of porous media, Journal of Physics. Condensed Matter 19(2007) 112101.

[165] N.K. Lee, J.G. Jang and H.K. Lee, Shrinkage characteristics of alkali-activated fly ash/slag paste and mortar at early ages, Cement and Concrete Composites 53(2014) 239-248.

[166] L. Kalina, V. Bílek, E. Bartoníčková, M. Kalina, J. Hajzler and R. Novotný, Doubts over capillary pressure theory in context with drying and autogenous shrinkage of alkali-activated materials, Construction and Building Materials 248(2020) 118620.

[167] J.G. Jang, N.K. Lee and H.K. Lee, Fresh and hardened properties of alkali-activated fly ash/slag pastes with superplasticizers, Construction and Building Materials 50(2014) 169-176.

[168] S. Li, J. Zhang, Z. Li, Y. Gao and C. Liu, Feasibility study of red mud-blast furnace slag based geopolymeric grouting material: effect of superplasticizers, Construction and Building Materials 267(2021) 120910.

[169] S. Sha, M. Wang, C. Shi and Y. Xiao, Influence of the structures of polycarboxylate superplasticizer on its performance in cement-based materials-a review, Construction and Building Materials 233(2020) 117257.

[170] V. Bílek, L. Kalina and R. Novotný, Polyethylene glycol molecular weight as an important parameter affecting drying shrinkage and hydration of alkali-activated slag mortars and pastes, Construction and Building Materials 166(2018) 564-571.

[171] F. Matalkah, T. Salem, M. Shaafaey and P. Soroushian, Drying shrinkage of alkali activated binders cured at room temperature, Construction and Building Materials 201(2019) 563-570.

[172] V. Bílek, L. Kalina, R. Dvořák, R. Novotný, J. Švec, J. Másilko and F. Šoukal, Correlating hydration of alkali-activated slag modified by organic additives to the evolution of its properties, Materials 16(2023).

[173] V. Bílek, L. Kalina, R. Novotný, J. Tkacz and L. Pařízek, Some issues of shrinkage-reducing admixtures application in alkali-activated slag systems, Materials 9(2016).

[174] H. Ye, C. Fu and A. Lei, Mitigating shrinkage of alkali-activated slag by polypropylene glycol with different molecular weights, Construction and Building Materials 245(2020) 118478.

[175] G. Roviello, C. Menna, O. Tarallo, L. Ricciotti, C. Ferone, F. Colangelo, D. Asprone, R. di Maggio, E. Cappelletto, A. Prota and R. Cioffi, Preparation, structure and properties of hybrid materials based on geopolymers and polysiloxanes, Materials & Design 87(2015) 82-94.

[176] S.Y. Oderji, B. Chen, C. Shakya, M.R. Ahmad and S.F.A. Shah, Influence of superplasticizers

and retarders on the workability and strength of one-part alkali-activated fly ash/slag binders cured at room temperature, Construction and Building Materials 229(2019) 116891.

[177] H. El Didamony, A. Amer and M. Arif, Impact of ethylene glycol addition on the physicochemical and mechanical properties of alkali activated ggbfs pastes, International Journal of Science and Research (Ijsr) 4(2015) 1596-1605.

[178] S. Wooh, N. Encinas, D. Vollmer and H. Butt, Stable hydrophobic metal-oxide photocatalysts via grafting polydimethylsiloxane brush, Advanced Materials 29(2017) 1604637.

[179] G. Liu, F. Xiangli, W. Wei, S. Liu and W. Jin, Improved performance of pdms/ceramic composite pervaporation membranes by zsm-5 homogeneously dispersed in pdms via a surface graft/coating approach, Chemical Engineering Journal 174(2011) 495-503.

[180] D. Wattanasiriwech, K. Yomthong and S. Wattanasiriwech, Characterisation and properties of class c-fly ash based geopolymer foams: effects of foaming agent content, aggregates, and surfactant, Construction and Building Materials 306(2021) 124847.

[181] V. Phavongkham, S. Wattanasiriwech, T. Cheng and D. Wattanasiriwech, Effects of surfactant on thermo-mechanical behavior of geopolymer foam paste made with sodium perborate foaming agent, Construction and Building Materials 243(2020) 118282.

[182] S. Petlitckaia and A. Poulesquen, Design of lightweight metakaolin based geopolymer foamed with hydrogen peroxide, Ceramics International 45(2019) 1322-1330.

[183] D. Yan, S. Ruan, S. Chen, Y. Liu, Y. Tian, H. Wang and T. Ye, Effects and mechanisms of surfactants on physical properties and microstructures of metakaolin-based geopolymer, Journal of Zhejiang University-Science A 22(2021) 130-146.

[184] L. Carabba, S. Manzi and M.C. Bignozzi, Superplasticizer addition to carbon fly ash geopolymers activated at room temperature, Materials 9(2016) 586.

[185] S. Pilehvar, M. Arnhof, R. Pamies, L. Valentini and A. Kjøniksen, Utilization of urea as an accessible superplasticizer on the moon for lunar geopolymer mixtures, Journal of Cleaner Production 247(2020) 119177.

[186] M. Verma and N. Dev, Effect of snf-based superplasticizer on physical, mechanical and thermal properties of the geopolymer concrete, Silicon 14(2022) 965-975.

[187] E. Paul, Influence of superplasticizer on workability and strength of ambient cured alkali activated mortar, Cleaner Materials 6(2022) 100152.

[188] S.H. Bong, B. Nematollahi, A. Nazari, M. Xia and J. Sanjayan, Efficiency of different superplasticizers and retarders on properties of 'one-part' fly ash-slag blended geopolymers with different activators, Materials 12(2019) 3410.

[189] B. Nematollahi and J. Sanjayan, Effect of different superplasticizers and activator combinations on workability and strength of fly ash based geopolymer, Materials & Design 57(2014) 667-672.

[190] N. Gupta, A. Gupta, K.K. Saxena, A. Shukla and S.K. Goyal, Mechanical and durability properties of geopolymer concrete composite at varying superplasticizer dosage, Materials

Today: Proceedings 44(2021) 12-16.

[191] Y. Alrefaei, Y. Wang, J. Dai and Q. Xu, Effect of superplasticizers on properties of one-part ca(oh)2/na2so4 activated geopolymer pastes, Construction and Building Materials 241(2020) 117990.

[192] N. Vanitha and R. Jeyalakshmi, The role of polyethylene glycol, a water entrainer on characteristics of silico alumino phosphate geopolymer to harvest enhanced gel phase and stability, Journal of Inorganic and Organometallic Polymers and Materials 33(2023) 2835-2847.

[193] O. Mikhailova and P. Rovnaník, Effect of polyethylene glycol addition on metakaolin-based geopolymer, Procedia Engineering 151(2016) 222-228.

[194] R.C. Pasquali, M.P. Taurozzi and C. Bregni, Some considerations about the hydrophilic–lipophilic balance system, International Journal of Pharmaceutics 356(2008) 44-51.

[195] S. Ghodke, P. Dandekar and R. Jain, Simplified evaluation aided by mathematical calculation for characterization of polyols by hydroxyl value determination, International Journal of Polymer Analysis and Characterization 26(2021) 169-178.

[196] X. Chen, G. Zhu, M. Zhou, J. Wang and Q. Chen, Effect of organic polymers on the properties of slag-based geopolymers, Construction and Building Materials 167(2018) 216-224.

[197] A.B.D. Cassie and S. Baxter, Wettability of porous surfaces, Transactions of the Faraday Society (1944) 546-551.

[198] I. Flores-Vivian, V. Hejazi, M.I. Kozhukhova, M. Nosonovsky and K. Sobolev, Self-assembling particle-siloxane coatings for superhydrophobic concrete, ACS Applied Materials & Interfaces 5(2013) 13284-13294.

[199] J. Zhang, S. Hong, B. Dong, L. Tang, C. Lin, Z. Liu and F. Xing, Water distribution modelling of capillary absorption in cementitious materials, Construction and Building Materials 216(2019) 468-475.

[200] H. Ma, H. Zhu, C. Wu, J. Fan, S. Yang and Z. Hang, Effect of shrinkage reducing admixture on drying shrinkage and durability of alkali-activated coal gangue-slag material, Construction and Building Materials 270(2021) 121372.

[201] J. Liu, N. Farzadnia, C. Shi and X. Ma, Shrinkage and strength development of UHSC incorporating a hybrid system of SAP and SRA, Cement and Concrete Composites 97(2019) 175-189.

[202] J. Lee and T. Lee, Effects of high CaO fly ash and sulfate activator as a finer binder for cementless grouting material, Materials 12(2019).

[203] V. BÍLEK JR, Evaluation of the surfactant leaching from alkali-activated slag-based composites using surface-tension measurements, Evaluation 33(2019) 38.

[204] P. Aïtcin and R.J. Flatt, Science and technology of concrete admixtures, Woodhead publishing 2015.

[205] C. Zhang, X. Kong, J. Yu, D. Jansen, J. Pakusch and S. Wang, Correlation between the adsorption behavior of colloidal polymer particles and the yield stress of fresh cement pastes,

Cement and Concrete Research 152(2022) 106668.

[206] N. Shirshova, A. Menner, G.P. Funkhouser and A. Bismarck, Polymerised high internal phase emulsion cement hybrids: macroporous polymer scaffolds for setting cements, Cement and Concrete Research 41(2011) 443-450.

[207] B. Pang, Y. Jia, S.D. Pang, Y. Zhang, H. Du, G. Geng, H. Ni, J. Qian, H. Qiao and G. Liu, The interpenetration polymer network in a cement paste–waterborne epoxy system, Cement and Concrete Research 139(2021) 106236.

[208] J. Mi, Z. Luo, X. Liu, M. Zhang, Y. Mu, C. Tian, M. Zhang and J. Guo, For the improvement of toughness and volume stability of alkali-activated slag with styrene-acrylic emulsion, Journal of Building Engineering 58(2022) 105040.

[209] X. Chen, M. Zhou, W. Shen, G. Zhu and X. Ge, Mechanical properties and microstructure of metakaolin-based geopolymer compound-modified by polyacrylic emulsion and polypropylene fibers, Construction and Building Materials 190(2018) 680-690.

[210] N.K. Lee, E.M. Kim and H.K. Lee, Mechanical properties and setting characteristics of geopolymer mortar using styrene-butadiene (SB) latex, Construction and Building Materials 113(2016) 264-272.

[211] H.E. El-Yamany, M.A. El-Salamawy and N.T. El-Assal, Microstructure and mechanical properties of alkali-activated slag mortar modified with latex, Construction and Building Materials 191(2018) 32-38.

[212] X. Xing, B. Wang, H. Liu, S. Luo, S. Wang, J. Wei, W. Xu and Q. Yu, The mechanism of silane-grafted sodium polyacrylate on the toughening of slag-based geopolymer: an insight from macroscopic–microscopic mechanical properties, Journal of Materials Science 58(2023) 8757-8778.

[213] C. Lu, Z. Zhang, J. Hu, Q. Yu and C. Shi, Relationship between rheological property and early age-microstructure building up of alkali-activated slag, Composites Part B: Engineering 247(2022) 110271.

[214] Z. Pan, J.G. Sanjayan and B.V. Rangan, Fracture properties of geopolymer paste and concrete, Magazine of Concrete Research 63(2011) 763-771.

[215] S.K. John, Y. Nadir, A. Cascardi, M.M. Arif and K. Girija, Effect of addition of nanoclay and SBR latex on fly ash-slag geopolymer mortar, Journal of Building Engineering 66(2023) 105875.

[216] S.Y. Yao and Y. Ge, Effect of styrene butadiene rubber latex on mortar and concrete properties, in: Trans Tech Publ, 2012,283-288.

[217] H. Yao, Z. Xie, C. Huang, Q. Yuan and Z. Yu, Recent progress of hydrophobic cement-based materials: preparation, characterization and properties, Construction and Building Materials 299(2021) 124255.

[218] A.M. Diab, H.E. Elyamany and A.H. Ali, Experimental investigation of the effect of latex solid/water ratio on latex modified co-matrix mechanical properties, Alexandria Engineering

Journal 52(2013) 83-98.

[219] G. Roviello, L. Ricciotti, O. Tarallo, C. Ferone, F. Colangelo, V. Roviello and R. Cioffi, Innovative fly ash geopolymer-epoxy composites: preparation, microstructure and mechanical properties, Materials 9(2016) 461.

[220] A. Maiorana, S. Spinella and R.A. Gross, Bio-based alternative to the diglycidyl ether of bisphenol a with controlled materials properties, Biomacromolecules 16(2015) 1021-1031.

[221] F. Jin, X. Li and S. Park, Synthesis and application of epoxy resins: a review, Journal of Industrial and Engineering Chemistry 29(2015) 1-11.

[222] X. Zhu, H. Qian, H. Wu, Q. Zhou, H. Feng, Q. Zeng, Y. Tian, S. Ruan, Y. Zhang, S. Chen and D. Yan, Early-stage geopolymerization process of metakaolin-based geopolymer, Materials 15(2022) 6125.

[223] V. Šmilauer, P. Hlaváček, F. Škvára, R. Šulc, L. Kopecký and J. Němeček, Micromechanical multiscale model for alkali activation of fly ash and metakaolin, Journal of Materials Science 46(2011) 6545-6555.

[224] L. Weng and K. Sagoe-Crentsil, Dissolution processes, hydrolysis and condensation reactions during geopolymer synthesis: part i-low Si/Al ratio systems, Journal of Materials Science 42(2007) 2997-3006.

[225] K. Benzarti, C. Perruchot and M.M. Chehimi, Surface energetics of cementitious materials and their wettability by an epoxy adhesive, Colloids and Surfaces a: Physicochemical and Engineering Aspects 286(2006) 78-91.

[226] J. Du, Y. Bu, Z. Shen, X. Hou and C. Huang, Effects of epoxy resin on the mechanical performance and thickening properties of geopolymer cured at low temperature, Materials & Design 109(2016) 133-145.

[227] G. Xiong, X. Guo and H. Zhang, Preparation of epoxy resin-geopolymer (erg) for repairing and the microstructures of the new-to-old interface, Composites Part B: Engineering 259(2023) 110731.

[228] J.L. Provis, P. Duxson, J.S.J. Van Deventer and G.C. Lukey, The role of mathematical modelling and gel chemistry in advancing geopolymer technology, Chemical Engineering Research and Design 83(2005) 853-860.

[229] I. Ismail, S.A. Bernal, J.L. Provis, R. San Nicolas, S. Hamdan and J.S.J. van Deventer, Modification of phase evolution in alkali-activated blast furnace slag by the incorporation of fly ash, Cement and Concrete Composites 45(2014) 125-135.

[230] J. Du, Y. Bu, X. Cao, Z. Shen and B. Sun, Utilization of alkali-activated slag based composite in deepwater oil well cementing, Construction and Building Materials 186(2018) 114-122.

[231] R.V.R. San Nicolas, B. Walkley and J.S.J. van Deventer, 7 - fly ash-based geopolymer chemistry and behavior, in:T. Robl, A. Oberlink, R. Jones(Eds.),Coal Combustion Products (CCP's),Woodhead Publishing, 2017, pp. 185-214.

[232] B. Pang, Y. Zhang, G. Liu and W. She, Interface properties of nanosilica-modified waterborne

epoxy cement repairing system, ACS Applied Materials & Interfaces 10(2018) 21696-21711.

[233] Y.J. Zhang, S. Li, Y.C. Wang and D.L. Xu, Microstructural and strength evolutions of geopolymer composite reinforced by resin exposed to elevated temperature, Journal of Non-Crystalline Solids 358(2012) 620-624.

[234] F.A.M.M. Gonçalves, M. Santos, T. Cernadas, P. Alves and P. Ferreira, Influence of fillers on epoxy resins properties: a review, Journal of Materials Science 57(2022) 15183-15212.

[235] M. Wu, B. Johannesson and M. Geiker, A review: self-healing in cementitious materials and engineered cementitious composite as a self-healing material, Construction and Building Materials 28(2012) 571-583.

[236] J. Wang, T. Huang, G. Cheng, Z. Liu, S. Li and D. Wang, Effects of fly ash on the properties and microstructure of alkali-activated FA/BFS repairing mortar, Fuel 256(2019) 115919.

[237] E. Gomaa, A. Gheni and M.A. ElGawady, Repair of ordinary Portland cement concrete using ambient-cured alkali-activated concrete: interfacial behavior, Cement and Concrete Research 129(2020) 105968.

[238] F. Djouani, C. Connan, M. Delamar, M.M. Chehimi and K. Benzarti, Cement paste–epoxy adhesive interactions, Construction and Building Materials 25(2011) 411-423.

[239] H.N. Yoon, S.M. Park and H.K. Lee, Effect of MgO on chloride penetration resistance of alkali-activated binder, Construction and Building Materials 178(2018) 584-592.

[240] F. Djouani, M.M. Chehimi and K. Benzarti, Interactions of fully formulated epoxy with model cement hydrates, Journal of Adhesion Science and Technology 27(2013) 469-489.

[241] T. Nochaiya, W. Wongkeo, K. Pimraksa and A. Chaipanich, Microstructural, physical, and thermal analyses of portland cement–fly ash–calcium hydroxide blended pastes, Journal of Thermal Analysis and Calorimetry 100(2010) 101-108.

[242] R. Singla, S. Kumar and T.C. Alex, Reactivity alteration of granulated blast furnace slag by mechanical activation for high volume usage in Portland slag cement, Waste and Biomass Valorization 11(2020) 2983-2993.

[243] P. Duxson, G.C. Lukey and J.S.J. van Deventer, Physical evolution of Na-geopolymer derived from metakaolin up to 1000 °c, Journal of Materials Science 42(2007) 3044-3054.

[244] C.E. White, J.L. Provis, T. Proffen and J.S.J. Van Deventer, The effects of temperature on the local structure of metakaolin-based geopolymer binder: a neutron pair distribution function investigation, Journal of the American Ceramic Society 93(2010) 3486-3492.

[245] S. Luo, J. Wei, W. Xu, Y. Chen, H. Huang, J. Hu and Q. Yu, Design, preparation, and performance of a novel organic–inorganic composite coating with high adhesion and protection for concrete, Composites Part B: Engineering 234(2022) 109695.

[246] S.A. Haddadi, A. Ramazani S. A., M. Mahdavian, P. Taheri, J.M.C. Mol and Y. Gonzalez-Garcia, Self-healing epoxy nanocomposite coatings based on dual-encapsulation of nano-carbon hollow spheres with film-forming resin and curing agent, Composites Part B: Engineering 175(2019) 107087.

[247] X. Xing, B. Wang, S. Luo, F. Lin, J. Wei, W. Xu, J. Hu and Q. Yu, Preparation and formation mechanism of high-toughness organic polymers modified geopolymers, Cement and Concrete Composites 150(2024) 105578.

[248] W.L. Zhong, Y.H. Zhang, L.F. Fan and P.F. Li, Effect of PDMS content on waterproofing and mechanical properties of geopolymer composites, Ceramics International 48(2022) 26248-26257.

[249] F. Tittarelli and G. Moriconi, Comparison between surface and bulk hydrophobic treatment against corrosion of galvanized reinforcing steel in concrete, Cement and Concrete Research 41(2011) 609-614.

[250] J. Zhao, X. Gao, S. Chen, H. Lin, Z. Li and X. Lin, Hydrophobic or superhydrophobic modification of cement-based materials: a systematic review, Composites Part B: Engineering 243(2022) 110104.

[251] A. Zhou, Z. Yu, H. Wei, L. Tam, T. Liu and D. Zou, Understanding the toughening mechanism of silane coupling agents in the interfacial bonding in steel fiber-reinforced cementitious composites, Acs Applied Materials & Interfaces 12(2020) 44163-44171.

[252] M.M. Camargo, T.E. Adefrs, J.A. Roether, R.D. Tilahun and A.R. Boccaccini, A review on natural fiber-reinforced geopolymer and cement-based composites, Materials 13(2020).

[253] K.A. Komnitsas, Potential of geopolymer technology towards green buildings and sustainable cities, Procedia Engineering 21(2011) 1023-1032.

[254] R. Siddique, J. Khatib and I. Kaur, Use of recycled plastic in concrete: a review, Waste Management 28(2008) 1835-1852.

[255] N. Bandow, S. Gartiser, O. Ilvonen and U. Schoknecht, Evaluation of the impact of construction products on the environment by leaching of possibly hazardous substances, Environmental Sciences Europe 30(2018) 14.

[256] K. Abora, I. Beleña, S.A. Bernal, A. Dunster, P.A. Nixon, J.L. Provis, A. Tagnit-Hamou and F. Winnefeld, Durability and testing–chemical matrix degradation processes, Alkali Activated Materials: State-of-the-Art Report, Rilem Tc 224-Aam(2014) 177-221.

[257] C.B. Godiya and B.J. Park, Removal of bisphenol a from wastewater by physical, chemical and biological remediation techniques. A review, Environmental Chemistry Letters 20(2022) 1801-1837.

[258] A.M. Kaja, K. Schollbach, S. Melzer, S.R. van der Laan, H.J.H. Brouwers and Q. Yu, Hydration of potassium citrate-activated bof slag, Cement and Concrete Research 140(2021) 106291.

[259] A.M. Kaja, S. Melzer, H. Brouwers and Q.L. Yu, On the optimization of bof slag hydration kinetics, Cement & Concrete Composites 124(2021).

[260] B.E. Glad and W.M. Kriven, Geopolymer with hydrogel characteristics via silane coupling agent additives, Journal of the American Ceramic Society 97(2014) 295-302.

[261] B.E. Glad, C. Han and W.M. Kriven, Polymer adhesion to geopolymer via silane coupling agent additives, Journal of the American Ceramic Society 95(2012) 3758-3762.

[262] C. Bai and P. Colombo, High-porosity geopolymer membrane supports by peroxide route with the addition of egg white as surfactant, Ceramics International 43(2017) 2267-2273.

[263] Y. Alrefaei, Y. Wang and J. Dai, The effectiveness of different superplasticizers in ambient cured one-part alkali activated pastes, Cement and Concrete Composites 97(2019) 166-174.

[264] C. Jithendra and S. Elavenil, Role of superplasticizer on ggbs based geopolymer concrete under ambient curing, Materials Today: Proceedings 18(2019) 148-154.

[265] T. Luukkonen, Z. Abdollahnejad, K. Ohenoja, P. Kinnunen and M. Illikainen, Suitability of commercial superplasticizers for one-part alkali-activated blast-furnace slag mortar, Journal of Sustainable Cement-Based Materials 8(2019) 244-257.

[266] B.A. Salami, M.A. Megat Johari, Z.A. Ahmad and M. Maslehuddin, Impact of added water and superplasticizer on early compressive strength of selected mixtures of palm oil fuel ash-based engineered geopolymer composites, Construction and Building Materials 109(2016) 198-206.

[267] F.N. Okoye, J. Durgaprasad and N.B. Singh, Mechanical properties of alkali activated flyash/kaolin based geopolymer concrete, Construction and Building Materials 98(2015) 685-691.

[268] M. Albitar, P. Visintin, M.S. Mohamed Ali and M. Drechsler, Assessing behaviour of fresh and hardened geopolymer concrete mixed with class-f fly ash, Ksce Journal of Civil Engineering 19(2015) 1445-1455.

[269] S. Demie, M.F. Nuruddin and N. Shafiq, Effects of micro-structure characteristics of interfacial transition zone on the compressive strength of self-compacting geopolymer concrete, Construction and Building Materials 41(2013) 91-98.

[270] F. Pacheco-Torgal, D. Moura, Y. Ding and S. Jalali, Composition, strength and workability of alkali-activated metakaolin based mortars, Construction and Building Materials 25(2011) 3732-3745.

[271] S. Demie, M.F. Nuruddin, M.F. Ahmed and N. Shafiq, Effects of curing temperature and superplasticizer on workability and compressive strength of self-compacting geopolymer concrete, in: IEEE, 2011,1-5.

[272] M.F. Nuruddin, S. Demie, M.F. Ahmed and N. Shafiq, Effect of superplasticizer and naoh molarity on workability, compressive strength and microstructure properties of self-compacting geopolymer concrete, International Journal of Geological and Environmental Engineering 5(2011) 187-194.

[273] M. Palacios, P.F.G. Banfill and F. Puertas, Rheology and setting of alkali-activated slag pastes and mortars: effect of organic admixture, Aci Materials Journal 105(2008) 140.

[274] P. Chindaprasirt, T. Chareerat and V. Sirivivatnanon, Workability and strength of coarse high calcium fly ash geopolymer, Cement and Concrete Composites 29(2007) 224-229.

[275] M. Catauro, F. Papale, G. Lamanna and F. Bollino, Geopolymer/peg hybrid materials synthesis and investigation of the polymer influence on microstructure and mechanical behavior, Materials Research 18(2015) 698-705.

[276] S. Zhang, K. Gong and J. Lu, Novel modification method for inorganic geopolymer by using water soluble organic polymers, Materials Letters 58(2004) 1292-1296.

[277] Y. Wang, J. Zhao and J. Chen, Effect of polydimethylsiloxane viscosity on silica fume-based geopolymer hybrid coating for flame-retarding plywood, Construction and Building Materials 239(2020) 117814.

[278] Z. Lu, J. Merkl, M. Pulkin, R. Firdous, S. Wache and D. Stephan, A systematic study on polymer-modified alkali-activated slag–part ii: from hydration to mechanical properties, Materials 13(2020).

[279] Z. Lu, J. Merkl, C. Schmidtke, M. Pulkin, F. Deschner, S. Wache, Y. Jin and D. Stephan, A systematic study on polymer modified alkali-activated slag - part i: stability analysis of colloidal polymer dispersion in sodium water glass, Construction and Building Materials 221(2019) 40-49.

[280] A. Kusbiantoro, N. Rahman, S.C. Chin and R. Bayu Aji, Effect of poly(ethylene-co-vinyl acetate) as a self-healing agent in geopolymer exposed to various curing temperatures, Materials Science Forum 841(2016) 16-20.

[281] A. Saludung, T. Azeyanagi, Y. Ogawa and K. Kawai, Alkali leaching and mechanical performance of epoxy resin-reinforced geopolymer composite, Materials Letters 304(2021) 130663.

[282] P.N. Lemougna, A. Adediran, J. Yliniemi, T. Luukkonen and M. Illikainen, Effect of organic resin in glass wool waste and curing temperature on the synthesis and properties of alkali-activated pastes, Materials & Design 212(2021) 110287.